INFORMATION TO USERS

This manuscript has been reproduced from the microfilm master. UMI films the text directly from the original or copy submitted. Thus, some thesis and dissertation copies are in typewriter face, while others may be from any type of computer printer.

The quality of this reproduction is dependent upon the quality of the copy submitted. Broken or indistinct print, colored or poor quality illustrations and photographs, print bleedthrough, substandard margins, and improper alignment can adversely affect reproduction.

In the unlikely event that the author did not send UMI a complete manuscript and there are missing pages, these will be noted. Also, if unauthorized copyright material had to be removed, a note will indicate the deletion.

Oversize materials (e.g., maps, drawings, charts) are reproduced by sectioning the original, beginning at the upper left-hand corner and continuing from left to right in equal sections with small overlaps. Each original is also photographed in one exposure and is included in reduced form at the back of the book.

Photographs included in the original manuscript have been reproduced xerographically in this copy. Higher quality 6" x 9" black and white photographic prints are available for any photographs or illustrations appearing in this copy for an additional charge. Contact UMI directly to order.

UMI

A Bell & Howell Information Company
300 North Zeeb Road, Ann Arbor MI 48106-1346 USA
313/761-4700 800/521-0600

Université d'Ottawa · University of Ottawa

The Effect of Spatial Statistics of Hydraulic Conductivity and Distribution Coefficient Fields on Solute Transport

by

© Ingrid E. Luffman

a thesis presented to the University of Ottawa
in fulfillment of the requirements of the Master of Science Degree.

May 16th, 1997

ABSTRACT

The purpose of this research is twofold. First, a tool is developed to assist in the reproduction of field correlation scenarios for input into a flow and transport simulator. Second, this tool is used to generate random fields with several different velocity/retardation relationships typical of the Canada Forces Base Borden aquifer in order to determine the effect of this relationship on the retardation and dispersive processes, specifically on the macrodispersivity.

The first section of the research involves making modifications to the input power spectrum of a random field generator and subsequently determining the effect of the modifications on the generated field. The power spectrum is modified by increasing the power at specific frequencies. The magnitude of the increase is directly proportional to the magnitude of the field variability, or noise. Increasing the power near the origin (at low frequencies) increases the low frequency or large scale variability. Similarly, increasing the power near the Nyquist (highest) frequency increases high frequency or small scale noise. An increase in power over several frequency increments results in noise at a wide range of scales, while increasing the power at a single frequency produces noise at a single scale. The symmetry of the input spectrum controls the orientation of the stratification in the generated fields. An asymmetrical input spectrum produces sloped layers while a symmetrical spectrum produces fields with horizontal stratification.

The second section of the research investigates the effect of different types of spatial

statistics on the behaviour of a contaminant travelling through saturated, heterogeneous porous media. The spatial statistics describe the spatial correlation (autocorrelation) of the velocity and of the retardation fields, and the spatial correlation between the velocity field and the retardation field (cross-correlation). A combination of three types of autocorrelation and three types of cross-correlation are studied, for a total of nine scenarios. Monte Carlo simulations are performed, and macrodispersivities are calculated from the output spatial moments. Only two Monte-Carlo realizations are used, however, because of the design of the experiment and the use of the Analysis of Variance (ANOVA) technique, significant results are obtained with a very limited number of realizations. The ANOVA technique is used to test for differences in the position of the plume centres of mass as well as differences in macrodispersivities between scenarios.

The non-reactive plume travels significantly farther than the reactive plume, even when considering the effects of retardation. The movement of the plume centre of mass for a reactive solute is significantly retarded when a positive correlation between velocity and retardation at scales greater than 1 m is added to an otherwise negative relationship, suggesting that the macroscopic retardation factor is dependent, in part, on the large-scale correlation between hydraulic conductivity and the distribution coefficient.

For a reactive solute, a small negative correlation between velocity and retardation increases longitudinal macrodispersivity whereas a positive correlation decreases it. Longitudinal macrodispersivity is also enhanced for fields with fine, periodic

stratification as opposed to fields with a coarser stratification and no periodicity. For a non-reactive solute, the type of autocorrelation had no effect on longitudinal macrodispersivity.

Transverse macrodispersivities are sensitive to changes to neither the correlation within fields, nor the correlation between velocity and retardation fields for both the reactive and non-reactive solute plumes.

Longitudinal macrodispersivity for a reactive solute is significantly different than that for a non-reactive solute: the effect of the chemical heterogeneities is to enhance reactive solute macrodispersivities relative to non-reactive macrodispersivities for a negative cross-correlation between velocity and retardation, and to decrease reactive solute macrodispersivities relative to non-reactive macrodispersivities when the cross-correlation is positive.

ACKNOWLEDGEMENTS

I would like to thank my advisor, Dr. Michel Robin for his assistance, guidance and interest in this project. I would also like to thank Rich Naff from the United States Geological Survey for his personal insights into the simulation program and also for his invaluable assistance in testing the code.

Sincere thanks go to my parents: to my Mother for countless hours of babysitting, and to my Father for hours of reading, proof-reading and revision (and yes, babysitting).

I would like to dedicate this thesis to my husband Robert and my son Benjamin, without whose loving attention this thesis would have been completed far sooner. Robert, I thank you for your unfailing support and optimism, this is for you.

TABLE OF CONTENTS

Abstract ..... (i)

Acknowledgements ..... (iv)

List of Tables ..... (vii)

List of Figures ..... (viii)

CHAPTER 1

Executive Summary 1

CHAPTER 2

Generating Random Fields With Specific Correlation Structures by Varying the Autocorrelation Function

ABSTRACT 6

INTRODUCTION 7

METHOD 11

RESULTS AND DISCUSSION 13
- Effect of Spike Height 13
- Effect of Spike Position 13
- Effect of Spike Shape 17

SUMMARY AND CONCLUSIONS 19

REFERENCES 20

CHAPTER 3

The Effect of Spatial Statistics of the Hydraulic Conductivity and Distribution Coefficient Fields on Solute Transport in 3-dimensional Heterogeneous Porous Media

ABSTRACT 31

INTRODUCTION 32

METHOD 36
- Calculation of Spatial Moments 44

ANALYSIS AND RESULTS 46
- Zeroth Moment (Mass in Solution) 49
- First Moment (Centre of Mass) 51
- Retardation Coefficient 52
- Second Moment 59
  - *Calculation of Macrodispersivities* 59
  - *Uniformity of Variances* 69
  - *Effect of Correlation Scenario* 70
  - *Effect of Solute Type* 75

SUMMARY AND CONCLUSIONS 79

REFERENCES 83

COMPILED REFERENCES 91

LIST OF TABLES

Chapter 2

Table I: Input parameters common to all simulations 12

Chapter 3

Table I: Monte-Carlo scenarios studied 40

Table II: First moments for reactive solute plumes at time T3 (400 days) (M_{100}) and for non-reactive solute plumes at times $T3/R_A$ (M^*_{100A}) and $T3/R_G$ (M^*_{100G})..... 55

Table III: Mean retardation factors for all scenarios 56

Table IV: Macrodispersivity values for Case 11 (non-reactive) 61

Table V: Longitudinal macrodispersivities for a) a reactive solute and b) a non-reactive solute. Each value is the mean of two or more realizations 64

Table VI: Macrodispersivities for the transverse horizontal (y) direction. Each value is the mean of two or more realizations 65

Table VII: Macrodispersivities for the transverse vertical (z) direction. Each value is the mean of two or more realizations 65

Table VIII: Theoretical and observed longitudinal macrodispersivities for the reactive (a) and non-reactive (b) solute 68

Table IX: P-values for significance of pairwise differences in longitudinal macrodispersivity (reactive solute) 73

Table X: A^* values from equation (38) for all scenarios, each entry is a mean over two realizations 78

LIST OF FIGURES

Chapter 2

Figure 1: Random fields (b) generated from spiked power spectra (a). Increased spike height produces increased variability. Note that only the perturbation magnitude is affected because the same random number seed was used for each spectrum..... 22

Figure 2: Random fields generated from spiked one-dimensional power spectra. The closer the spike to the Nyquist frequency, the closer together the peaks in the field (an increase in variability at small scales) 23

Figure 3: Base case field of (unitless) dependent variable for two-dimensional simulations..... 24

Figure 4: Transects from two-dimensional fields. X-direction transects (a) show increased variability at small scales as spike is moved from (0,0) towards (x-Nyquist, 0). Y-direction transects (b) show no change in variability since y coordinates of spike do not change 25

Figure 5: Example of symmetry properties used by RFG packing routine for (a) a vertical stripe and (b) a partial horizontal stripe 26

Figure 6: Power spectra and resulting random fields for horizontal stripes in the power spectrum. A stripe with a "step up" (a) produces lenses with negative slopes. A continuous stripe at y=0 (b) increases variability in the y direction at infinitely large scales . 27

Figure 7: Random fields generated from one-dimensional power spectra with the spike centred on frequency 0.8. Increased spike width causes increased variability over a wider range of scales..... 28

Figure 8: Transects of two-dimensional random fields. Removal of high-frequency component of stripe in spectrum causes a reduction in low-frequency noise in the x direction (a) and a reduction in high-frequency noise in the y-direction (b)..... 29

Figure 9: Random field resulting from two spikes in the input spectrum. Dimensions of lenses are controlled by positions of spikes. Because spikes are located at both high and low x-frequencies, lenses with both small and large x-lengths are observed. Similar observations can be made for the y-direction 30

Chapter 3

Figure 1: Scatter plot of field means versus variances for all individual realizations. Upper half of each cluster corresponds to cases with increased field variability from addition of high-frequency spike to input power spectrum..... 85

Figure 2: Transverse vertical transects of K and K_d fields showing effects of different auto and cross-correlation structures..... 86

Figure 3: Three orthogonal slices from the full K field for vertical correlation lengths of a) 20 cm, b) 20 cm with small-scale periodicity and c) 7 cm. Field dimensions are 30 x 11 x 4.4 meters and vertical exaggeration is 3x..... 87

Figure 4: Reactive tracer plume longitudinal macrodispersivity is enhanced for small negative cross-correlation (a) compared to perfect positive correlation (b). Vertical correlation lengths are 20 cm. Concentration plume isosurface is 0.1% at time 450 days. Field dimensions are 30 x 11 x 4.4 meters, vertical exaggeration is 3x 88

Figure 5: Enhanced longitudinal macrodispersivity results from an increase in small scale variability due to periodicity in velocity and retardation fields with $\lambda_3 = 20$ cm (a) compared to $\lambda_3 = 7$ cm (b). There is a small negative cross-correlation between velocity and retardation and the 0.1% concentration isosurface is shown. Field dimensions are 30 x 11 x 4.4 meters, vertical exaggeration is 3x 89

Figure 6: Plume longitudinal macrodispersivity is enhanced for a reactive solute. Reactive plume for time 300 days (with K_d field in the background) (a) has more spatial spreading than non-reactive plume at 103 days (with the common K field in the background). There is a small negative cross-correlation between K and K_d. Field dimensions are 30 x 11 x 4.4 metres and vertical exaggeration is 3x, 0.1% concentration isosurface is shown 90

CHAPTER 1

Executive Summary

The organization of this thesis is non-traditional. Each chapter is written as a self-contained unit with an introduction and set of conclusions. As a consequence of this layout, some repetition may occur in the introductory sections of each chapter in order to provide the necessary background information.

The purpose of this research is to investigate the dispersion of a contaminant through saturated heterogeneous porous media. The research focused in particular on the effects on macrodispersivity of the spatial correlation structure of the hydraulic conductivity (K), of the distribution coefficient (K_d) and of the correlation between K and K_d. One factor which makes this research unique is the scale of the features in the simulated fields: fields generated with vertical correlation scales of 20 centimetres were compared to fields with 7 centimetre correlation lengths. The physical interpretation of the vertical correlation length is the thickness of layered heterogeneities, or lenses, in the porous media. A comparison between the two scales provides an estimate of the effect of thin versus thick sedimentary facies on solute macrodispersivity. Differences in sedimentary facies are the result of variations in depositional environments, and such environments are generally cyclical, having arisen from mechanisms of deposition. Thus periodicity should be considered when performing these types of simulations. For the reasons outlined above, a comparison

of periodic versus non-periodic sedimentary facies, as well as thin versus thick facies is undertaken.

A second factor by which this research differs from similar studies is in the cross-correlation model used to generate the random fields. Rather than using the more common linear model, a cross-spectrum based on the two power spectra and the coherency is used.

The first part of the research (Chapter 2) investigates the generation of random fields with specific correlation structures based on changes to the input autocorrelation function (ACF). A recipe for producing specific characteristics is developed based on trial runs of the random field generator (RFG).

The second section of the research (Chapter 3) investigates the flow and transport of a contaminant through heterogeneous porous media. Here, the RFG studied in the first section is used to generate random fields which mirror as closely as possible several different geological scenarios typical of the Canada Forces Base Borden aquifer in Ontario, Canada. Specifically, input statistics of the natural logs of the hydraulic conductivity (ln(K)) and the distribution coefficient ($\ln(K_d)$) measured from cores by *Halket et al. [1996]* are used as the base statistics for all scenarios and then two cross-correlated fields are generated. The type of correlation within and between the fields is varied to assess the impact on macrodispersivity.

Monte Carlo simulations of solute transport through these fields are performed, and the statistical technique Analysis of Variance (ANOVA) is used to analyse the resulting calculated macrodispersivities. This innovation enabled conclusions to be drawn from a very limited number of realizations.

Three-dimensional flow and transport simulations through heterogeneous porous media were performed on nine different Monte Carlo scenarios. Each scenario encompassed one each of three types of auto and cross-correlation functions, determined from field studies at Borden. The following is a summary of the results from the two parts of the research.

Increasing the power at specific frequencies in the power spectrum of a random field generator affects the physical characteristics of the generated field. Noise at a particular scale (or scales) can be added to the field by increasing the power spectrum at the desired frequency (or frequencies). The typically horizontal stratification of the generated field can be given a sloped orientation by using an asymmetrical input spectrum. These tools provide a way for modelers to fine-tune a random field to represent a specific aquifer for which physical and chemical correlation information is available. Such is the case for the Borden aquifer.

Flow and transport simulations through fields with properties similar to those found at Borden were performed and the effect of changing the correlation structure of the

velocity and retardation fields was studied. A non-reactive plume travels significantly farther overall than the reactive plume, even when retardation is taken into account. The movement of the plume centre of mass for a reactive solute is significantly retarded when a positive correlation between velocity and retardation at scales greater than 1 m is added to an otherwise negative relationship. This suggests that the macroscopic retardation factor depends, in part, on the large-scale correlation between hydraulic conductivity (K) and the distribution coefficient (K_d).

Retardation coefficients based on the arithmetic mean K_d provide a better estimate of macro-retardation than those based on the geometric mean K_d.

Macrodispersivity is dependent on the type of correlation between velocity and retardation. Specifically, a small negative correlation enhances longitudinal macrodispersivity, however, transverse macrodispersivity is not dependent on the correlation scenario. The type of autocorrelation also has a significant effect: longitudinal macrodispersivity is enhanced for fields with fine, periodic stratification compared to fields with a more coarse non-periodic stratification.

Macrodispersivities for a reactive solute are significantly larger than those for a non-reactive solute, depending on the type of cross-correlation and to some extent on the type of autocorrelation. Even a weak correlation between K and K_d can lead to significantly enhanced mixing.

The Analysis of Variance (ANOVA) procedures to process the results of numerical experiments are extremely powerful: conclusions could be drawn from a very limited number of realizations. However, the confidence level of the conclusions could have been improved by using a larger number of realizations. By increasing the number of realizations, the probability of committing a Type II error would be reduced.

The results of these simulations are important because they show how the dispersive process is sensitive to small-scale changes to the correlation structure of the velocity and retardation fields. In the case of a reactive tracer, the simulations showed that even a weak correlation between K and K_d can produce more mixing than can be accounted for in an equivalent homogeneous medium.

CHAPTER 2

Generating Random Fields With Specific Correlation Structures by Varying the Autocorrelation Function

ABSTRACT

One-, two- and three-dimensional random fields were generated using the magnitude of the inverse Fourier transform of the auto-correlation function, the power spectrum. The purpose of this research was to discover the effects of increasing the value of the power spectrum at specific frequencies (i.e. adding a spike to the power spectrum) on the resulting random fields. The results of the simulations indicated that increasing the height of the spike increases the field variability. The position of the spike in the power spectrum governs the presence of noise, for example, a spike located near the origin increases the low frequency noise in the field, while a spike located near the Nyquist frequency increases the high frequency noise. The frequency of the noise is also affected by the shape of the spike: a spike with a wide base covering several frequency increments produces noise at a wide range of scales while a spike with a narrow base produces field variability at a single scale. The orientation of lenses in two- and three-dimensional fields is controlled by the symmetry of the input spectrum. Asymmetrical input spectra produce sloped lenses, while symmetrical input spectra have no affect on the orientation of the lenses.

INTRODUCTION

Over the past twenty years, models of solute flow and transport have expanded from uni-dimensional, deterministic, homogeneous and isotropic system simulations, to three-dimensional models that allow for heterogeneity and anisotropy, having random components which better represent spatial variability. One of the first steps in modelling contaminant transport is to define the media through which the contaminant travels. Random field generators can produce fields representing the physical characteristics of the media based on statistical parameters provided as input by the user. Other areas of hydrogeology in which random field generators may be used, are groundwater sampling, aquifer remediation and the design and operation of waste management facilities (e.g., *Massman and Freeze [1987a,b], Wagner and Gorelick [1987], [1989]*) as well as in sensitivity analysis, forecasting or verification of existing theories of groundwater flow and solute transport (e.g. *Black and Freyberg [1987], Frind et al. [1987], Sudicky et al. [1990], Thompson and Gelhar [1990], Vomvoris and Gelhar [1990]*).

Often, computer simulations of contaminant transport are performed in concert with field tests and/or lab experiments. The advantage of this is that Monte Carlo simulations produce an average behaviour of the plume over a number of repetitions of the experiment, called realizations, whereas field tests represent only one realization out of an infinite number of possible realities. In order to be able to compare simulations with actual experiments, generated fields must match as closely as possible the porous media through which the solute is travelling. An analysis of cores gives an idea of the structure

of the porous media, and this information can then be used to generate random fields representing the same structure.

The purpose of this part of the research is to develop a recipe for generating random fields which mirror, as closely as possible, specific field scenarios.

Generation of the random field requires input data and statistics, which include the mean and variance of the parameter in question, the spatial correlation scales in each dimension, and the shape of the auto-correlation function or power spectrum. The auto-correlation function (ACF) and power spectrum are, by definition, a Fourier transform pair. They are expressions of variability as a function of the scale over which the measurement is made (*Brigham [1989]*).

The power spectrum is a function of frequency, which can be interpreted as the number of measurements per unit length. Frequency is equal to 1/wavelength where the wavelength represents the distance between measurements or the scale of measurement.

The random field generator (RFG) used in this research was developed by *Robin et al. [1993]* to generate two random fields that are cross-correlated in space. The fields can represent any two parameters of interest. They specify nodal values for a pair of physical parameters for which the mean, variance, correlation lengths, and type and degree of correlation between the pair is known. For this first portion of the research, the second

field is disregarded in order to separate the effects of the changes to the power spectrum from the effects of the cross-correlation between the two fields.

One of the ACF models used by the RFG, and the one chosen for this study, is an exponentially decaying anisotropic function of the form:

$$R_{hh}(\xi) = \sigma_h^2 \exp\left\{ - \left\{ \frac{\xi_1^2}{\lambda_{h1}^2} + \frac{\xi_2^2}{\lambda_{h2}^2} + \frac{\xi_3^2}{\lambda_{h3}^2} \right\}^{\frac{1}{2}} \right\} \qquad (1)$$

where R_{hh} is the auto-covariance function for variable h , σ_h^2 is the variance, ξ is the lag vector (distance separating pairs of measurements), and λ_{hi} (i=1,2,3) is the correlation scales vector (*Robin et al. [1993], Gelhar and Axness [1983]*).

The ACF (1) has the power spectrum

$$S_{hh}(f) = \frac{(2\pi)^3 \sigma_f^2 \lambda_{h1} \lambda_{h2} \lambda_{h3}}{\pi^2 \left\{1 + (2\pi f_1 \lambda_{h1})^2 + (2\pi f_2 \lambda_{h2})^2 + (2\pi f_3 \lambda_{h3})^2\right\}^2} \qquad (2)$$

where S_{hh} is the Power Spectral Density function (PSD) (also called the power spectrum) and $f=(f_1, f_2, f_3)$ is the frequency vector. It is interesting to note that integrating the spectrum over all frequencies yields the variance, and an increase to the power spectrum at any frequency will therefore increase the overall variance of the field.

To generate a random field, we begin with the power spectrum for the dependent variable

h using equation (2), with the variance and correlation scales provided as input. The power spectrum is then discretized, truncated and randomized, and the random field is generated from the randomized discrete spectrum by inverse Fourier transformation. The effect of truncation on the spectrum depends on the shape of the spectrum and the value of the Nyquist frequency (largest frequency of the discrete spectrum). The truncation error is controlled by the input field spacing which dictates the magnitude of the Nyquist frequency as shown in the formula below

$$f_{N_j} = \frac{1}{2\Delta X_j} \tag{3}$$

where f_{Nj} is the Nyquist frequency and ΔX_j is the nodal spacing in the j direction (j =1,2,3). Since the Nyquist frequency is the cut off point for the spectrum, a flat power spectrum with a wide base could lose a significant amount of variance (integrated spectrum) if too large a nodal spacing was chosen.

Similarly, the spectral discretization error is affected by the frequency spacing, which is controlled by the size of the field:

$$\Delta f_j = \frac{1}{L_j} = \frac{1}{2N_j\Delta X_j} \tag{4}$$

where Δf_j is the frequency spacing, L_j is the field length and N_j is the number of nodes in the j direction (j = 1, 2, 3). A tall, thin power spectrum could be inaccurately represented if too large a frequency spacing was chosen (for instance, a spacing of the same order as the thickness of the power spectrum). Since N_j and ΔX_j are input functions set by the

user, a trial and error method is used to clamp the discretization and truncation errors within acceptable limits. See *Robin et al. [1993]* for further details.

METHOD

Rather than simply trying to echo given aquifer characteristics in generated random fields, the problem is studied from another perspective: instead of answering the question "What changes to the power spectrum are needed to reproduce this specific aquifer?", we attempt to answer "How will different changes to the power spectrum affect the generated field?". This new perspective provides a recipe for reproducing specific field situations in random fields.

Because the Random Field Generator (RFG) produces a power spectrum defined in three-dimensions, yet field measurements generally produce orthogonal one-dimensional power spectra, one cannot simply plug the field power spectral densities (PSDs) into the RFG. The original RFG code allows the user to specify the basic shape of the power spectrum (either a bell-shaped or an exponentially decaying curve); here the code is altered so that the user can modify the input PSD to mirror that seen in the measured PSD.

The base-case model for the power spectrum is an exponentially decaying function, which is based on field measurements at C.F.B. Borden (*Robin et al. [1991]*). This base model was modified by increasing the power at different frequencies or frequency intervals, in effect, a spike was added to the PSD. By changing the physical characteristics of this

spike (i.e. position, height, shape), its effect on the generated field was studied.

The reason for selecting this type of modification to the power spectrum was thus: in the second section of the research, the effect of periodic sedimentary facies on the dispersive process was investigated, and by studying how the addition of a spike to the PSD changed the random field, the desired form of the periodicity was determined.

The first step in determining the effect of a spike in the power spectrum on the field involved investigating the one-dimensional case. Subsequently fields in two and three dimensions were studied. The effects of three variables were investigated: i) the spike height, ii) the spike position, and iii) the spike shape.

Table I displays the input variables that remain constant for each of the one-, two- and three-dimensional simulations. Because the full field is periodic (the period in each

Table I: Input parameters common to all simulations.

Number of dimensions	Nodal dimensions (x,y,z)	Nodal dims (truncated field) (x,y,z)	Mean (h)	Variance (h)	Correlation scales (x,y,z) (m)
1	(64,1,1)	(49,1,1)	8.3	0.3	(1.5,-,-)
2	(64,32,1)	(49,25,1)	8.3	0.3	(1.5,2,-)
3	(64,32,32)	(49,25,25)	8.3	0.3	(1.5,2,1)

Random number generator seed for all simulations was -8.

direction equals the field size in that direction), it must be truncated by one or two correlation lengths in order to eliminate the periodicity *[Robin et al. 1993]*.

RESULTS AND DISCUSSION

Effect of spike height

Figure 1 shows the base case one-dimensional power spectrum with the added spikes, and the resulting fields. (The figures are given at the end of each chapter). The spike height was varied from 0.2 to 0.8 compared to a maximum spectral density in the original spectrum of 0.9. As the spike height was increased, an increase in field variability was observed because the area under the power spectrum is equal to the variance of the field. Because the same random number generator seed was used for the cases presented in Figure 1, the effect of increasing the spike height was simply to amplify the perturbations. The increase in variability occurred at small scales because the spike was located at high frequencies. In the two and three-dimensional cases, the same increase in variability was observed. It is interesting to note that a large enough spike could produce sufficient noise to mask the original field characteristics.

Effect of spike position

The height of the spike in the one-dimensional power spectrum was kept constant at 0.8 and a constant width of one frequency increment was used, while the position of the spike was varied from frequency 0.5625 to 0.9375. As the spike was moved closer to the Nyquist (highest) frequency, the resulting peaks in the field appeared closer together (see

Figure 2). Notice that for a spike at frequency 0.5625 (wavelength 1/0.56 = 1.79 m), the peaks are located about 2 m apart and for frequency 0.9375 (wavelength 1/0.94 = 1.06 m), the peaks are approximately 1 m apart. This demonstrates that the addition of a region of higher power in the PSD (i.e. a spike) introduces periodicity in the generated field at a scale specified by the position of the spike in the power spectrum.

The base-case field for the two-dimensional case is shown as Figure 3. It was generated according to the parameters outlined in Table I.

To examine the effects of the spike position, first a spike with a rectangular footprint measuring 0.05 x 0.1 frequency units was inserted into the power spectrum and moved along each axis. The value, or height of the spike was 100 for the two-dimensional simulations, in order to dwarf the original spectrum and isolate the effects of the spike position and shape. The effects are best visualized by looking at transects rather than the entire field since categorizing the data for two-dimensional viewing causes small changes in the field values to be lost. Transect AB cuts the field along the x-axis at node 1 while transect AC cuts the field along the y-axis at the same node.

Figure 4a) shows that there is an increase in small-scale variability in the x-direction (the x-length of the lenses shortens) as the spike is moved from the origin to the x-Nyquist frequency. There is no change, however, in the y-length of the lenses (Fig. 4b). Similarly, as the spike is moved from the origin to the y-Nyquist frequency, small-scale

variability in the y-direction is increased but there is no change in the x-direction lenses.

Second, a spike was used with a footprint extending the entire length of the spectrum (as in a band or a stripe) in one direction and then in the other. When a y-direction stripe was at x = 0, the lenses stretch horizontally across the entire field. These horizontal lenses are a result of the increase in variability in the x-direction at frequency zero. As the stripe is moved to increasingly positive x values, the x-length of the lenses decreases because of the increased high-frequency component of the power spectrum, but the lenses preserve their orientation. When an x-direction stripe is used the effects are equivalent (but in the other direction).

When specifying a spike location in the input array of the RFG, one must consider the symmetry properties of the power spectrum. The power spectrum of a real variable is an even function, that is, $S_{hh}(f) = S_{hh}(-f)$ (in n dimensions, f is an n-dimensional vector (n = 1, 2, 3)). The RFG exploits this property by calculating only half of the theoretical input spectrum and packing the other half using the symmetry properties. Therefore, when introducing a spike in the spectrum, the RFG packing routine automatically introduces a second spike at the symmetry location. The process is illustrated in Figure 5 for a two-dimensional spectrum.

The effect of introducing a spike in only one quadrant of the spectrum (as in Figure 5b) is illustrated in Figure 6, which shows the full spectrum and resulting fields for an input

spectrum with an x-direction stripe in quadrant I. The resulting packed array has stripes in quadrants I and III. For a stripe located at $y \neq 0$ the resulting field has sloping lenses. A horizontal stripe in quadrants I and III induces a positive slope in the orientation of the lenses in the field (Figure 6a). A horizontal stripe in quadrants II and IV produces a negative slope in the orientation of the lenses. As the stripe is moved closer to the origin, the slope of the lenses becomes steeper and the y-length of the lenses increases as a result of the increase in variability produced by the lower frequency component of the spectrum. When the stripe is located at $y = 0$, the resulting field displays lenses that stretch vertically across the entire field (Figure 6b). This is indicative of the increase in variability at frequency zero (wavelength approaching infinity). The x-length of the lenses do not change significantly as the stripe is shifted, since the range of x-coordinates of the stripe do not change over the series of simulations.

It is the discontinuity in the x-direction stripe in the packed array which causes the lenses to have an orientation other than horizontal. Because of the packing routine used by the RFG, the smaller the discontinuity in the full spectrum, the larger the discontinuity in the packed array, and the steeper the slope of the lenses in the field. The direction of the discontinuity governs the direction of the slope: a step up in the full spectrum (from left to right) produces positively sloped lenses while a step down produces lenses with negative slopes.

The third type of spike that was investigated had a square footprint measuring a unitless

0.1 x 0.1. This spike was moved off the axes and it was determined that the x-and y-lengths of the lenses was controlled by the x- and y-coordinates of the spike: the closer the spike to the x-Nyquist frequency, the shorter the x-length of the lenses, and similarly for the y direction. Because the spike is located in quadrant I or IV of the input spectrum (producing an asymmetrical full spectrum), the lenses are sloped either positively or negatively as outlined in the previous paragraphs. The addition of two symmetrical spikes, one in each of quadrants I and IV of the input spectrum, affects the x- and y-lengths of the lenses but not their slopes (since the full power spectrum is symmetrical).

Just as in the two-dimensional case, in three dimensions the RFG calculates power spectrum values for only half of the full spectrum (i.e. four of the eight octants), and exploits the symmetry properties of the power spectrum to pack the full array. In this case, four symmetrical spikes are required (one in each of the four input octants) to produce a symmetrical spectrum. The effects produced are equivalent to the two-dimensional case but are more difficult to visualize.

Effect of spike shape

To study the effect of the spike shape (or width, in one dimension), a spike was centred at frequency 0.8 (wavelength 1/0.8) in the one-dimensional power spectrum and its width was varied from a single frequency increment to almost one third of the spectrum range. Because the spike height was kept constant, an increase in width caused the area under the spectrum to increase also. This in turn led to an increase in field variability. As the

spike width increased, there was more variability over a wider range of scales (as shown by the varying distance between peaks in the field). This was caused by the higher and lower frequency components of the power spectrum. Figure 7 illustrates these observations for a spike of height 0.8.

In the two-dimensional simulations, the stripes studied in the previous section were shortened to study the effect of a change in the spike shape. As the y-direction stripe in the spectrum was shortened, there was a decrease in variability over the entire field. Figure 8 shows transects of fields generated using spikes with two different shapes. Along transect AC (y-direction) a reduction in small-scale variability (high frequency noise) occurs due to the removal of the high-frequency component of the stripe in the y-direction. Because the stripe is located at x-frequency=zero, a reduction in large-scale variability (low frequency as opposed to high frequency noise) occurs along transect AB (x-direction). As the x-direction stripe in the spectrum is shortened similar effects are observed.

Along the transect oriented in the same direction as the stripe (x-direction in this case), a reduction in high-frequency noise is noted as the stripe is shortened. The effects on the transect perpendicular to the stripe depend on the position of the stripe in the power spectrum (in this case, because the stripe is located at high y-frequencies, there is a reduction in high frequency noise in the y-direction).

Two spikes were added to the power spectrum at different locations, and effects of both spikes were incorporated into the resulting field. Both sets of x- and y- frequency ranges affect the dimensions of the lenses. For example, Figure 9 shows that a spectrum with one spike at high x and low y frequencies and a second spike at low x and high y frequencies produces three shapes of lenses: i) large x-length, small y-length, ii) small x-length, large y-length, and iii) small x-length, small y-length. The fourth possible permutation (large x-length, large y-length) is not observed.

Three-dimensional simulations produce the same results as discussed in one-and two-dimensions, however the results are not as easily seen due to the difficulty of viewing fields in three-dimensions.

SUMMARY AND CONCLUSIONS

An increase in the height of the spike in the power spectrum increases field variability. The scale at which the variability increase occurs depends on the position of the spike. A spike located near the origin in the power spectrum increases the low-frequency (or large-scale) noise, while a spike located near the Nyquist frequency increases the high-frequency (or small-scale) noise. The scale of periodicity (i.e. wavelength) of the generated field is controlled by the position of the spike.

The shape of the spike also affects the frequency of the noise. A spike with a narrow base covering only a few frequency increments produces field variability at a single scale and

noticeable periodicity between the high and low valued areas of the field. Variability over a wider range of scales is produced by spikes with a wider base spanning several frequency increments. It is more difficult to see the periodicity in this case since a wider range of frequency scales for the spike produces periodicity at several wavelengths.

An input stripe in the x-direction in opposite quadrants of the spectrum affects the orientation of the lenses. The closer the stripes to the Nyquist frequency, the shallower the slope of the lenses, while the closer the stripes to the origin, the steeper the slope of the lenses. Stripes located in quadrants I and III produce positively sloped lenses while stripes in quadrants II and IV result in lenses with negative slopes.

This portion of the research provides a recipe for reproducing specific aquifer characteristics in a random field, by using properties of the power spectrum. The addition of one or more spikes to the power spectrum can affect the shape and orientation of the lenses in the simulated field as well as introduce periodicity between high- and low-valued lenses. The ability to control the orientation of the lenses can be useful when attempting to model a field situation where the geological formation has been subjected to uplift and the lenses are no longer horizontal.

REFERENCES

Brigham, E.O., 1989, *The fast Fourier transform and its applications*, Prentice Hall,

Englewood Cliffs, New Jersey, 448 p.

Black, T.C., and Freyberg, D.L., 1987, Stochastic modelling of vertically averaged concentration uncertainty in a perfectly stratified aquifer, *Water Resources Research*, 23(6), p. 997-1004.

Frind, E.O., Sudicky, E.A., and Schellenberg, S.L., 1987, Micro-scale modelling in the study of plume evolution in heterogeneous media, *Stochastic Hydrol.*, 1, p. 241-262.

Gelhar, L.W., and Axness, C.L., 1983, Three-dimensional stochastic analysis of macrodispersion in aquifers, *Water Resources Research*, 19(1), p. 161-180.

Massman, J., and Freeze, R.E., 1987a, Groundwater contamination from waste management sites: The interaction between risk-based engineering and regulatory policy, 1, Methodology, *Water Resources Research*, 23(2), p. 351-367.

Massman, J., and Freeze, R.E., 1987b, Groundwater contamination from waste management sites: The interaction between risk-based engineering and regulatory policy, 2, Results, *Water Resources Research*, 23(2), p. 368-380.

Robin, M.J.L., Gutjahr, A.L., Sudicky, E.A., and Wilson, J.L., 1993, Cross-correlated random field generation with the direct Fourier transform method, *Water Resources Research*, 29(7), p. 2385-2397.

Robin, M.J.L., E.A. Sudicky, R.W. Gillham and R.G. Kachanoski, Spatial variability of strontium distribution coefficients and their correlation with hydraulic conductivity in the Canadian Forces Base Borden aquifer, *Water Resources Research*, 27(10), 2619-2632, 1991.

Sudicky, E.A., Schellenberg, S.L., and MacQuarrie, K.T.B., 1990, *Assessment of the behaviour of conservative and biodegradable solutes in porous media*, (J. H. Cushman, editor), Academic Press, p. 429-461.

Thompson, A.F.B., and Gelhar, L.W., 1990, Numerical simulation of solute transport in three-dimensional, randomly heterogeneous porous media, *Water Resources Research*, 26(10), p. 2541-2562.

Vomvoris, E.G., and Gelhar, L.W., 1990, Stochastic analysis of the concentration variability in a three-dimensional heterogeneous aquifer, *Water Resources Research*, 26(10), p. 2591-2602.

Wagner, B.J., and Gorelick, S.M., 1987, Optimal groundwater quality management under parameter uncertainty, *Water Resources Research*, 23(7), p. 1162-1174.

Wagner, B.J., and Gorelick, S.M., 1989, Reliable aquifer remediation in the presence of spatially varying hydraulic conductivity: From data to design, *Water Resources Research*, 24(4), p. 566-578.

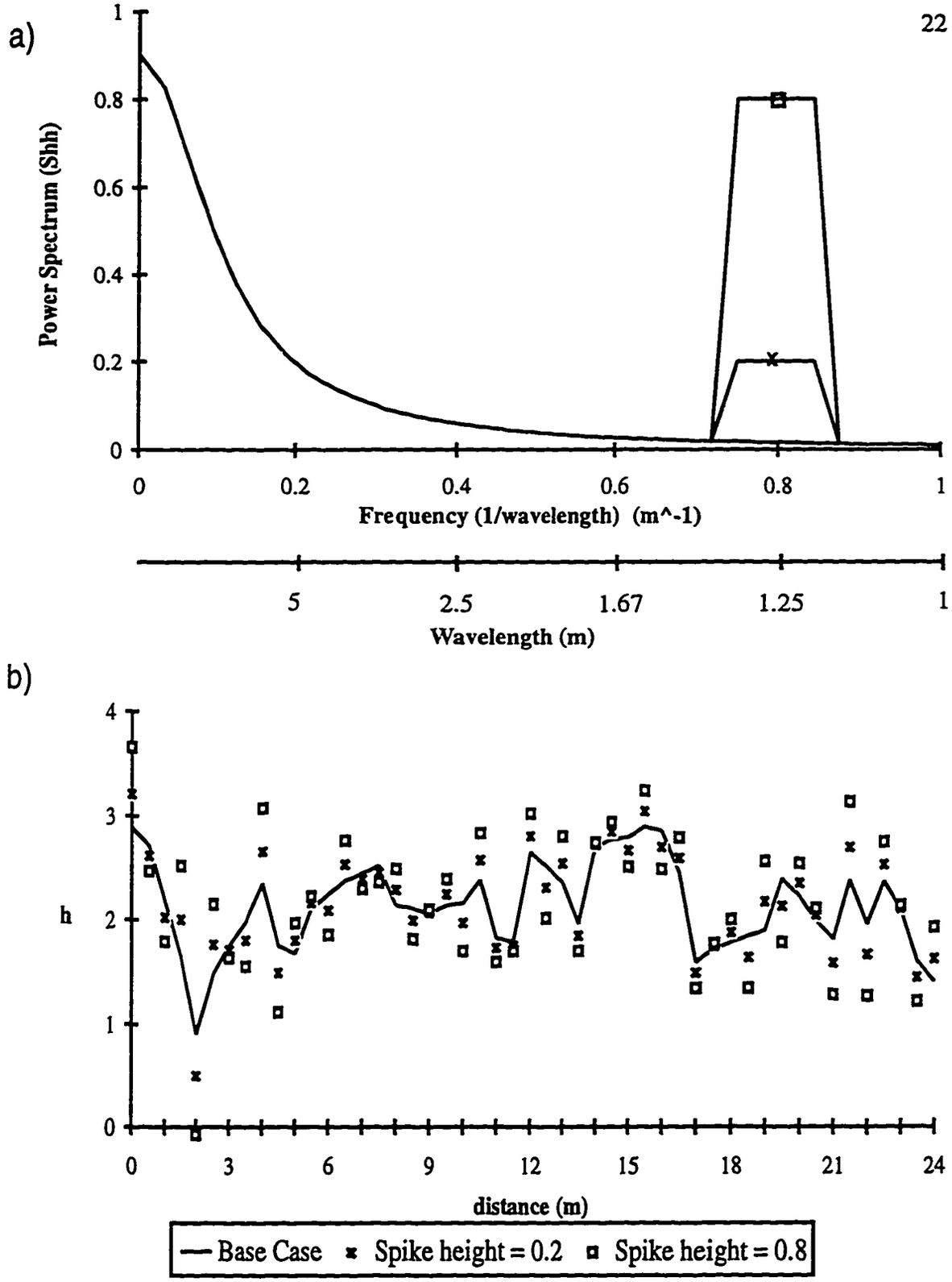

Figure 1: Random fields (b) generated from spiked power spectra (a). Increased spike height produces increased variability. Note that only the pertubation magnitude is affected because the same random number seed was used for each spectrum.

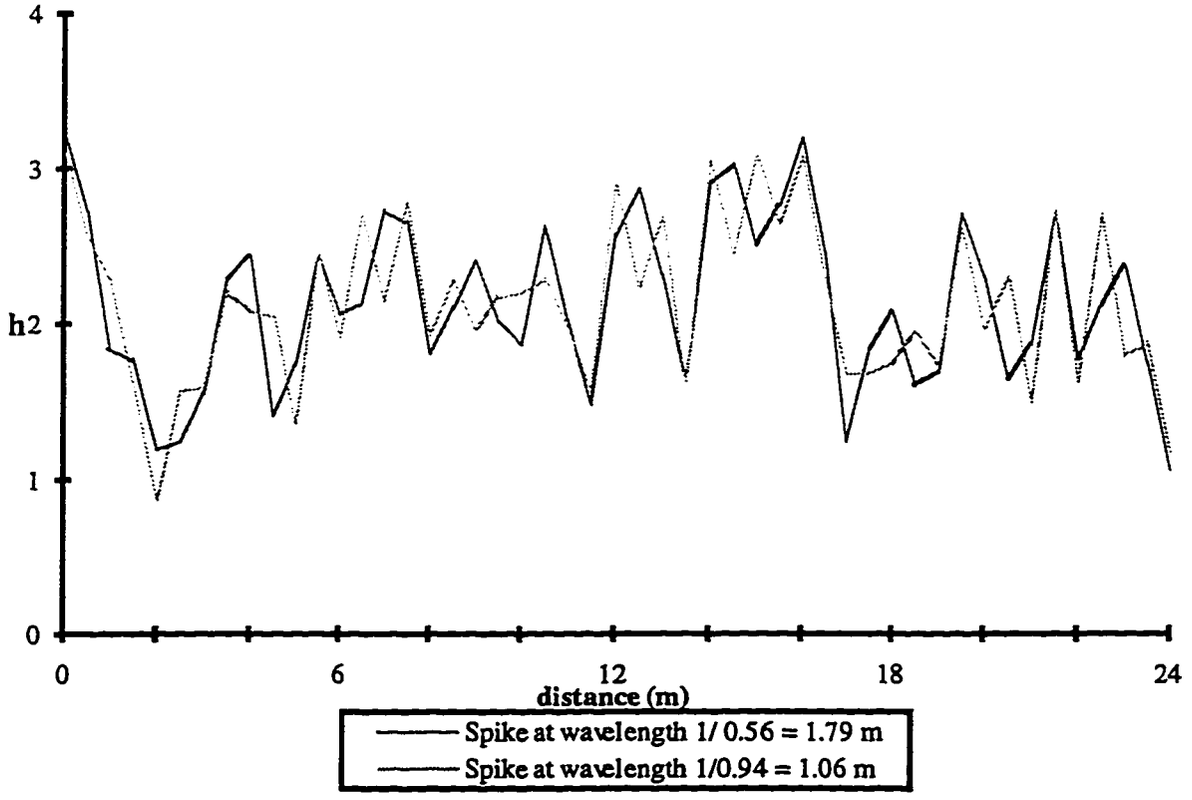

Figure 2: Random fields generated from spiked one-dimensional power spectra. The closer the spike to the Nyquist frequency, the closer together the peaks in the field (an increase in variability at small scales).

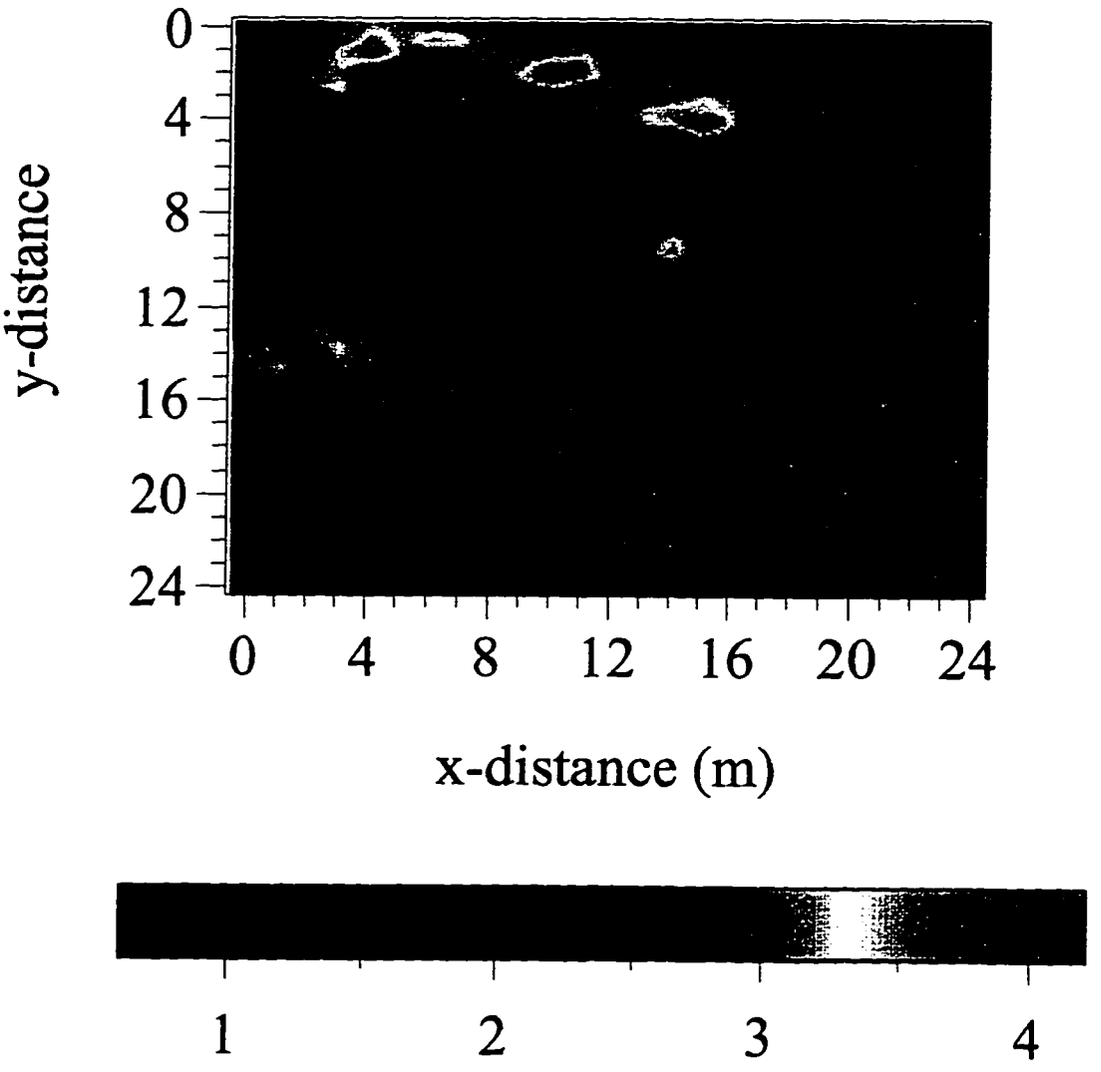

Figure 3: Base case field of (unitless) dependent variable for two-dimensional simulations

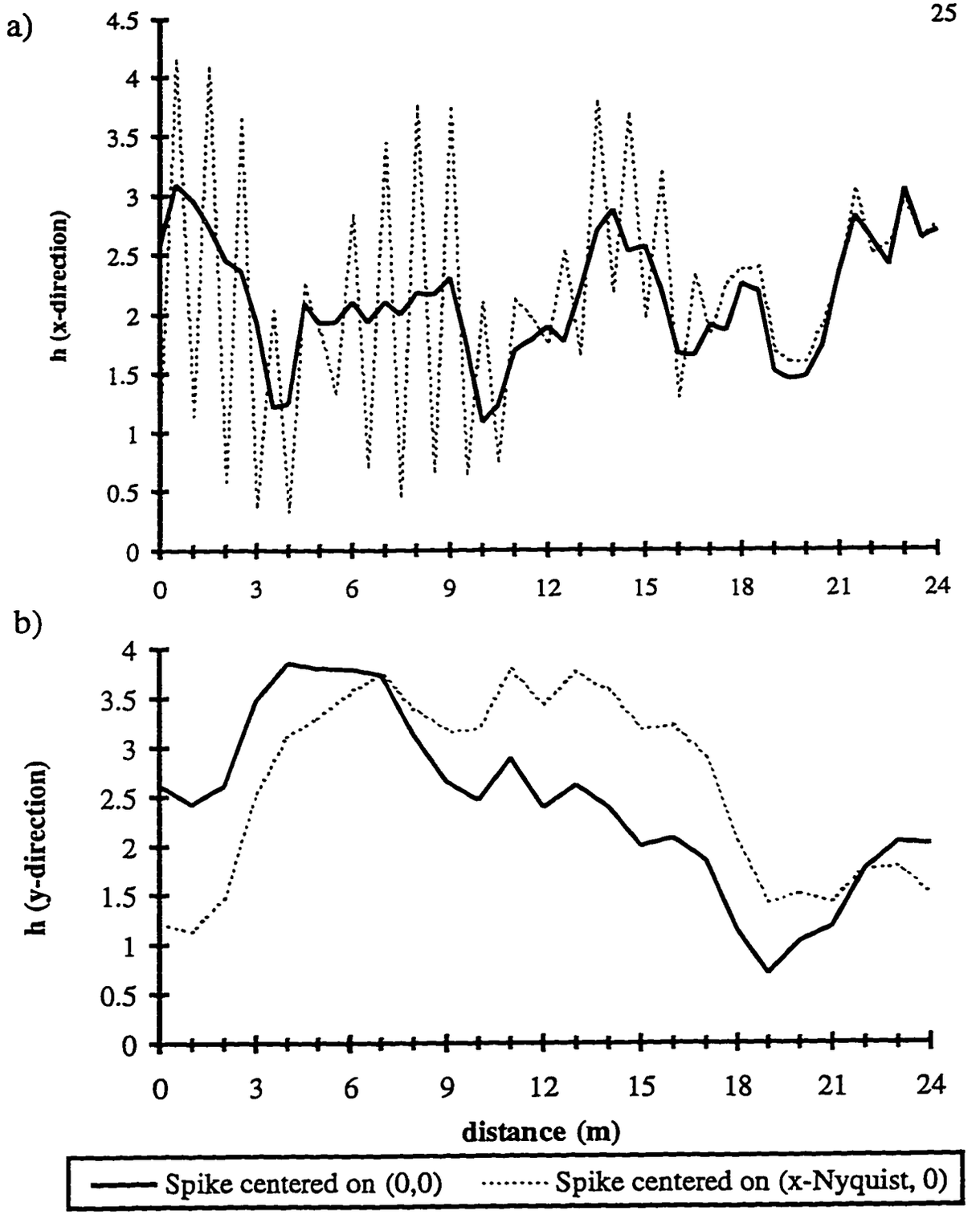

Figure 4: Transects from two-dimensional fields. X-direction transects (a) show increased variability at small scales as spike is moved from (0,0) towards (x-Nyquist, 0). Y-direction transects (b) show no change in variability since y coordinates of spike do not change.

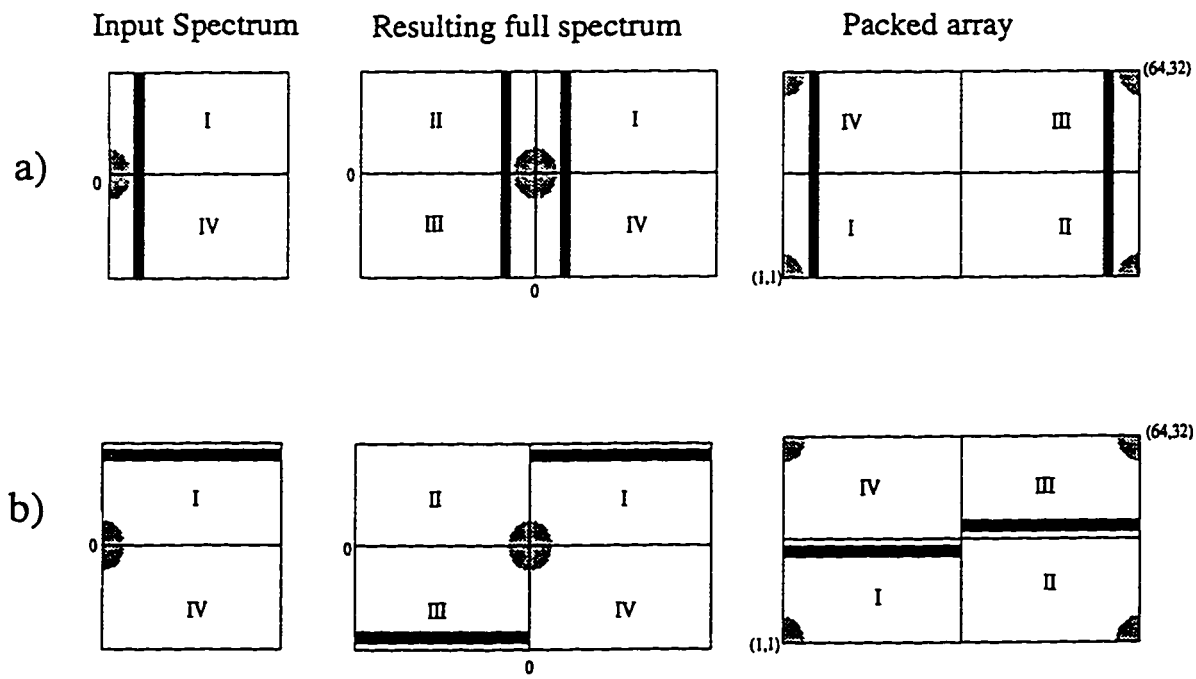

Figure 5: Example of symmetry properties used by RFG packing routine for a) a vertical stripe and b) a partial horizontal stripe

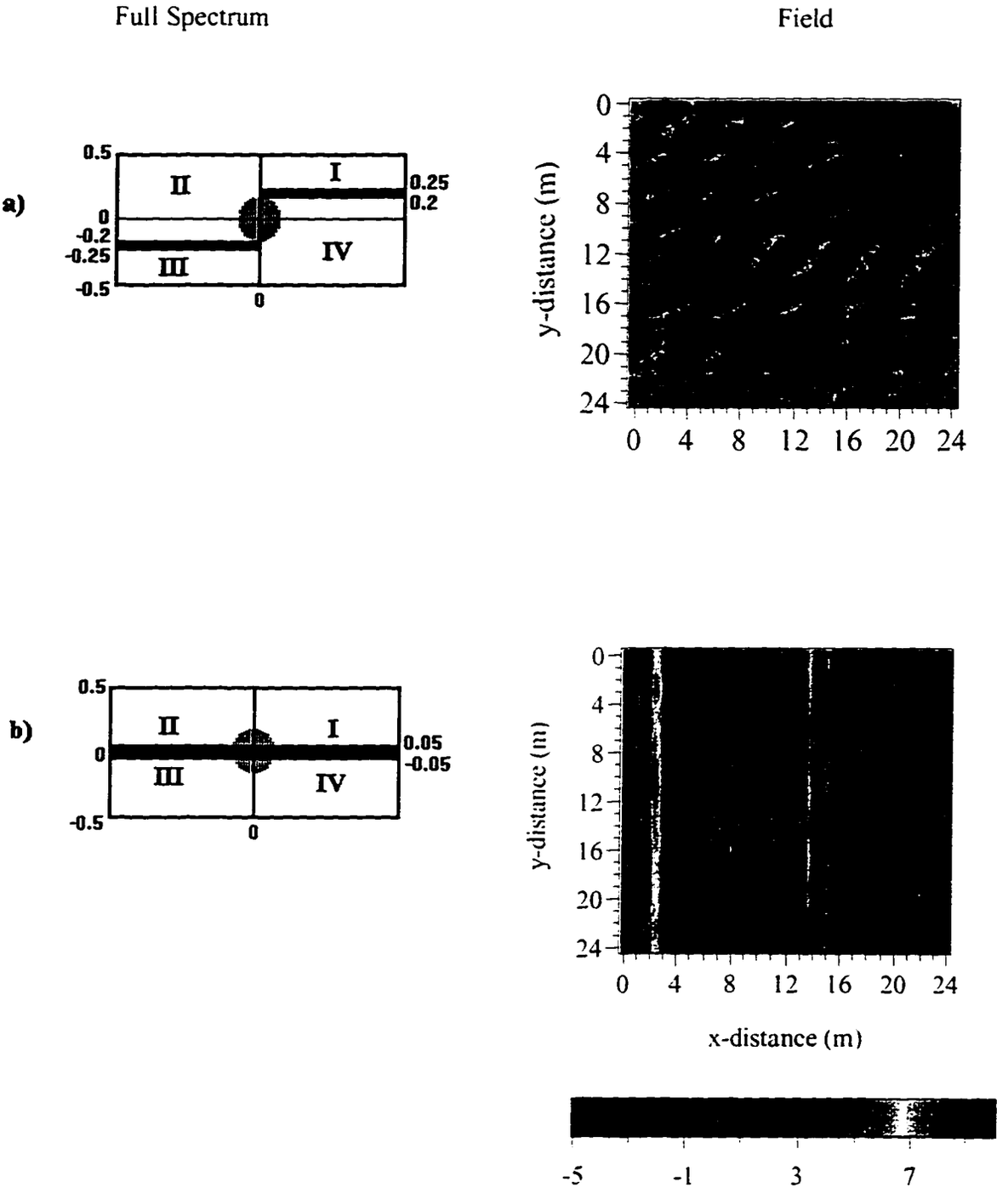

Figure 6: Power spectra and resulting fields for horizontal stripes in the power spectrum. A stripe with a step up (a) produces lenses with positive slopes. A continuous stripe at y=0 (b) increases variability in the y-direction at infinitely large scales.

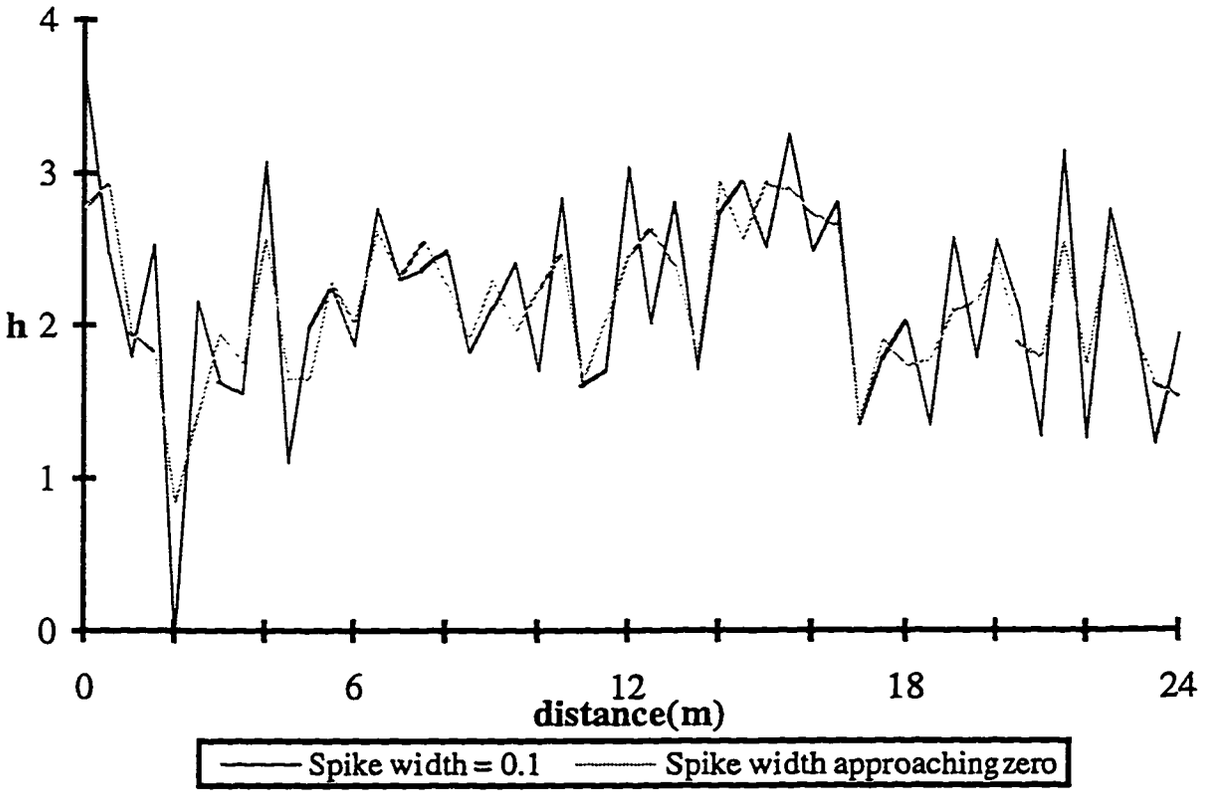

Figure 7: Random fields generated from one-dimensional power spectra with spike centered on frequency 0.8. Increased spike width causes increased variability over a wider range of scales.

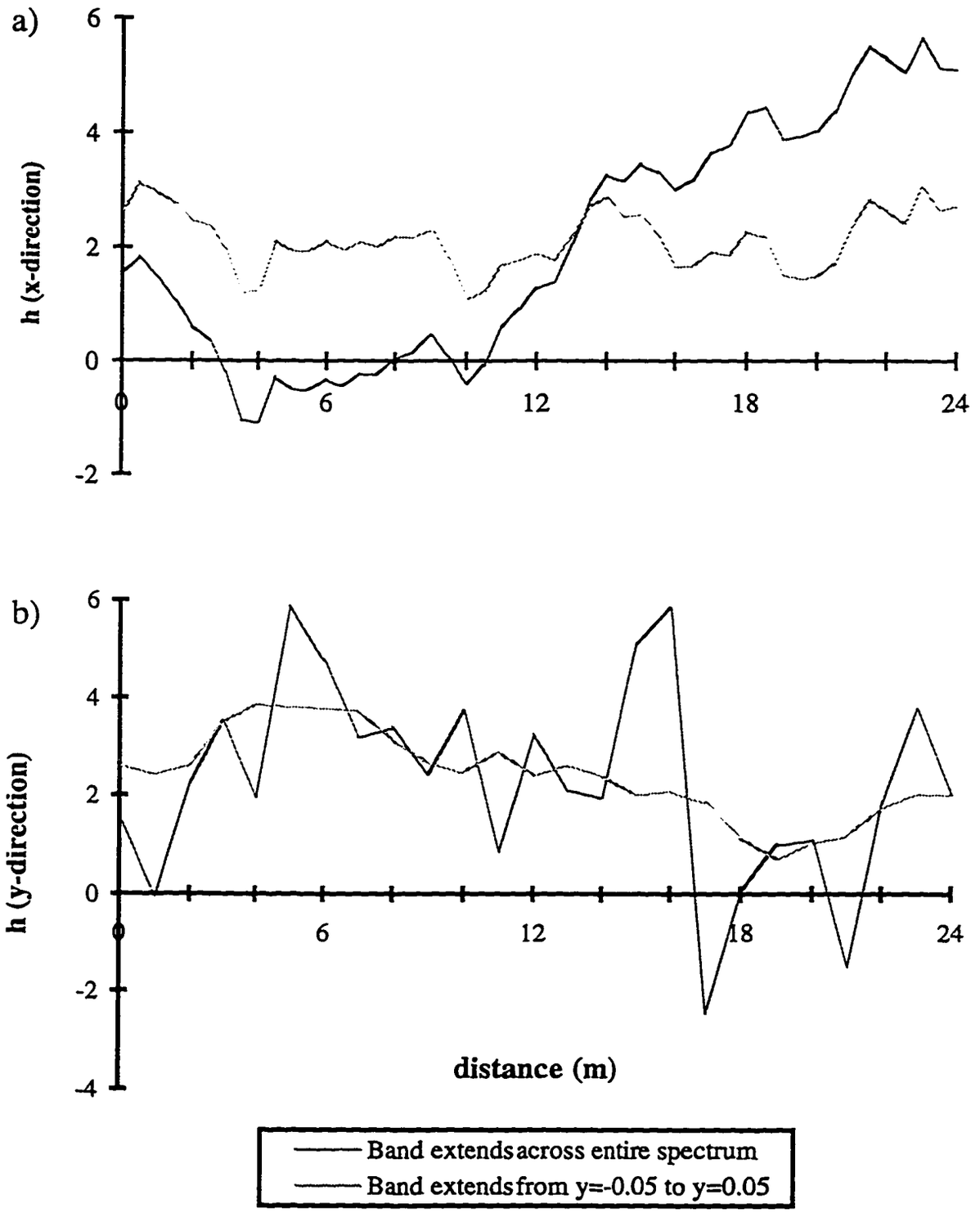

Figure 8: Transects of two-dimensional random fields. Removal of high-frequency component of stripe in spectrum causes a reduction in low-frequency noise in x-direction (a) and a reduction in high-frequency noise in y-direction (b).

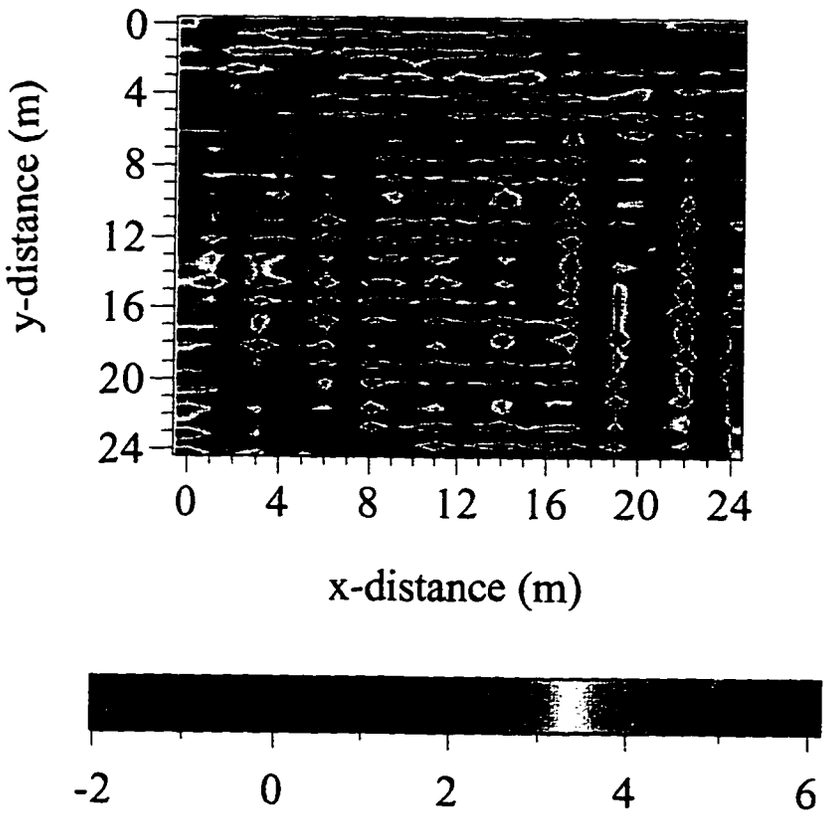

Figure 9: Random field resulting from two spikes in the input spectrum. Dimensions of lenses are controlled by position of spikes. Because spikes are located at both high and low x-frequencies, lenses with both small and large x-lengths are observed. Similar observations can be made for the y-direction.

CHAPTER 3

The Effect of Spatial Statistics of the Hydraulic Conductivity and Distribution Coefficient Fields on Solute Transport in 3-dimensional Heterogeneous Porous Media

ABSTRACT

The purpose of this study is to determine the effect of the relationship between the velocity of the fluid and the degree of reactivity between the contaminant and the porous media on the behaviour of the contaminant plume. The study also investigates the effect of the type of self-correlation within the velocity and reactivity fields, on the plume. Computer simulations of contaminant transport in three-dimensional saturated, heterogeneous porous media are performed. The effects of the type of autocorrelation and cross-correlation on plume behaviour are examined with a limited number of Monte-Carlo simulations in a factorial-design numerical experiment. The output from the simulations is used to measure the mass of contaminant in solution, the macroscopic plume velocity, and the macrodispersivity (a measure of the rate of spatial spreading). The results showed that the addition of a positive correlation between velocity and retardation at scales greater than 1 metre to otherwise negatively correlated fields inhibits the movement of the center of mass and increases the retardation coefficient. A small negative correlation between groundwater velocity and retardation increases longitudinal macrodispersivity, but a positive correlation decreases macrodispersivity. The effect of autocorrelation is to enhance longitudinal macrodispersivity for fields with fine, periodic stratification as opposed to fields with

a coarser stratification and no periodicity. Transverse macrodispersivities are not sensitive to changes to the correlation within fields, or the correlation between velocity and retardation fields.

INTRODUCTION

Computer simulation of contaminant transport is a popular and cost-effective method of predicting the impact of solutes in groundwater systems. The work of hydrogeologists who model the development of contaminant plumes is valuable since simulations provide an arguably accurate assessment of plume behaviour; and remediation techniques and field experiments are comparatively expensive. Perhaps the most valuable aspect of computer modelling, however, is in evaluating the sensitivity of the system to input parameters and to different scenarios. This study evaluates the effects on the dispersion process of the spatial statistics of two important parameters, the hydraulic conductivity, K and the distribution coefficient, K_d; and it examines the effects of possible correlations between K and K_d.

The approach used here is to perform computer simulations of solute transport in highly detailed fields of K and K_d with prescribed statistical properties and to examine the effect of the prescribed statistic on the large-scale behaviour of the plume. The macro-scale parameters resulting from the simulations are then examined using factorial-design Analysis of Variance (ANOVA) procedures, thereby allowing conclusions to be drawn from a very limited number of Monte-Carlo realizations.

In recent years, it has been shown that an increase in the degree of non-linearity of the sorption isotherm increases plume spreading and tail formation *(Thompson [1993])*, an increase in physical heterogeneity enhances transverse spreading more than longitudinal spreading *(Zang and Chi [1995])* and increasing the chemical heterogeneity (increasing the K_d variance) has no effect on plume dispersion *(Bosma et al. [1996])*.

The effect of the type of correlation between velocity and retardation on plume dispersion has also been examined. *Robin [1991]* found that a weak cross-correlation between K and K_d could not produce enhanced mixing for a reactive solute. *Haley et al. [1994]* performed Monte-Carlo simulations to determine the effect of the type and degree of cross-correlation between K and K_d on dispersion. For a reactive solute, a negative correlation between K and K_d produced enhanced longitudinal mixing. Both *Robin* and *Haley* used correlation scales on the order of tens of centimetres in the horizontal directions and a few centimetres in the vertical direction, with linear cross-spectra.

The scenarios studied here are combinations of one of three types of autocorrelation and one of three types of cross-correlation. The types of autocorrelation studied are: 1) correlation lengths of 20 cm; 2) correlation lengths of 20 cm with increased small-scale periodicity; and 3) correlation lengths of 7 cm. The types of cross-correlation studied are: 1) small negative cross-correlation; 2) small negative cross-correlation at small scales with positive cross-correlation at scales larger than 1 m; and 3) perfect

positive correlation at all scales. The cross-spectrum model is non-linear and based on the power spectra of both the K and K_d fields. The cross-spectrum model is elaborated in the section entitled "Method". The resulting nine combinations of auto and cross-correlation (scenarios) were examined using the standard statistical tools of Analysis of Variance (ANOVA).

The first cross-correlation scenario (small negative correlation at all scales) was selected to represent the behaviour of a positively charged contaminant sorbing onto negatively charged sites. Intuitively, one would expect zones of high affinity (and high retardation), such as fine-textured materials, to be associated with zones of low permeability, giving a negative correlation. *Haley et al. [1994]* have shown that a negative correlation will produce significantly enhanced dispersions of the reactive tracer plume. However, it is not clear whether the strength, or coherency, of the correlation plays a role. For instance, it is not clear if a weak correlation such as the one observed by *Robin et al. [1991]* at the Canada Forces Base, Borden site in Ontario, Canada for strontium, will also produce significant mixing.

The second cross-correlation scenario is based on the observation of *Robin et al. [1991]* at C. F. B. Borden. They observed a small but significant negative correlation (regions of high velocity corresponding to regions of low retardation) at all scales except at large scales, where the cross-correlation was positive. This large-scale positive correlation, however, could not be shown to be significant. The large-scale trends (on the order of several metres) could be due to larger scale depositional

features. The question we attempt to answer here is: "how will the addition of large-scale positive correlation to an otherwise weak negative correlation affect the dispersive behaviour of the reactive contaminant plume?".

The last cross-correlation scenario studied (7 cm correlation lengths and perfect positive correlation between velocity and retardation) was chosen to correspond to the findings of a field study performed by *Halket et al. [submitted 1996]*, which measured K and K_d values for perchloroethene on two cores at C. F. B. Borden. *Halket* separated the cores into very small samples that did not cross sedimentary facies boundaries. This method provided lab measurements of K and K_d for relatively homogeneous segments of the cores. The auto and cross-correlation functions were calculated, as well as the power spectrum and cross-spectrum in order to investigate the correlation between K, K_d and sedimentary facies in the Borden aquifer. They found a perfect positive correlation between velocity and retardation, and an autocorrelation structure with correlation lengths of approximately 7 cm.

The range of cross-correlation scenarios covered in this study is based on a mildly heterogeneous aquifer: C. F. B. Borden. It is expected that in more highly heterogeneous aquifers (such as the Columbus, Mississippi site mentioned in *Gelhar et al., 1992]*), the effects on dispersion of the cross-correlation scenario will be amplified.

METHOD

The Advection-Dispersion Equation (ADE) was used to solve the solute transport problem:

$$R\frac{\partial(\epsilon c)}{\partial t} + \nabla\cdot(\epsilon c\vec{v}) - \nabla\cdot(\epsilon D_{ij}\cdot\nabla c) = 0 \qquad (1)$$

where R is the retardation coefficient, ε is the porosity, $c(\vec{x},t)$ is the solute concentration, t is the time, $\vec{v}=(v_1, v_2, v_3)$ is the average linear porewater velocity, and D_{ij} is the local dispersion tensor:

$$D_{ij} = (\alpha_T|\vec{v}| + D_d) + (\alpha_L - \alpha_T)\frac{v_i v_j}{|\vec{v}|}, \qquad i, j = 1, 2, 3 \qquad (2)$$

where α_L and α_T are the longitudinal and transverse local dispersivities, and D_d is the effective diffusion coefficient in the porous media.

For a solute undergoing linear sorption, the retardation coefficient in (1) is given by

$$R(x,y,z) = 1 + \frac{\rho_b}{\epsilon} K_d(x,y,z) \qquad (3)$$

where ρ_b is the bulk density, and $K_d(x,y,z)$ is a random but spatially correlated distribution coefficient for the solute in question.

The velocity field, $\vec{v}$, is characterized by the hydraulic conductivity field ($K(x,y,z)$) of

the porous medium, which is also random yet spatially correlated:

$$\vec{v} = -\frac{[K]\ \nabla h}{\epsilon} \qquad (4)$$

where h is the hydraulic head. An increase in K at node (x,y,z) results in an increase in $\vec{v}$ at the same node. Similarily, an increase in K_d results in an increase in R. Another way by which R can be obtained is from the ratio of the non-reactive solute plume to the reactive solute plume velocities. If the retardation process is linear, then R is constant. This is so for a homogeneous porous medium at large scales, and locally (at the nodal scale) in this study. However, introducing a cross-correlation between K and K_d, and therefore between the groundwater velocity and the retardation factor may affect the apparent large-scale retardation factor. This is one of the main questions posed by this study. Another important question is whether this cross-correlation will affect the rate of spreading of the plume (as measured by the apparent macroscopic dispersion coefficient).

Cross-correlated random fields were generated according to the spectral technique of *Robin et al. (1993)*. Because K and K_d were assumed to be log-normally distributed, the Random Field Generator (RFG) generated log-hydraulic conductivities and log-distribution coefficients for each node in the field. Each pair of fields was generated using a different seed for the pseudo-random number generator, and different auto- and cross-correlation properties. The RFG initially produced two fields of perturbations about zero, $f(x)$ and $g(x)$, with variances σ^2_f and σ^2_g. Subsequently, the

specified input means (F and G) were added to the perturbations:

$$\begin{aligned} \ln(K) &= F + f(x) \\ \ln(K_d) &= G + g(x) \end{aligned} \tag{5}$$

An exponentially decaying autocovariance function (6) describes the correlation

$$R_{ii}(\xi) = \sigma_i^2 \exp\left\{ - \left\{ \frac{\xi_1^2}{\lambda_{i1}^2} + \frac{\xi_2^2}{\lambda_{i2}^2} + \frac{\xi_3^2}{\lambda_{i3}^2} \right\}^{\frac{1}{2}} \right\} \qquad i = h,g \tag{6}$$

within each field i, where ξ is the lag vector, and λ_{ij} are the correlation scales in the j direction. The corresponding power spectral density function (power spectrum) is defined by (7), where $f = (f_1, f_2, f_3)$ is the frequency vector.

$$S_{ii}(f) = \frac{(2\pi)^3 \ \sigma_i^2 \ \lambda_{i1} \ \lambda_{i2} \ \lambda_{i3}}{\pi^2 \left\{1 + (2\pi f_1 \lambda_{i1})^2 + (2\pi f_2 \lambda_{i2})^2 + (2\pi f_3 \lambda_{i3})^2\right\}^2} \qquad i = h,g \tag{7}$$

The correlation between fields is defined by the cross-spectrum:

$$S_{hg}(f) = \pm\left\{C_{hg}^2(f) \ S_{hh}(f) \ S_{gg}(f)\right\}^{1/2} \tag{8}$$

In equation (8), $C^2_{hg}(f)$ is the squared coherency spectrum, which can be thought of as the correlation coefficient between the random coefficients of the components in $S_{hh}(f)$ and $S_{gg}(f)$. In other words, C^2 is a measure of the degree of correlation between the

two fields ($C^2 = 1$ for perfectly correlated fields, and $C^2 = 0$ for uncorrelated fields). For this research, $C^2_{hg}(f) = C^2$ was assumed constant over all frequencies. For further details, refer to *Robin [1991].*

The flow problem was solved using a finite element program FLOW3D (University of Waterloo). Each element is a parallelepiped (brick-shaped) and thus has eight elemental nodes. Head values at these eight nodes, along with the elemental hydraulic conductivity produced by the RFG, were used to calculate the components of the specific discharge for each element. By dividing the elemental specific discharge by the porosity, the elemental velocity vector $\vec{v}=(v_x, v_y, v_z)$ was obtained, which characterized the flow field. For further details, refer to *Burr et al. (1994)* and *Naff et al. (submitted 1996-1).*

The transport problem was solved using a form of the advection-dispersion equation (ADE) which considers the effects of sorption and intra particle diffusion. By using the Laplace transform of the ADE, the temporal derivative was eliminated and then a finite element technique based on the Galerkin procedure was used to solve for the Laplace-transformed concentrations at each node. The numerical inversion process developed by *de Hoog et al. [1982]* was applied to invert the concentrations from Laplace-space. This technique is referred to as the Laplace Transform Galerkin (LTG) technique and is described in more detail in *Sudicky [1989].*

The RFG generated two cross-correlated fields: ln(K) and ln(K_d). By varying the type

and degree of correlation within and between the fields, it was possible to evaluate the sensitivity of the dispersion behaviour of the contaminant plume to these parameters. The three types of correlation within fields (autocorrelation) and three types of correlation between fields (cross-correlation) described earlier, were compared using a factorial-design numerical experiment. The experimental design is outlined in Table I. Only two replications (reps), or realizations, of each case were performed because the variability associated with the change in seed for the random number generator (i.e. the variance within scenarios) was independent of the correlation scenario and therefore the variability in the measured parameters is expected to be uniform from one scenario to another. The implications of this assumption will be discussed in a later section entitled "Uniformity of variances".

Table I: Monte Carlo scenarios studied

Cross-correlation	**Autocorrelation**		
	λ = (5, 5, 0.2) (m) no periodicity	**λ = (5, 5, 0.2) (m) periodicity (spike at z-frequency (-.05-.05, -.12-.12, 12.0-12.35))**	**λ = (5,5,0.07) (m) no periodicity**
negative correlation C^2=0.1	Case 11: Standard Borden scenario.	Case 12	Case 13
variable correlation C^2=0.1	Case 21: *Robin et al. (1991)*	Case 22	Case 23
positive correlation C^2=1	Case 31	Case 32	Case 33: *Halket et al. (submitted 1996)*

Case 33 is characterized by a perfect positive correlation between velocity and retardation for all directions. As mentioned earlier, this case corresponds to the type of correlation observed by *Halket et al. [submitted 1996]* on a limited number of cores at C.F.B. Borden. Because of the limited number of cores, there was no cross-correlation information available for the longitudinal and transverse horizontal directions; therefore, it was assumed that the perfect positive correlation between velocity and retardation occurred at all scales and in all directions. This assumption is physically plausible and does not compromise the results of these simulations.

Correlation within the fields was controlled by the input correlation lengths and by the shape of the power spectrum. As described in the previous chapter, in order to introduce periodicity in the vertical (z) direction, a spike was added to the input power spectrum in the z direction at high frequencies ($f_z \in (12.0, 12.35)$), and about the origin in the x-and y-directions ($f_x \in (-0.05, 0.05)$ and $f_y \in (-0.12, 0.12)$). The value of the power spectrum in this block was chosen as 6.54 for the ln(K) field and 11.60 for the $\ln(K_d)$ field, such that the integrated spectrum was 25% more than the input variance. In other words, the addition of the spike in the power spectrum increased the variability within the fields by 25%.

Correlation between the fields was controlled by the cross-spectrum model. A positive correlation was obtained by using the positive version of formula (8), while a negative correlation was obtained by the addition of a negative sign before the square root. The variable correlation was produced by the cross-spectrum shown in (9):

$$S_{hg}(f) = \left\{ \begin{array}{ll} 2 * \left\{ C_{hg}^2(f) * S_{hh}(f) * S_{gg}(f) \right\}^{1/2} & , \; 0 < f_z < 1 \\ -\left\{ C_{hg}^2(f) * S_{hh}(f) * S_{gg}(f) \right\}^{1/2} & , \; f_z \geq 1 \;\; all \; f_x, \; f_y \end{array} \right\} \qquad (9)$$

higher positive correlation for frequencies less than 1 (scales larger than 1 metre) in the transverse vertical direction, and negative correlation for all other scales and directions. As mentioned earlier, this type of cross correlation was observed at Borden by *Robin [1991]*; however, the positive correlation at large scales in the vertical direction could not be shown significant at the 95% confidence level.

The generated fields were truncated (1, 1, 3) correlation lengths from the edge in the (x, y, z) directions, respectively. It is necessary to truncate the fields since the random field generator produces fields that are periodic over the entire field (period 1 in each direction) *[Robin et al., 1993]*. If the fields were used without truncation, it would be necessary to consider possible effects of the field scale periodicity in the analysis, which is an artifact of the RFG. This study does consider the effect of periodicity, but at high frequencies (small scales) in the transverse vertical direction only.

The dimensions of the truncated random fields are 30 m x 11 m x 4.4 m (or 50 x 44 x 110 elements), with nodal spacing 0.6 m x 0.25 m x 0.04 m for a total of 254,745 nodes. In the direction of mean groundwater flow (x-direction), an instep node is added between each node for the flow and transport solutions which reduces nodal spacing to 0.3 m in order to meet Peclet criteria, while minimizing hardware memory

requirements. An instep node is a node added in between existing nodes in the random field. It assumes mean ln(K) and ln(K_d) values of the surrounding nodes and its function is to reduce nodal spacing thus reducing oscillation in the flow and transport solutions. *[Naff et al. (submitted 1996-1,2)].*

The source was centred on (3.5, 5.5, 2.25) (m) with dimensions 1 m x 1 m x 0.3 m. The remaining flow parameters are :

Upstream Head = 3.38 m
Downstream Head = 3.2 m
Local Dispersivity (longitudinal) α_L = 0.05 m
Local Dispersivity (transverse) α_T = 0.01 m
Porosity ϵ = 0.35
Bulk Density ρ_b = 1.75 g/cm^3
Diffusion Coefficient D_d = 1.1664x10^{-4} m^2/d

The input mean for K was 5.62 m/day (ln(K) = 1.73) with the ln(K) variance equal to 0.19. The K_d input mean was 0.58 mL/g (ln(K_d) = -0.54) and the ln(K_d) variance was 0.39. The input mean and variance of the log hydraulic conductivity and log distribution coefficient were measured by *Halket et. al [submitted 1996]* for perchloroethene (PCE) at C.F.B Borden.

The physical parameters and flow parameters outlined in the previous paragraphs are common to all cases. The simulations were performed on a Silicon Graphics Crimson Elan, with a 64 bit-processor and 208 megabytes of RAM using a modified version of the code MONTE3D (Waterloo Centre for Groundwater Research). The code was also used by *Haley [1994]* and *Naff et al. [submitted 1996-1,2].* Each realization

used approximately five hours of CPU time.

Calculation of spatial moments

Concentration plumes for six time steps were simulated, and spatial moments up to order two were calculated for each realization according to (10), where $C(x,y,z,t)$ is the concentration field, n is the porosity, and x, y, and z are the spatial coordinates

$$M_{ijk}(t) = \int_{-\infty}^{\infty}\int_{-\infty}^{\infty}\int_{-\infty}^{\infty} n\, C(x,y,z,t)\, x^i y^j z^k \, dx\,dy\,dz \qquad (10)$$

[Freyberg, 1986]. The indices i, j, and k ($i, j, k = 0, 1, 2$) refer to the moment in question; the sum $i + j + k$ indicates the order of the moment, and the respective values of i, j, and k indicates the moment direction (for example, M_{200} refers to the second spatial moment in the x-direction).

Because the spatial moments are obtained from a piecewise integration over the finite elements, the elemental concentrations, $C_e(x,y,z,t)$, were calculated as a weighted sum of the nodal concentrations at each corner of the element

$$C_e(x,y,z,t) = \sum_{n=1}^{8} \phi_n(x,y,z)\; C(x_n,y_n,z_n,t) \qquad (11)$$

where $\phi_n(x,y,z)$ are shape functions as described in *Desai and Abel [1972, Table 5-1]* and (x_n,y_n,z_n) is a nodal location of element e. The raw elemental moment calculations consisted of a triple integral over the scale of the element, defined by coordinates $x_m \le x \le x_{m+1}$, $y_n \le y \le y_{n+1}$, $z_p \le z \le z_{p+1}$. The elemental moments were then summed to

produce the moment for the current simulation (12) where N_e is the total number of elements *[Naff et al. (submitted 1996-2)]*.

$$M_{ijk}(t) = \sum_{e=1}^{N_e} \int_{x_m}^{x_{m+1}} \int_{y_n}^{y_{n+1}} \int_{z_p}^{z_{p+1}} x^i y^j z^k \, C_e(x,y,z,t) \, dx dy dz \qquad (12)$$

The moments in (12) were scaled to give estimates of the mass, centre of mass and degree of spreading of the contaminant plume over time. Specifically, the spatial moments can be used to obtain the following physical interpretations based on *Sudicky [1986]*:

Moment Expression	Physical Interpretation
M_{000}	mass of solute in solution;
$X_c = M_{100}/M_{000}$	x-coordinate of centre of mass;
$Y_c = M_{010}/M_{000}$	y-coordinate of centre of mass;
$Z_c = M_{001}/M_{000}$	z-coordinate of centre of mass;
$\sigma_{xx}^2 = M_{200}/M_{000} - X_c^2$	spatial variance about X_c;
$\sigma_{yy}^2 = M_{020}/M_{000} - Y_c^2$	spatial variance about Y_c;
$\sigma_{zz}^2 = M_{002}/M_{000} - Z_c^2$	spatial variance about Z_c.

Note that this method of calculating the spatial variance σ_{ij}^2 is equivalent to calculating spatial moments centred on X_c, Y_c, and Z_c. The off-diagonal terms of the symmetrical spatial variance tensor (i.e. σ_{xy}^2, σ_{xz}^2 and σ_{yz}^2) are defined as, for example, $\sigma_{xy}^2 = M_{110}/M_{000} - X_c Y_c$. These terms are non-zero if the principal axes of the plume do not line up with the principal axes of the flow system. In this case, the eigenvalues of the σ_{ij}^2 tensor provide an estimate of the degree of spreading along each of the three

eigenvectors (principal axes of the plume). For the cases where the off-diagonal terms of the second moment tensor were non-zero, the subroutine JACOBI, obtained from Numerical Recipes, the Art of Scientific Computing, (Press, W.H., B.P. Flannery, S.A. Teukolski, W.T. Vetterling, Cambridge University Press, 1986), was used to calculate the eigenvalues, in effect realigning the plume along the axes of the flow system.

Because of the Analysis of Variance model used, the individual realization moments, rather than the mean moments were used for the analysis. It is important to realize that it is the time-rate of change of the spatial moments that are of interest. For example, the time-rate of change of the first moment is the plume velocity, and the time-rate of change of the second moment is equal to two times the macroscopic dispersion coefficient.

ANALYSIS AND RESULTS

The K and K_d field means and variances for each scenario were calculated to determine to what degree they differed from the input mean and variance. Figure 1 plots the mean versus the variance for each realization of the ln(K) and ln(K_d) fields. The upper half of both groups in the scatter plot (fields with a high variance) corresponds to the fields generated using the second type of auto-correlation (correlation lengths equalling 20 cm and increased variability at small scales in the transverse vertical direction). The increase in variance caused by the addition of a spike to the power spectrum is clearly apparent in Figure 1.

Before performing a detailed statistical analysis of the moment results, a qualitative visual analysis of the fields was performed. First, transects of the K and K_d fields were compared for cases 11, 22 and 33. Second, the entire K-field was compared for cases 21, 22 and 23.

Figure 2 shows K and K_d values for transects in the transverse vertical direction. Figure 2a) shows negatively correlated K and K_d fields with coherency 0.1 and correlation lengths of 20 cm. Notice that regions of high K often correspond to regions of low K_d. This is not always the case because the coherency, which can be thought of as the strength of the correlation, is low. Also notice that for the individual fields, the thickness of the features (the distance between peaks or valleys in the graph) is approximately five elements. Multiplying by the nodal spacing of 0.04 m gives us a value of 0.2 m, or 20 cm, which corresponds to the input correlation length in the transverse vertical direction.

In Figure 2b), the distance between the peaks (which represents the thickness of the features) is diminished due to the addition of the spike to the power spectrum at high frequencies (small scales). It is difficult to see the effect of a variable cross-correlation on the fields, however the reader may notice that a region of high K located at element e corresponds to a region of high K_d located at element e + 25 ((25 elements)*(0.04 m spacing) = 1 m) which demonstrates a positive correlation between K and K_d at scales of 1 m. At small scales the negative cross-correlation is apparent, as in a).

Figure 2c) shows fields that are perfectly and positively correlated (regions of high K correspond to regions of high K_d at all scales). The correlation lengths within each field were reduced to 0.07 m, the effect of which can be seen in the width of the lenses: the distance between peaks is approximately two elements, a distance of 0.08 m.

Figure 3 shows the full K field for Cases 21, 22 and 23 with auto-correlation characteristics corresponding to Figure 2 a), b) and c) above: the field in a) has correlation lengths of 20 cm in the vertical direction, the field in b) has correlation lengths of 20 cm and also has a spike added at high frequencies in the vertical direction, and the field shown in c) has correlation lengths of 7 cm. The effect of correlation length on the field is apparent when comparing Figures 3 a) and c); the lenses are thinner in c), corresponding to a shorter vertical correlation length. The effect of increasing the power spectrum at high frequencies is two-fold: small-scale periodicity is introduced, characterized by the periodic repetition of very thin low K lenses. Also, the overall field variability is increased, however, this feature is difficult to see.

Each field was generated using a different seed and therefore high and low-valued lenses are not necessarily located in the same parts of the field for every scenario, however, the statistical behaviour of the fields is identical, from realization to realization.

Zeroth moment (mass in solution)

The amount of mass input into the system was 0.168, based on the source box having a unitless concentration of 1, a volume of 0.48 m^3 and a porosity of 0.35. Zeroth moments (M_{000}) for the non-reactive simulations remained constant at 0.168, however, for the reactive simulations, M_{000} values fluctuated strongly, varying over an order of magnitude for all simulations. Since there was no effect on M_{000} for the non-reactive case, the change was attributed to the effect of the $\ln(K_d)$ field: a source box located in a region of high K_d caused the mass to increase as the plume travelled away from the source area into lower K_d regions, or lenses. Similarly, when the source was located in a region of low K_d, the mass decreased as the plume travelled into high K_d areas and more contaminant was sorbed onto the porous media.

This behaviour arises from the imposed initial condition, which forces the liquid phase concentration to 1 in the source box, and from instantaneous sorption behaviour imposed by the underlying transport equation. In the source box, the solution concentration is 1 but the amount of solute associated with the solid depends on the value of K_d that happens to be present in the source box area; the larger the K_d value in the source area, the larger the total amount of mass present in the system.

To confirm this hypothesis, the source box mean K_d was compared to the field K_d mean, and it was discovered that a drop in M_{000} over time corresponded to a source mean smaller than the field mean K_d. Similarly, an increase in M_{000} over time coincided with a source mean K_d greater than the field mean K_d. Because the K_d

variance was comparatively large, there were large fluctuations in K_d over small areas of the field which accounted for the differences between source mean K_d and field mean K_d.

Preliminary analyses of the zeroth moments indicated that the type of autocorrelation, and even the interaction between the type of autocorrelation and cross-correlation may have affected the total mass of reactive tracer in the system. To test this hypothesis, a repeated measures Analysis of Variance (ANOVA) was performed on the zeroth moments as a function of time. The ANOVA model was

$$T_{ijk} = \mu + \alpha_i + \beta_j + (\alpha\beta)_{ij} + \epsilon_{ijk} \qquad (13)$$

where T_{ijk} is the zeroth moment at the k^{th} time step ($k = 1,...,6$) and is expressed as the sum of a general mean μ, an auto-correlation effect α, a cross-correlation effect β, an interaction effect ($\alpha\beta$), and a random error term ϵ. The subscripts i and j ($i, j = 1, 2, 3$) refer to the type of auto and cross-correlation, respectively. A repeated measures ANOVA is used because we expect a correlation in the zeroth moments between the time steps of a given realization. A simplified version of equation (13) will be used henceforth to describe the type of ANOVA, where

$$Mass = time + time*cross + time*auto + time*cross*auto + \epsilon \qquad (14)$$

is equivalent to (13).

The results of the ANOVA indicate that the effect of the time step on the amount of

mass is not significant (p=0.054) (*p* indicates the probability of committing an error in declaring an effect significant; *(1 - p)* is the confidence level) and thus there was as much variability in the amount of mass present at different times as there was for different realizations. The effect of time on the amount of mass present did not depend on the type of cross-correlation (p=0.077); or on the type of autocorrelation (p=0.956); or on the scenario (combination of cross- and autocorrelation) (p=0.998). The lack of significance indicates that variations in mass over time are random, which is what we would expect if a plume encounters zones of high and low K_d at random. Calculated zeroth moments, and the full ANOVA results are attached as Appendix A.

First moment (centre of mass)

In this section we examine the effect of the type of auto and cross-correlation on the macroscopic average plume velocity. In order to do this, we compare the locations of the center of mass of the solute plumes at a given time.

For the non-reactive solute the following ANOVA was performed:

$$M_{100} = auto + \epsilon \qquad (15)$$

The type of cross-correlation is not included in this model since it has no impact on the non-reactive simulations. The ANOVA results show that the position of the centre of mass was not affected by the type of autocorrelation (p=0.115) (Appendix B). This result is plausible because the correlation structure of the K field in the

horizontal direction was not varied.

In the case of the reactive solute the effects of the cross-correlation were also included in the ANOVA model, giving:

$$M_{100} = cross + auto + cross*auto + \epsilon \qquad (16)$$

The results (Appendix B) show that for a reactive solute, the location of the centre of mass (M_{100}) depends on the type of cross-correlation (p=0.003) but not on the type of autocorrelation (p=0.088) nor on the interaction between auto and cross-correlation (p=0.121). Post-hoc pairwise comparisons (Appendix B) further reveal that the centre of mass travels significantly less far for a variable correlation (small negative correlation between the fields at small scales, and a positive correlation at scales larger than 1 m) than for a small negative correlation (p=0.006) or for a perfect positive correlation (p=0.009). This indicates that large-scale features (large-scale cross-correlation) can have a more significant impact on the macro-scale retardation factor than the small-scale features. This is not unexpected, considering that the size of the source was smaller than the large-scale features (but larger than the small-scale features).

Retardation coefficients

In this section, the centres of mass for the reactive solute were compared to those for the non-reactive solute. For a homogeneous K_d field of a linearly retarded solute, the

ADE predicts that the location of the centre of mass of a reactive contaminant plume at time t should be the same as that of a non-reactive plume at time t/R, where R is the retardation coefficient. Since the K field was the same for both the non-reactive and the reactive simulations, any discrepancy between the centre of mass of the reactive tracer at time t and the centre of mass of the non-reactive tracer at time t/R can be attributed to heterogeneities in the K_d field and to correlation between K and K_d. However, the output retardation factor for the plumes varied from one realization to another, and therefore the centre of mass of the reactive solute plume at time t could not be compared directly to the centre of mass of the non-reactive solute at time t/R. This necessitated an adjustment to the first moments for the non-reactive cases before they could be compared directly to the reactive cases. This adjustment took the following form: because the first moment versus time (velocity) curves were linear, a linear interpolation was performed to determine the adjusted first moment values. The formula used was:

$$M^{*}_{100} = \frac{dM_{100}}{dt} t^{*} + 3.45 \qquad (17)$$

where M^{*}_{100} is the adjusted centre of mass location of the non-reactive solute, dM_{100}/dt is the average non-reactive solute plume velocity, t^{*} is the time value adjusted to account for retardation, and the final term (3.45) is the x-coordinate of the centre of mass of the source, in metres. The adjusted time value was calculated from:

$$t^{*} = \frac{t}{R} \qquad (18)$$

where t is the corresponding time for the reactive case, and R is the output macroscopic retardation factor specific to the current realization. For this exercise, the macroscopic retardation coefficient was calculated in two ways for each realization: the first was based on the arithmetic mean of the truncated K_d field (R_A), and the second based on the geometric mean of the truncated K_d field (R_G), according to

$$R_A = 1 + \frac{\rho_b \langle K_d \rangle_A}{\epsilon} \qquad R_G = 1 + \frac{\rho_b \langle K_d \rangle_G}{\epsilon} \tag{19}$$

where $\langle K_d \rangle_A$ is the arithmetic mean of the elemental K_d values in the truncated field, and $\langle K_d \rangle_G$ is the geometric mean of the elemental K_d values in the truncated field. The resulting non-reactive first moments were denoted M^*_{100A} when calculated using R_A, and M^*_{100G} when calculated using R_G In effect, the non-reactive first moment was shifted backwards according to R_A or R_G, and then compared to M_{100} for the reactive case. Sample calculations are given in Appendix C.

The adjusted non-reactive first moments (M^*_{100A} and M^*_{100G}) were compared to the raw reactive first moments (M_{100}) (Table II) using the Analysis of Variance (ANOVA) technique. The third time step (400 days for the reactive solute) was chosen at random to provide a representative assessment of the degree of correlation between the two data sets (non-reactive adjusted versus reactive). In the ANOVA, the non-reactive and reactive first moments (variable "*solute*") were treated as repeated measures because they are correlated through the flow field. The ANOVA model (20)

was applied to compare M^*_{100A} with M_{100}, and then to compare M^*_{100G} with M_{100}.

Table II: First moments for reactive solute plumes at time T3 (400 days) (M_{100}) and for non-reactive solute plumes at times $T3/R_A$ (M^*_{100A}) and $T3/R_G$ (M^*_{100G}).

Cross	Auto	M_{100} Reactive	M^*_{100A} Non-reactive	M^*_{100G} Non-reactive
1	1	14.25	13.45	14.42
1	2	14.05	15.08	17.08
1	3	13.30	11.98	12.85
2	1	10.8	12.82	13.85
2	2	10.98	12.19	13.60
2	3	11.12	13.41	14.44
3	1	13.89	12.25	13.33
3	2	12.63	12.93	14.40
3	3	12.66	12.82	13.91

$$M_{100} = solute + solute*cross + solute*auto + solute*cross*auto + \epsilon \quad (20)$$

The detailed results of the ANOVA are given in Appendix D. There was no significant difference between M^*_{100A} and M_{100} ($p>0.149$) which means that there is no significant difference between the location of the centre of mass for a non-reactive solute at time t/R_A and the location of the centre of mass for a reactive solute at time t (where R_A is the retardation factor based on the arithmetic mean K_d).

However, when comparing M^*_{100G} and M_{100}, the centres of mass were significantly farther along for the non-reactive case at time t/R_G ($p=0.003$). This difference did not depend on the type of auto or cross-correlation, nor on the individual scenario. A

third method for evaluating a macroscopic retardation factor consists of using the ratio of the velocity of the non-reactive solute plume (V_{NR}) to that of the reactive solute plume (V_R):

$$R_V = \frac{V_{NR}}{V_R} \tag{21}$$

where $V_i = dM_{100}/dt$ for $i = NR, R$ for the realization in question. A detailed explanation of the procedure used to measure V_i is found at the beginning of the section on second moments.

The values of R calculated according to (21) are presented in Table III along with the values obtained from the arithmetic averages of K_d (R_A) and from the geometric averages of K_d (R_G). These results indicate that for the scenarios considered here, a

Table III: Mean Retardation factors for all scenarios, the standard error on the means is 0.153, 0.021, and 0.013 for R_V, R_A and R_G, respectively, with nine degrees of freedom.

Cross-correlation	Autocorrelation								
	λ_3=20 cm			λ_3=20 cm, periodicity			λ_3=7 cm		
	R_V	R_A	R_G	R_V	R_A	R_G	R_V	R_A	R_G
small negative	4.24	4.44	4.03	5.20	4.86	4.15	5.79	4.51	4.08
variable	5.85	4.55	4.11	5.62	4.84	4.17	5.93	4.51	4.09
perfect positive	3.83	4.50	4.00	5.28	4.92	4.26	4.75	4.68	4.19

$R_V = V_R/V_{NR}$, where V is velocity, R and NR refer to reactive and nonreactive solutes, respectively.
R_A based on arithmetic averageK_d
R_G based on geometric averageK_d

retardation factor evaluated from the arithmetic mean K_d gives a better representation of the macroscopic retardation than a retardation factor based on the geometric mean K_d, which tends to underestimate the macroscopic retardation factor. The values in Table III are averages of two realizations.

The data presented in Table III was examined with the ANOVA model below, applied successively to R_A, R_G, and R_V.

$$R = cross + auto + cross*auto + \epsilon \qquad (22)$$

The ANOVA results showed that the addition of small scale periodicity to the autocorrelation structure of the fields significantly increased R_A ($p=0.003$), however, R_A depended on neither the type of cross-correlation ($p=0.532$) nor the interaction ($p=0.847$). The geometric mean retardation coefficient, R_G, did not depend on the autocorrelation ($p=0.139$), the cross-correlation ($p=0.636$), or on the interaction ($p=0.696$).

In all cases R_A was higher than R_G as a result of the differences in the averaging process between the arithmetic and geometric means of the $\ln(K_d)$ fields. Because the K_d fields are log-normally distributed, the distribution of the K_d fields is skewed. An increase in variability (such as that which occurs from the addition of small-scale periodicity), further skews the K_d distribution, causing the arithmetic mean to be artificially increased. For the case of the geometric mean of the K_d distribution, an

increase in variability in the $\ln(K_d)$ field does not have the same effect since the geometric mean is the exponential of the arithmetic mean of $\ln(K_d)$ which is added deterministically to perturbations in the random field generation process.

The ANOVA results on R_V showed that R_V depends on the type of cross-correlation between velocity and retardation ($p=0.002$), on the type of autocorrelation within the fields ($p=0.010$) and to a lesser degree of confidence on the interaction between the auto and cross-correlation scenarios ($p=0.039$).

Pairwise post-hoc comparisons on R_V revealed that retardation coefficients were significantly elevated when there was a variable cross-correlation between K and K_d compared to a small negative cross-correlation ($p=0.046$) or compard to a perfect positive cross-correlation ($p=0.002$). This observation concurs with the results obtained in the previous section for center of mass: the movement of the plume center of mass was inhibited for a variable correlation between K and K_d. This result suggests that even a weak, large-scale positive correlation between the fields can significantly change the apparent macroscopic retardation factor.

R_V was also elevated when the correlation lengths were 20 cm compared to the same correlation lengths with the addition of periodicity ($p=0.044$), or compared to correlation lengths of 7 cm and no periodicity ($p=0.013$).

Because of the differences in results between R_V and R_G, a repeated measures

ANOVA was performed to determine whether there was a significant difference between the two variables and if so, whether the differences were random. A repeated measures ANOVA was used since R_V and R_G are calculated from the same random fields, and are thus correlated. The ANOVA model was

$$R = retard + retard*cross + retard*auto + retard*cross*auto + \epsilon \quad (23)$$

where *retard* refers to either R_V or R_G (which were the repeated measure). The values of R_V were significantly higher than the values based on the mean $\ln(K_d)$ values ($p=0.2E-05$), and the effect of the calculation method depended on the type of cross-correlation ($p=0.003$) and on the type of autocorrelation ($p=0.027$) but not on the interaction ($p=0.072$). This means we cannot show that the differences between R_V and R_G are random, and therefore, the velocity of a reactive solute plume should not be calculated based solely on the mean field K_d; the effects of the hydraulic conductivity field, and particularly it's correlation with K_d must also be considered.

The ratio of R_V to R_G was tested using (22), with similar results. The full ANOVA results for R_A, R_G, and R_V can be viewed in Appendix E.

Second Moment

Calculation of macrodispersivities

Macrodispersivity is defined as the dispersion coefficient divided by velocity, where the dispersion coefficient is half the time rate of change of the plume's second

moment. Because Monte-Carlo simulations were performed, the question arises of whether to use the realization dispersion coefficient (calculated from a single realization), the mean dispersion coefficient over all realizations (the arithmetic average of the realization dispersion coefficients for a single scenario), or even the dispersion coefficient based on the mean plume (calculated from the second moments of the mean plume, averaged over the realizations). The latter two are, in fact, identical as shown in *Naff et. al [submitted 1996-2].*

There exist several similar formulae which have recently been used in macrodispersivity calculations. Formula (24) outlines three of these methods, used by *Burr et al. [1994]* (method 1), *Garabedian et al. [1991]* (methods 1 and 2), and *Naff et al. [submitted 1996-2]* (methods 2 and 3):

$$A_{ii}^{(1)} = \frac{1}{2}\frac{d\sigma_{ii}^2}{dX_c} \qquad A_{ii}^{(2)} = \frac{1}{2V}\frac{d\sigma_{ii}^2}{dt} \qquad A_{ii}^{(3)} = \frac{1}{2\langle V\rangle}\frac{d\langle\sigma_{ii}^2\rangle}{dt} \tag{24}$$

where i is an indice representing direction (x, y or z), $V = d|X_c|/dt$ is the realization velocity, and $\langle\bullet\rangle$ is the realization arithmetic mean of $\bullet$. Method 3 is inappropriate to use for this type of analysis since $A_{ii}^{(3)}$ is the scenario average, which eliminates individual realization macrodispersivities needed for the Analysis of Variance. Therefore, a new version of the formula is presented below:

$$A_{ii}^{(4)} = \frac{1}{2\langle V\rangle}\frac{d\sigma_{ii}^2}{dt} \tag{25}$$

which preserves the realization macrodispersivities and allows comparisons between non-reactive and reactive cases.

Macrodispersivities were calculated using $A_{ii}^{(1)}$, $A_{ii}^{(2)}$, and $A_{ii}^{(4)}$ for three scenarios in order to make a comparison between calculation methods. Table IV shows longitudinal macrodispersivities for one of the three scenarios, Case 11 (non-reactive). This particular case was chosen in an attempt to study the worst-case scenario since it exhibited the largest velocity variance of all cases. Because macrodispersivity depends on velocity according to equations (24) and (25), a large change in velocity from realization to realization increases the realization variance of $A_{ii}^{(1)}$ and $A_{ii}^{(2)}$, in effect maximizing the difference between the three methods.

Table IV: Macrodispersivity values for Case 11 (non-reactive)

	$A_{ii}^{(1)}$	$A_{ii}^{(2)}$	$A_{ii}^{(4)}$
Real#1	0.2212	0.2198	0.2661
Real#2	0.5057	0.4953	0.3908
Average	0.3635	0.3575	0.3285

The results shown in Table IV were analysed by the ANOVA model

$$A_{ij} = method + realization + method*realization + \epsilon \qquad (26)$$

and it was determined that the variability between methods was not significant ($p=0.852$). In other words, the choice of method by which macrodispersivity was calculated had no effect on the conclusions drawn from the ANOVA results due to the high degree of variability between realizations.

Before choosing a particular method by which to perform the remaining macrodispersivity calculations, the sources of error associated with these calculations were evaluated. For all methods, it was necessary to estimate slopes of curves, and the method used to estimate these slopes was somewhat subjective. The general procedure used to estimate the slope was: 1) discard all data-points where plume has encountered a boundary, 2) discard early-time data-points showing a large degree of oscillation, and 3) perform a regression analysis on the remaining data-points to obtain the slope of the line of best fit. The choice of whether or not to discard data points was subjective in that one had to set limits for the oscillation and determine what constituted the plume having encountered a boundary.

The slope-estimation procedure outlined above was used to calculate the realization velocity, dispersion coefficients, and macrodispersivity. For a more detailed discussion into the problems associated with this technique, refer to *Naff et al. [submitted 1996-1,2].*

For all simulations, the amount of oscillation in the solution was monitored. This constituted two variables: the first was the ratio of negative nodes to positive nodes

(nodes with concentrations less than $c_{max}(t)$E-04 were considered to be zero), the second was the value of the minimum concentration, $c_{min}(t)$, usually a negative number. If either the ratio of negative to positive nodes was greater than 0.2, or $c_{min}(t)$ was less than -0.2, the concentration field was discarded. If the absolute values of both variables were greater than 0.02, the concentration field was also discarded. Levels of oscillation were far below these limits, except for the case where there was a perfect positive correlation between the K and K_d fields.

In most cases, too much oscillation coincided with a loss of mass of three percent or more, indicating the plume had encountered a boundary. However, for a reactive solute, the amount of mass in solution varied by an order of magnitude and it was difficult to ascertain whether a loss of mass indicated increased sorption or the plume encountering a boundary. Here, the plume centre of mass (X_c, Y_c, Z_c) and spatial spreading (σ^2_x, σ^2_y, σ^2_z) values were helpful: sudden stagnation or a sudden drop in the rate of spreading indicated that something was amiss and further investigation was needed.

A minimum of four data points were used to calculate the macrodispersivities presented in the following tables, except for one case which will be discussed separately. The second formula, $A^{(2)}_{ii}$ was used for the remaining calculations for several reasons: $A^{(1)}_{ii}$ was discarded due to the large number of data points which were unusable in the σ^2_{ii} versus X_c slope calculation, and $A^{(2)}_{ii}$ was chosen over $A^{(4)}_{ii}$ so that the macrodispersivities were particular to the realization in question. The

choice of $A^{(2)}_{ii}$ ensured that large differences in velocity from realization to realization were not smoothed by the averaging process, which would have reduced the macrodispersivity variance and decreased the error term in the ANOVA.

The calculated macrodispersivities for the longitudinal direction are shown in Table V, and those for the transverse horizontal, and transverse vertical directions are shown in Tables VI and VII, respectively.

Table V: Longitudinal macrodispersivities for a) a reactive solute and b) a non-reactive solute. Each value is the mean of two or more realizations with standard error 0.110 (reactive solute) and 0.045 (non-reactive solute). The numbers at the left hand side of each cell correspond to the case number for that particular scenario.

a) Reactive

Cross-correlation	Autocorrelation		
	λ_3=20 cm	λ_3=20 cm periodicity	λ_3=7 cm
small negative	11 0.614	12 1.746	13 0.546
variable	21 0.557	22 1.234	32 0.365
perfect positive	31 0.021	32 0.049	33 0.059

b) Non-Reactive

Cross-correlation	Autocorrelation		
	λ_3=20 cm	λ_3=20 cm periodicity	λ_3=7 cm
small negative	11 0.358	12 0.581	13 0.194
variable	21 0.460	22 0.553	32 0.285
perfect positive	31 0.460	32 0.340	33 0.363

A comparison of specific scenario results from Tables V, VI and VII with *Robin [1991]* shows similar findings. For vertical correlation lengths of 20 cm and a small

Table VI: Macrodispersivities for the transverse horizontal (y) direction. Each value is the mean of two or more realizations, with standard error 0.44E-05 (reactive) and 0.16E-04 (non-reactive).

a) Reactive

Cross-correlation	Autocorrelation		
	λ_3=20 cm	λ_3=20 cm periodicity	λ_3=7 cm
small negative	$_{11}$ 0.013	$_{12}$ 0.013	$_{13}$ 0.013
variable	$_{21}$ 0.010	$_{22}$ 0.011	$_{32}$ 0.010
perfect positive	$_{31}$ 0.011	$_{32}$ 0.011	$_{33}$ 0.012

b) Non-Reactive

Cross-correlation	Autocorrelation		
	λ_3=20 cm	λ_3=20 cm periodicity	λ_3=7 cm
small negative	$_{11}$ 0.013	$_{12}$ 0.010	$_{13}$ 0.012
variable	$_{21}$ 0.011	$_{22}$ 0.010	$_{32}$ 0.011
perfect positive	$_{31}$ 0.011	$_{32}$ 0.011	$_{33}$ 0.012

Table VII: Macrodispersivities for the transverse vertical (z) direction. Each value is the mean of two or more realizations, with standard error 0.16E-04 (reactive) and 0.15E-05 (non-reactive)

a) Reactive

Cross-correlation	Autocorrelation		
	λ_3=20 cm	λ_3=20 cm periodicity	λ_3=7 cm
small negative	$_{11}$ 0.014	$_{12}$ 0.009	$_{13}$ 0.012
variable	$_{21}$ 0.006	$_{22}$ 0.012	$_{32}$ 0.013
perfect positive	$_{31}$ 0.008	$_{32}$ 0.009	$_{33}$ 0.010

b) Non-Reactive

Cross-correlation	Autocorrelation		
	λ_3=20 cm	λ_3=20 cm periodicity	λ_3=7 cm
small negative	$_{11}$ 0.013	$_{12}$ 0.007	$_{13}$ 0.009
variable	$_{21}$ 0.010	$_{22}$ 0.014	$_{32}$ 0.008
perfect positive	$_{31}$ 0.009	$_{32}$ 0.010	$_{33}$ 0.010

negative or variable cross-correlation (Cases 11 and 21), longitudinal macrodispersivities ranged from 0.453 m to 0.661 m for all realizations. A similar scenario simulated by *Robin [1991]*, but using an inorganic solute and a linear cross-spectrum model (*Robin*'s Case 3) produced a value of 0.5038 m for longitudinal macrodispersivity. Transverse macrodispersivities had fewer similarities, with results from this study near 0.01 m compared to 0.0058 m (horizontal) and a range of 0.003 m to 0.009 m from this study, compared to 0.0012 m (vertical), both for *Robin* 's simulations.

The results of Case 31 (perfect positive correlation), with longitudinal macrodispersivities of 0.021 m compare favourably with the Monte Carlo results of *Haley et al. [1994]* (Case 2) (0.04 m).

Following the procedure used by *Robin [1991]*, theoretical macrodispersivities for the non-reactive case were calculated using the method of *Gelhar and Axness [1983]* (their equation 65):

$$A_{11} = \frac{\sigma_f^2 \lambda_1 \mu}{\gamma^2 \xi} \tag{27}$$

where

$$\gamma = \frac{\exp\left[\sigma_f^2 (0.5 - g_{33})\right]}{\sin^2\theta + \beta\cos^2\theta}$$

$$\mu = \lambda_3/\lambda_1 \qquad (28)$$

$$\xi = (\sin^2\theta + \mu^2\cos^2\theta)^{1/2}$$

$$\beta = \exp\left[\sigma_f^2 (g_{11} - g_{33})\right]$$

and also

$$g_{11} = g_{22} = \frac{1}{2}\,\frac{1}{\rho^2 - 1}\left\{\frac{\rho^2}{(\rho^2-1)^{1/2}}\tan^{-1}(\rho^2-1)^{1/2} - 1\right\}$$

$$g_{33} = \frac{\rho^2}{\rho^2 - 1}\left\{1 - \frac{1}{(\rho^2-1)^{1/2}}\tan^{-1}(\rho^2-1)^{1/2}\right\} \qquad (29)$$

where $\rho = \lambda_1/\lambda_3 > 1$. Table VIII shows that the theoretical values are larger than the observed values, by a factor of two to three, depending on the autocorrelation scenario. *Robin* calculated theoretical macrodispersivities which were approximately twice the observed values, and *Thompson and Gelhar [1990]* also saw similar discrepancies between theoretical and observed macrodispersivities.

For the reactive case, the method used by *Garabedian [1987]* and subsequently modified by *Robin*, was followed. Theoretical longitudinal macrodispersivities were calculated according to

$$A_{11} = \frac{\sigma_f^2 \lambda_1}{\gamma^2} \left\{ 1 - \frac{\gamma \, b}{\epsilon \bar{R}^2} \right\} + \rho_b^2 \left\{ \frac{\sigma_{K_d}^2}{\sigma_g^2} \right\} (1 - C^2) \frac{\lambda_1}{(\epsilon \bar{R})^2} \qquad (30)$$

where ϵ is the porosity, is the macroscopic retardation factor based on the arithmetic mean of K_d, C is the coherency and the remaining parameters are as in the method of *Gelhar and Axness [1983]*, above. Refer to *Robin [1991]* for further details and for an explanation of the simplifying assumptions associated with the procedure. For these reactive cases, theoretical macrodispersivities (Table VIII) were four to fifty times higher than the observed macrodispersivities. The largest discrepancies were

Table VIII: Theoretical and observed longitudinal macrodispersivities for the reactive (a) and non-reactive (b) solute.

a) Reactive

Cross-correlation	Autocorrelation					
	λ_3=20 cm		λ_3=20 cm periodicity		λ_3=7 cm	
	Garabedian [1987]	Observed	*Garabedian [1987]*	Observed	*Garabedian [1987]*	Observed
small negative	^{11} 4.809	^{11} 0.614	^{12} 6.857	^{12} 1.746	^{13} 5.000	^{13} 0.546
variable	^{21} 5.053	^{21} 0.557	^{22} 6.668	^{22} 1.234	^{23} 4.983	^{23} 0.365
perfect positive	^{31} 1.162	^{31} 0.021	^{32} 0.853	^{32} 0.043	^{33} 1.018	^{33} 0.059

b) Non-Reactive

	Autocorrelation		
	λ_3=20 cm	λ_3=20 cm periodicity	λ_3=7 cm
Gelhar and Axness (1983)	^{11} 0.795	^{12} 0.950	^{13} 0.789
Observed	^{21} 0.416	^{22} 0.491	^{23} 0.280

observed for the case where the ln(K) and ln(K_d) fields were perfectly and positively correlated indicating that the theoretical calculations did not reflect the effect of the positive correlation to a large enough degree.

For the cases were the ln(K) and ln(K_d) fields were negatively correlated, the theoretical macrodispersivities were four to thirteen times larger than the observed values. These discrepancies are also significantly higher than those calculated by *Robin* (*Robin's* theoretical macrodispersivities were approximately two to four times larger than the observed values). Discrepancies between the predicted values and the measured values may be the result of the simple cross-correlation structure used in *Garabedian's* work and the simplifying assumptions that were necessarily made in order to carry out the calculations.

For Case 12 (non-reactive), only three data points were used in the macrodispersivity calculation because the plume encountered the downstream boundary by the fourth time step (155 days) and thus the last three data points were discarded. Because the σ^2_{ii} versus time curves are linear for the remaining three data points in all directions and for all realizations, the calculated macrodispersivities were accepted as representative of typical values for the scenario in question.

Uniformity of variances

The Analysis of Variance technique is based on the assumption that the variance is the same for each treatment, that is, the variability between realizations is the same for

each case. However, the calculated variance in macrodispersivity within each treatment was not constant from one case to another. Because the Analysis of Variance is robust, it operates well even when variances are not homogeneous (*Zar, 1984*). Nevertheless, since the log-transformed macrodispersivities had a more acceptable level of variability between the variances, A_{ii} was replaced by $\log(A_{ii})$ in (32) to determine if a more strict adherence to the rules of the ANOVA would affect the outcome of the tests. The conclusions based on the $\log(A_{ii})$ data were no different from those based on the actual macrodispersivity values and so further ANOVA's were performed on A_{ii}.

Effect of correlation scenario

Analyses of variance were performed on the calculated macrodispersivities to determine whether there was a significant effect due to the type of cross-correlation and autocorrelation and also to see if there was evidence of interaction between the auto and the cross-correlation.

For the non-reactive case the effect of cross-correlation has no physical meaning since K_d doesn't enter into the calculation of the non-reactive plume. The following ANOVA model was therefore used:

$$A_{ii} = auto + \epsilon \qquad (31)$$

The results of the ANOVA (Appendix F) showed that there was no significant difference between types of auto-correlation in any direction for the non-reactive case

(p=0.250, p=0.090, p=0.685 for the x, y and z directions respectively). This suggests that the longitudinal macrodispersivity is relatively insensitive to the type of transverse spatial correlation in the ln(K) field compared to the differences between realizations for the range of autocorrelations used here. The most likely explanations for this phenomenon are as follows. First, the range of possible ln(K) scenarios was not extreme, especially when considering that all scenarios had the same horizontal input statistics, and second, the size of the source was fairly large relative to the vertical correlation scales, which, in effect, allows the plume to sample a wide range of heterogeneities in the flow field from the very start. It should be noted, however, that even though there was no significant difference between scenarios, the macrodispersivity values were larger than the input local dispersivity by a factor of ten, which is in line with values predicted from stochastic theory.

The ANOVA model of equation (32) was constructed for each direction (longitudinal, transverse horizontal, transverse vertical) for the reactive simulations (a total of three ANOVAs).

$$A_{ii} = cross + auto + cross * auto + \epsilon \qquad (32)$$

In the transverse horizontal and transverse vertical directions the type of auto and cross-correlation had no significant effect on macrodispersivity (p>0.1427), and there was no interaction between the auto and cross-correlation (p>0.3993). In the longitudinal direction, both the effects of the type of cross-correlation and autocorrelation were found to be significant (p=0.0002 and p=0.0076, respectively).

Periodicity in the autocorrelation produced significantly higher macrodispersivities especially when the cross-correlation was negative. However, this effect may have been caused by the increased variance caused by the periodicity rather than by the periodicity itself. Generally, the macrodispersivities were enhanced when the cross-correlation between K and K_d was negative. The effect of the interaction was not significant (p=0.1087) indicating that the effect of the type of autocorrelation did not depend on the type of cross-correlation and vice-versa. See Appendix F for the complete ANOVA results.

Post-hoc pairwise comparisons can be used to identify which particular scenario produced macrodispersivities that were significantly different from another scenario. Only the longitudinal macrodispersivities for the reactive case were analysed using post hoc tests since these were the only values significantly affected by differing correlation scenarios.

First, the results were grouped in sixes according to type of cross-correlation (ignoring differences in auto-correlation). The results of these comparisons indicated that macrodispersivity was significantly smaller for a perfect positive cross-correlation when compared to a small negative (p=0.0002) or variable (p=0.0087) cross-correlation.

Second, the results were re-grouped according to type of auto-correlation, and ignoring cross-correlation. Post-hoc analysis indicated that macrodispersivity was

enhanced for vertical correlation lengths of 20 cm with periodicity, compared to 7 cm vertical correlation lengths with no periodicity ($p = 0.0078$). All other pairwise comparisons were not significant.

Third, both auto- and cross-correlation were taken into account, and macrodispersivities for every scenario were compared pairwise. Table IX shows the results of the post-hoc analysis; shaded regions indicate non-significant pairwise differences ($p>0.05$). Because the table is symmetrical, only the lower triangle is used.

Table IX: P-values for significance of pairwise differences in longitudinal macrodispersivity (reactive solute)

Case	11	12	13	21	22	23	31	32	33
11	1.0	X	X	X	X	X	X	X	X
12	1.0	1.0	X	X	X	X	X	X	X
13	1.0	1.0	1.0	X	X	X	X	X	X
21	1.0	0.1332	1.0	1.0	X	X	X	X	X
22	1.0	1.0	1.0	1.0	1.0	X	X	X	X
23	1.0	0.0465	1.0	1.0	0.7963	1.0	X	X	X
31	0.2274	0.0078	1.0	1.0	0.1166	1.0	1.0	X	X
32	0.0838	0.0018	1.0	1.0	0.0385	1.0	1.0	1.0	X
33	0.2814	1.0	1.0	1.0	0.1439	1.0	1.0	1.0	1.0

The results shown in Table IX indicate that Case 12 (periodic autocorrelation with small negative cross-correlation at all scales) has a significantly higher

macrodispersivity than the cases with positive cross-correlation and Case 23 (variable cross-correlation and a short (7 cm) vertical correlation scale). Cases 22 and 32 were also significantly different. This suggests that adding periodicity to the K and K_d fields in the vertical direction increases dispersion significantly when the cross-correlation between K and K_d is positive, somewhat less when the cross-correlation is partly negative and partly positive, and insignificantly when the cross-correlation is negative. Conversely, in the presence of periodicities, the effect of the cross-correlation on dispersion is significant (Case 22 was marginally different than Case 32 ($p=0.0385$), which was different than Case 12 ($p=0.0018$)).

Simply reducing the correlation scale to 7 cm (from 20 cm) did not have a significant effect on macrodispersivity, whereas including small-scale periodicity did. This may be due to the large size of the source relative to the correlation scale, and to the increase of variance caused by the added periodicity. The raw ANOVA results, and the results of the post-hoc tests are attached as Appendix F.

It would be useful at this point to demonstrate the results of the ANOVA by showing the physical effects of the different types of auto and cross-correlation on the shape and behaviour of the plume. Images of the plume at each of the six time steps were recorded, and were super-imposed on an image of either the K or K_d field. By viewing the results in this way, it was possible to gain better insight in to the effects of the type of cross-correlation and autocorrelation on the evolution of the contaminant plume.

Figure 4 demonstrates the differences between a perfect positive correlation and a weak negative correlation between the fields. Figure 4a) shows the 0.1% concentration isosurface of the reactive tracer plume at 450 days, for the case where the cross-correlation is negative with a coherency of 0.1. Figure 4b) shows the 0.1% isosurface for the case of a perfect positive cross-correlation. The hydraulic conductivity field is shown in the background. Notice how the longitudinal macrodispersivity is enhanced when the correlation between the K and K_d field is negative (regions of high K correspond to regions of low K_d).

Figure 5 shows the effects of differing correlation lengths in the transverse vertical direction, and the addition of periodicity to the layering. Figure 5a) shows the K field and the reactive tracer plume at a time of 300 days when the vertical correlation lengths were 20 cm and there was increased small-scale variability due to periodicity. Figure 5b) shows the K field and the plume at the same time step, but for vertical correlation lengths of 7 cm with no periodicity. Macrodispersivity is enhanced in a), notice how the plume lags in regions of low K and channels into high K regions.

Effect of type of solute

This section focuses on comparing macrodispersivities obtained from the non-reactive simulations with those of the reactive case. Theoretically, for a homogeneous medium and a linearly sorbing solute, dispersivity is a property of the porous medium if all phenomena are properly accounted for in the ADE. In this particular study, the non-reactive simulations were performed using the same random number generator

seed as the reactive simulations, therefore the sole difference between the non-reactive and the reactive cases was in the $\ln(K_d)$ field. This procedure ensured that differences in macrodispersivity were due only to the $\ln(K_d)$ field.

The feasibility of comparing macrodispersivities for a non-reactive and a reactive solute is not inherently obvious. However, considering a linear retardation process, the entire Advection-Dispersion Equation (ADE) is divided through by R (the retardation factor), and therefore

$$D_r = \frac{D_{nr}}{R} \qquad V_r = \frac{V_{nr}}{R} \tag{33}$$

where D is the dispersion coefficient, V is the velocity and the subscripts r and nr refer to reactive and non-reactive solute, respectively.

Ignoring diffusion, we have

$$D = Av \quad \textit{so that} \quad D_r = A_r V_r \quad \textit{also} \quad D_{nr} = A_{nr} V_{nr} \tag{34}$$

and by manipulating these equations we obtain

$$D_r = \frac{A_{nr} V_{nr}}{R} = A_r V_r \tag{35}$$

which cancels to

$$A_{nr} = A_r \tag{36}$$

Therefore, if retardation is properly accounted for, the macrodispersivity is expected to be the same for the non-reactive and the reactive case.

The ANOVA model which was used to perform the repeated measures analysis was

$$A_{ij} = solute + solute*xcor + solute*auto + solute*xcor*auto + \epsilon \quad (37)$$

where the type of solute was the repeated measure (either reactive or non-reactive) because of the inherent correlation due to the same flow field. When all values were taken together (ignoring differences between reactive and non-reactive simulations), there was a marginally significant effect of cross-correlation (p=0.021) and of auto-correlation (p=0.055) on macrodispersivity. However, when reactive and non-reactive macrodispersivities were taken as repeated measures, the effect of the type of solute was significant and depended on the type of cross-correlation (p=0.001) but less significantly on the type of auto-correlation (p=0.095). The ANOVA results are given in detail in Appendix G.

Because the macrodispersivities are significantly different according to the results of the ANOVA, then it may be said that the effect of the $\ln(K_d)$ heterogeneities is to enhance the macrodispersivity of the reactive solute relative to the non-reactive case when the correlation between K and K_d is negative, and to decrease it when the correlation is positive.

Figure 6 illustrates the enhanced spreading of the reactive versus the non-reactive case, where K and K_d are negatively correlated (Case 11). Figure 6a) shows the reactive tracer plume at time 300 days, with the K_d field in the background (the corresponding K field is shown in Figure 6b). Notice how the plume fingers into regions of high K and low K_d, and avoids, or lingers in regions of high K_d. Figure 6b) shows the same K field and the non-reactive plume at time 103 days. The different degree of spatial spreading that is seen is due to the spatial cross-correlation.

A more meaningful comparison of the non-reactive versus reactive longitudinal macrodispersivities can be obtained by comparing:

$$A^* = \frac{A_r - A_{nr}}{A_{nr}} \tag{39}$$

Positive values of A^* correspond to enhanced spreading of the reactive plume relative to the non-reactive plume, and negative values correspond to reduced spreading. Mean A^* values for the nine scenarios are presented in Table X.

Table X: A^* values from equation (38) for all scenarios, each entry is a mean over two realizations.

Cross-correlation	Autocorrelation		
	λ_s=20 cm	λ_s=20 cm periodicity	λ_s=7 cm
small negative	2.031	2.077	1.925
variable	1.552	1.117	0.308
perfect positive	-0.949	-0.777	-0.768

The ANOVA model (39) applied to A^* indicated that there was reduced spreading for the case of a perfect positive cross-correlation (p=0.002), however neither the type of autocorrelation nor the interaction between autocorrelation and cross-correlation significantly affected A^* (p=0.755 and p=0.864, respectively).

$$A^* = cross + auto + cross*auto + \epsilon \qquad (40)$$

Post-hoc pairwise comparisons indicated that there were no specific pairs of cases which significantly differed from one another. In fact, this ANOVA model procured no new information, simply confirming the results obtained from previous ANOVA's. Full ANOVA results are presented in Appendix H.

SUMMARY AND CONCLUSIONS

This study demonstrates how the relationship between the groundwater velocity field and the retardation field can affect the behaviour of a contaminant plume in a heterogeneous aquifer. It also shows how the spatial correlation of the groundwater field can affect plume behaviour. The parameters used to measure plume behaviour were the time-rate of change of the first and second spatial moments of the plume; the latter is used to derive the macrodispersivity.

The effects of three types of vertical self-correlation for ln(K) and ln(K_d) were examined: large (20 cm) and small (7 cm) correlation scales without periodicity; and

large correlation scales (20 cm) with small scale periodicity. Horizontally, the fields were statistically isotropic with correlation scales of 5 m. Three types of cross-correlation between ln(K) and ln(K_d) were examined: a weak negative correlation at all scales, a weak negative correlation at small scales with a weak positive correlation at large scales and a weak positive correlation at all scales. The resulting numerical experiment had nine possible scenarios that were compared using standard factorial design Analysis of Variance (ANOVA) procedures. This allowed conclusions to be drawn from a very limited number of realizations.

For a non-reactive solute, the correlation scenario had no significant effect on the location of the plume centre of mass, however, for a reactive solute, a variable correlation between K and K_d inhibited the movement of the centre of mass. Also, the non-reactive solute plume had travelled significantly farther at time t/R_G than the corresponding reactive solute plume at time t (R_G is the geometric retardation coefficient based on the geometric mean K_d).

Confirming the results of the previous paragraph, retardation coefficients were significantly elevated when there was a variable cross-correlation between K and K_d, which suggests that even a weak large-scale positive correlation can significantly change the apparent macroscopic retardation coefficient. This is an important result since it suggests that when predicting macro-retardation coefficients, one must consider not only the distribution coefficient field, but also the hydraulic conductivity field and particularly the type and degree of the cross-correlation between them.

For both non-reactive and reactive solutes, macrodispersivity in the directions transverse to flow was not sensitive to changes in the correlation structure of the ln(K) field.

In the longitudinal direction, however, there were significant effects. For a reactive solute, a small negative correlation between velocity and retardation caused enhanced spatial spreading while a perfect positive correlation caused reduced spreading. The addition of a small positive correlation at scales greater than 1 m to an otherwise negative cross-correlation did not have a significant effect on the longitudinal macrodispersivity.

The introduction of small-scale periodicity in the transverse vertical direction had no effect if the correlation lengths were held constant at 20 cm. Likewise, a decrease in correlation lengths from 20 cm to 7 cm had no effect on the longitudinal macrodispersivity; however, the macrodispersivity values were significantly higher for the periodic, 20 cm case compared to the non-periodic 7 cm case. However, this effect may have been caused by the increase in variance introduced with the periodicity rather than by the periodicity itself.

For the non-reactive cases the autocorrelation structure of the ln(K) field used in this study had no significant effect on the longitudinal macrodispersivity.

A comparison of macrodispersivities for the reactive versus the non-reactive case determined that macrodispersivity is enhanced for a reactive solute. This effect depends largely on the type of cross-correlation and to a lesser degree on the type of autocorrelation. Thus, even a weak correlation between K and K_d can lead to significantly enhanced mixing for a reactive solute.

The results of this study are important because they show that the macroscopic retardation factor depends on the type of correlation between hydraulic conductivity and the distribution coefficient, and that the longitudinal macrodispersivity for a reactive solute is sensitive to the relationship between velocity and retardation, even when the relationship is weak. Weak correlations between K and K_d are common and are highly dependent on the type of solute, as evidenced by the work at C.F.B. Borden (*Robin et al. [1993], Halket et al. [submitted 1996]*).

This study demonstrates that the standard statistical tools of Analysis of Variance can be extremely powerful in analysing Monte-Carlo-type simulations. The use of experimental design methods to plan the numerical experiments enables the use of the ANOVA, which can provide meaningful conclusions with a very limited number of realizations. The experimental design methods used here are applicable to most sensitivity analyses and may provide significant time savings, and hence financial savings.

The results of this type of study can be used to assist in the design of field

experiments, to assist in designing strategies for sampling and also to calculate uncertainties in concentration predictions.

Future areas which could be studied using the same principles outlined here include the effects of horizontal anisotropy, the effect of source size on plume displacement and dispersion, and the effect of temporal variations in the flow field (non-steady-state flow).

REFERENCES

Bosma, W.J.P., S.E.A.T.M. van der Zee and C.J. van Duijn, Plume development of a nonlinearly adsorbing solute in heterogeneous porous formations, *Water Resources Research*, 32(6), 1569-1584, 1996.

Burr, D.T., E.A. Sudicky and R.L. Naff, Nonreactive and reactive solute transport in three dimensional heterogeneous porous media: Mean displacement, plume spreading and uncertainty, *Water Resources Research*, 30(3), 791-815, 1994.

Dagan, G., *Flow and Transport in Porous Formations*, Springer-Verlag, 1989.

de Hoog, F.R., J.H. Knight and A.N. Stokes, An improved method for numerical inversion of Laplace transforms, *SIAM J. Sci. Stat. Comput.*, 3(3), 357-366, 1982.

Desai, C.S., and J.F. Abel, *An Introduction to the Finite Element Method*, Van Nostrand Reinhold, 1972.

Freyberg, D.L., A natural gradient experiment on solute transport in a sand aquifer 2. Spatial moments and the advection and dispersion of nonreactive tracers,*Water Resources Research*, 22(13), 2031-2046, 1986.

Garabedian, S.P., *Large-scale dispersive transport in aquifers: field experiments and reactive transport theory*, PhD Thesis, Massachusetts Institute of Technology, 1987.

Garabedian, S.P., D.R. LeBlanc, L.W. Gelhar and M.A. Celia, Large-scale natural gradient tracer test in sand and gravel, Cape Cod, Massachusetts 2. Analysis of spatial moments for a nonreactive tracer, *Water Resources Research*, 27(5), 911-924, 1991.

Gelhar, L.W., C. Welty, and K.R. Rehfeldt, A critical review of data on field-scale dispersion in aquifers, *Water Resources Research*, 28(7), 1955-1974, 1992.

Haley, D.F., E.A. Sudicky and R.L. Naff, Three-dimensional Monte Carlo analysis of spatial spreading during reactive solute transport by groundwater, in *Transport and Reactive Processes in Aquifers*, Dracos and Stauffer (eds), pp 437-443,

A.A.Balkema/ Brookfield, Rotterdam, 1994.

Halket, R.M., R.M. Allen-King, D.R. Gaylord and M.J.L. Robin, PCE sorption and hydraulic conductivity correlation with sedimentary facies in the Borden aquifer, *Water Resources Research* (submitted 1996).

Naff, R.L., D.F. Haley and E.A. Sudicky, High-resolution Monte-Carlo simulation of flow and conservative transport in heterogeneous porous media: 1, Methodology and flow results, *Water Resources Research* (submitted 1996).

Naff, R.L., D.F. Haley and E.A. Sudicky, High-resolution Monte-Carlo simulation of flow and conservative transport in heterogeneous porous media: 2, Transport results, *Water Resources Research* (submitted 1996).

Press, W.H., B.P. Flannery, S.A. Teukolski, W.T. Vetterling, *Numerical Recipes, The Art of Scientific Computing,* Cambridge University Press, 1986.

Robin, M.J.L., *Migration of Reactive Solutes in Three-Dimensional Heterogeneous Porous Media*, PhD Thesis, University of Waterloo, 1991.

Robin, M.J.L., A.L. Gutjahr, E.A. Sudicky and J.L. Wilson, Cross-correlated random field generation with the direct Fourier transform method, *Water Resources Research*, 29(7), 2385-2397, 1993.

Robin, M.J.L., E.A. Sudicky, R.W. Gillham and R.G. Kachanoski, Spatial variability of strontium distribution coefficients and their correlation with hydraulic conductivity in the Canadian Forces Base, Borden aquifer, *Water Resources Research*, 27(10), 2619-2632, 1991.

Sudicky, E.A., A natural gradient experiment on solute transport in a sand aquifer: spatial variability of hydraulic conductivity and its role in the dispersion process, *Water Resources Research*, 22(13), 2069-2082, 1986.

Sudicky, E.A., The Laplace Transform Galerkin technique: a time-continuous finite element theory and application to mass transport in groundwater, *Water Resources Research*, 25(8), 1833-1846, 1989.

Thompson, A.F.B., Numerical simulation of chemical migration in physically and chemically heterogeneous porous media, *Water Resources Research*, 29(11), 3709-3726, 1993.

Thompson, A.F.B., and L.W. Gelhar, Numerical simulation of solute transport in three-dimensional, randomly heterogeneous porous media, *Water Resources Research*, 26(10), 2541-2562, 1990.

Zhang, Y.-K. and J.A. Chi, An evaluation of nonlinearity in spatial second moments of ensemble mean concentration in heterogeneous porous media, *Water Resources Research*, 31(12), 2991-3005, 1995.

Zar, J.H., *Biostatistical Analysis, 2nd Ed.*, Prentice-Hall, New Jersey, 1984.

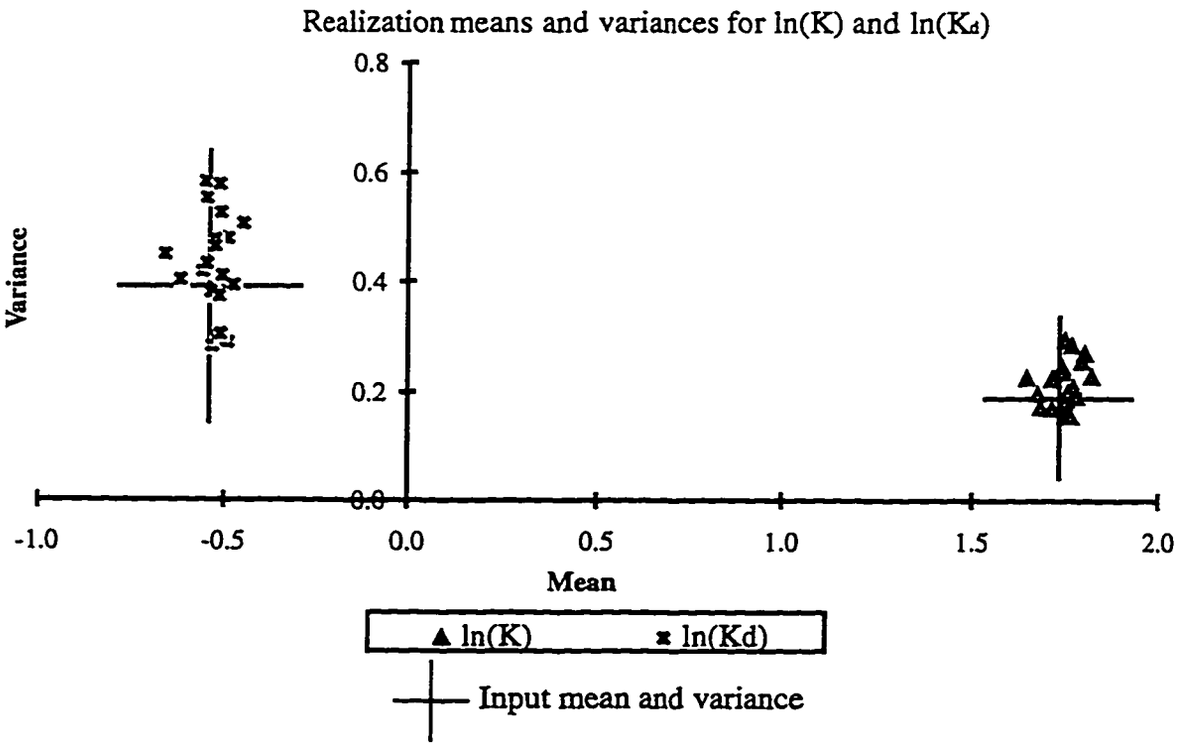

Figure 1: Scatter plot of field means versus variances for all individual realizations. Upper half of each cluster corresponds to cases with increased field variability from addition of high-frequency spike to input power spectrum.

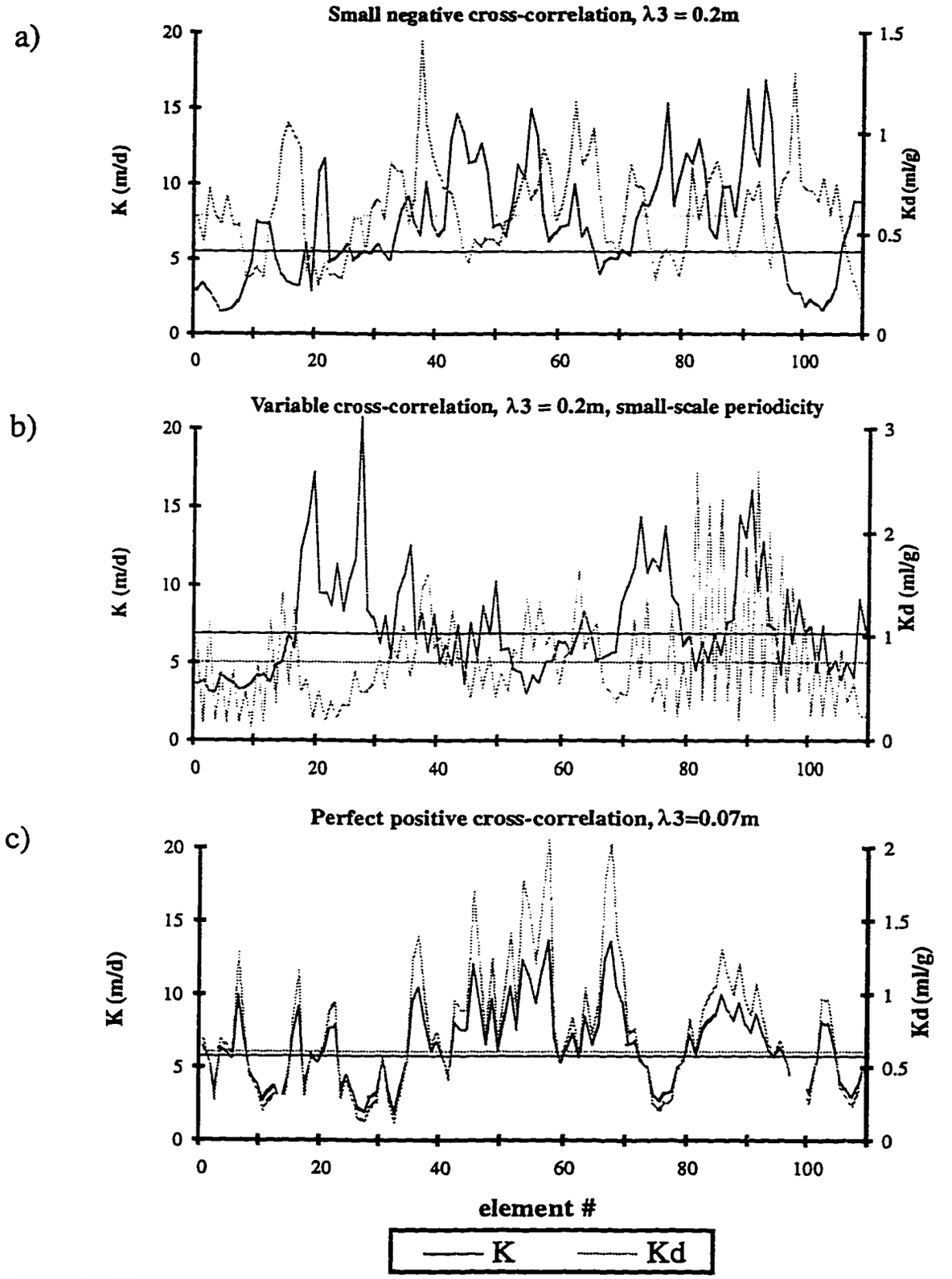

Figure 2: Transverse vertical transects of K and K_d fields showing effects of different auto and cross-correlation structures. Horizontal lines indicate means.

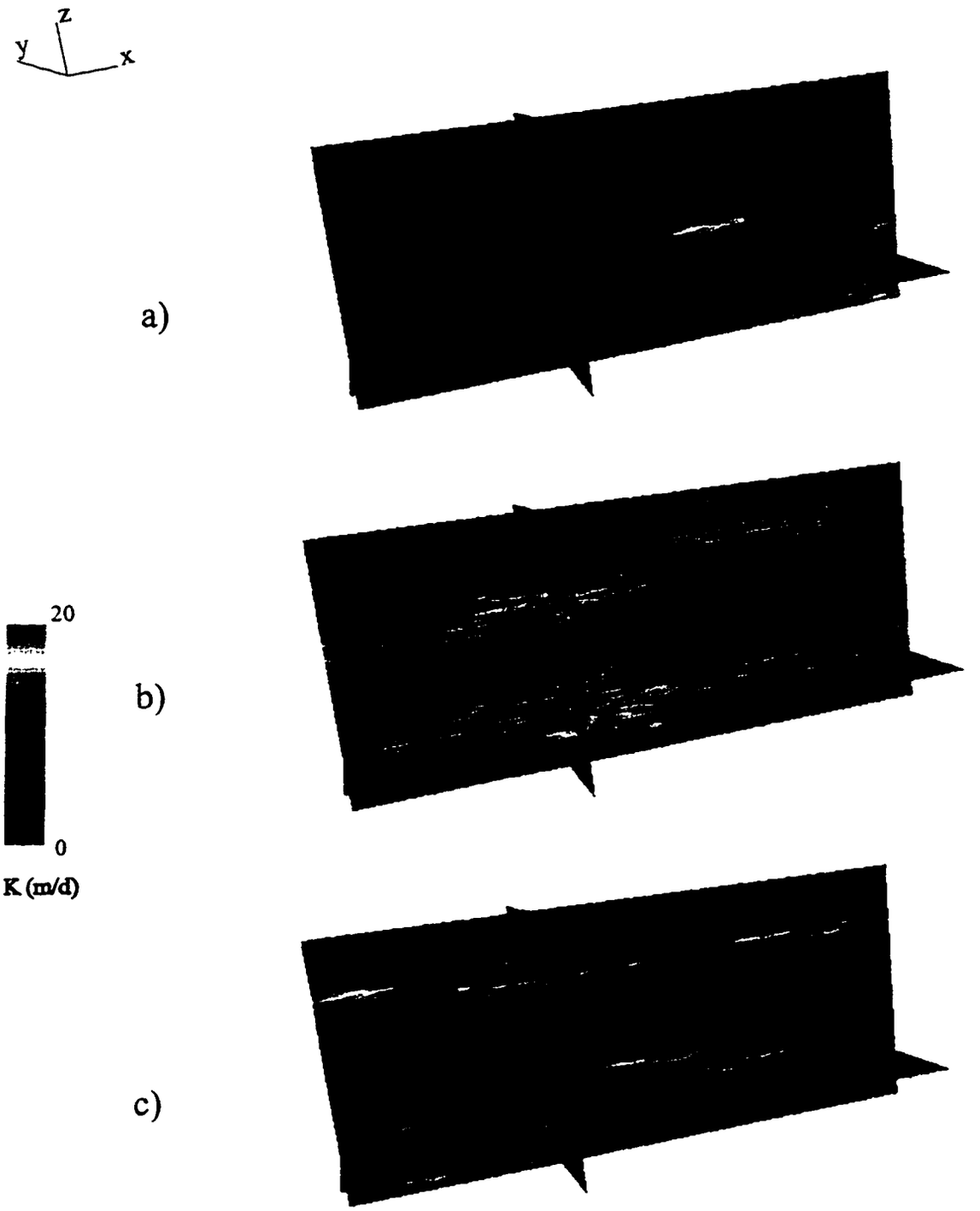

Figure 3: Three orthogonal slices from the full K field for vertical correlation lengths of a) 20 cm, b) 20 cm with small-scale periodicity and c) 7 cm. Field dimensions are 30 x 11 x 4.4 meters and vertical exaggeration is 3x.

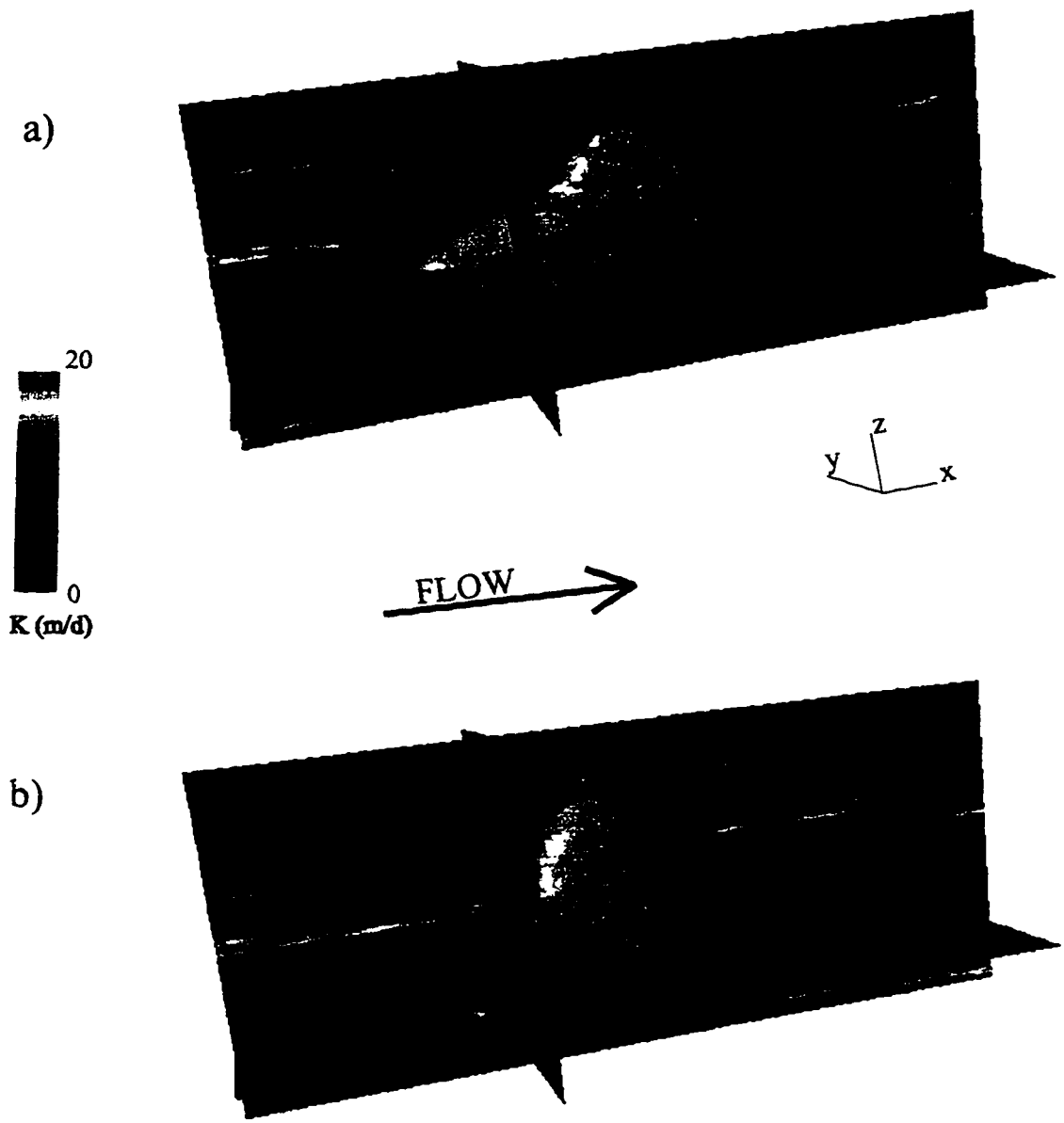

Figure 4: Reactive tracer plume longitudinal macrodispersivity is enhanced for small negative cross-correlation (a) compared to perfect positive correlation (b). Vertical correlation lengths are 20 cm. Concentration plume isosurface is 0.1% at time 450 days. Field dimensions are 30 x 11 x 4.4 meters, vertical exaggeration is 3x.

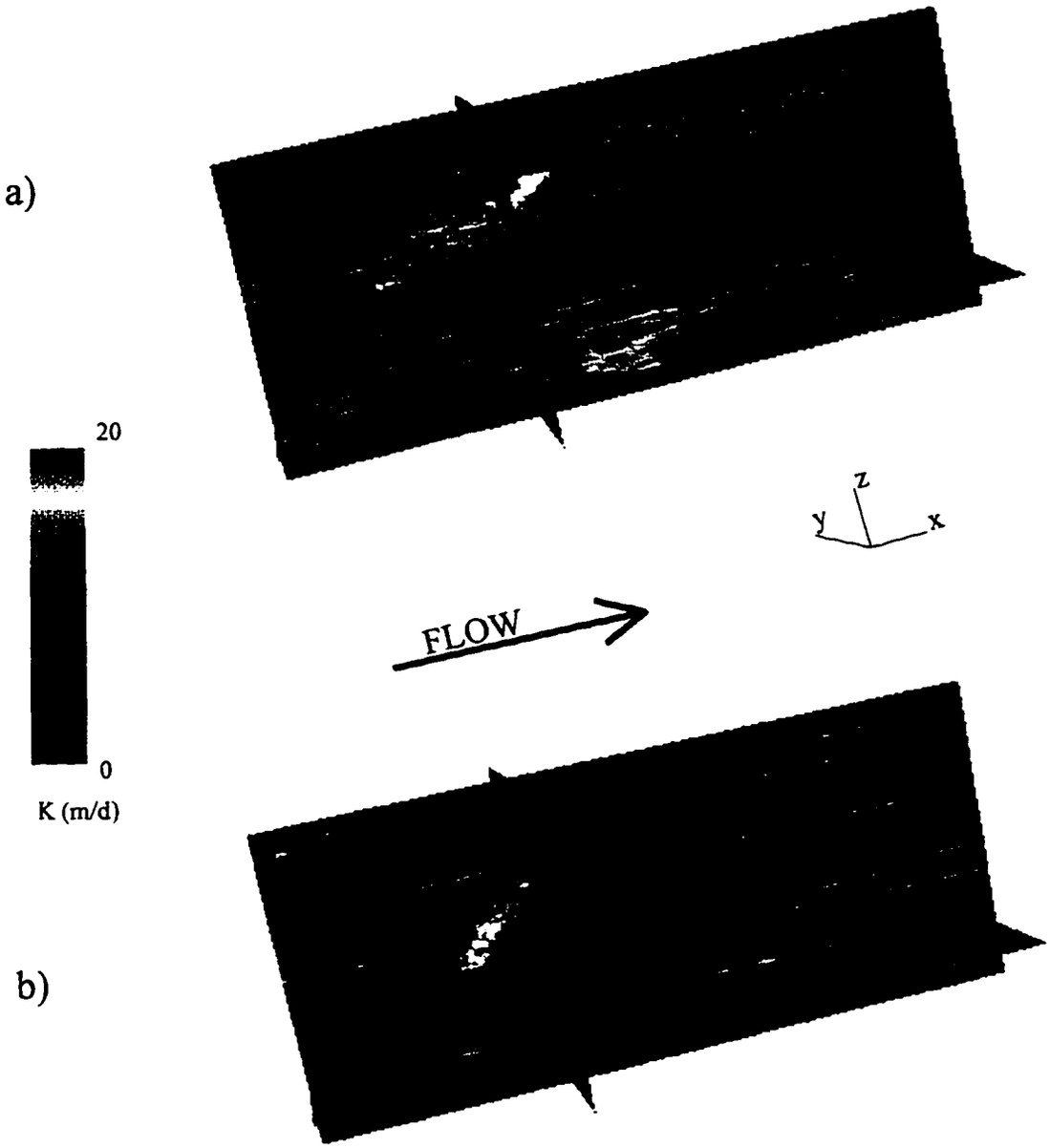

Figure 5: Enhanced longitudinal macrodispersivity results from an increase in small scale variability due to periodicity in velocity and retardation fields with λ_3=20 cm (a) compared to λ_3=7 cm (b). There is a small negative cross-correlation between velocity and retardation, and the 0.1% concentration isosurface is shown. Field dimensions are 30 x 11 x 4.4 meters, vertical exaggeration is 3x.

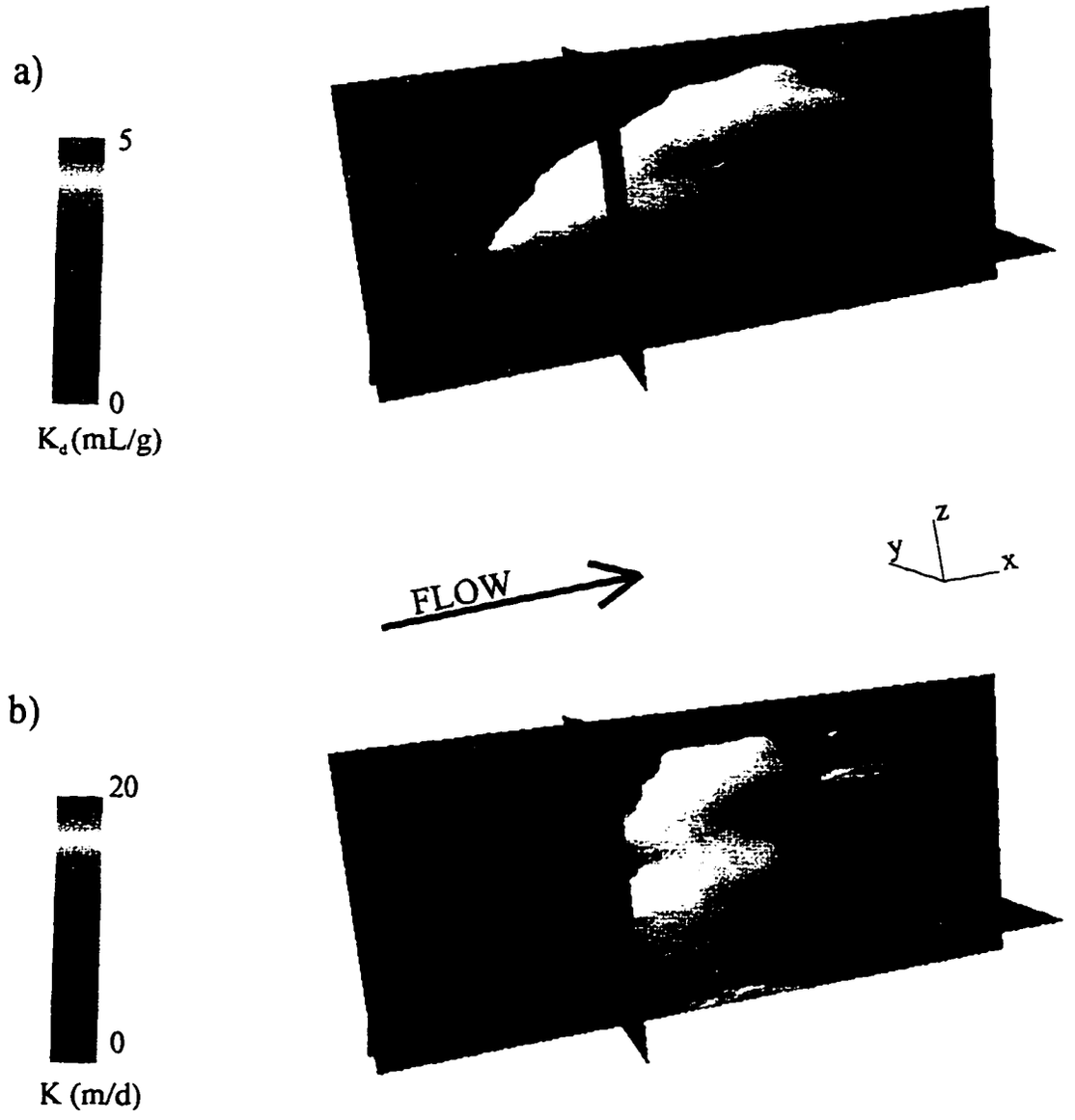

Figure 6: Plume longitudinal macrodispersivity is enhanced for a reactive solute. Reactive plume for time 300 days (with K_d field in the background) (a) has more spatial spreading than non-reactive plume at 103 days (with the common K field in the background). There is a small negative cross-correlation between K and K_d. Field dimensions are 30 x 11 x 4.4 meters, vertical exaggeration is 3x, and 0.1% concentration isosurfaces are shown.

COMPILED REFERENCES

Black, T.C. and D.L. Freyberg, Stochastic modelling of vertically averaged concentration uncertainty in a perfectly stratified aquifer, *Water Resources Research*, 23(6), 997-1004, 1987.

Bosma, W.J.P., S.E.A.T.M. van der Zee and C.J. van Duijn, Plume development of a nonlinearly adsorbing solute in heterogeneous porous formations, *Water Resources Research*, 32(6), 1569-1584, 1996.

Brigham, E.O., *The Fast Fourier Transform and its Applications*, Prentice Hall, Englewood Cliffs, New Jersey, 1989.

Brillinger, D.R., *Time Series: Data Analysis and Theory, Second Edition*, San Francisco: Holden-Day, 1981.

Burr, D.T., E.A. Sudicky and R.L. Naff, Nonreactive and reactive solute transport in three dimensional heterogeneous porous media: Mean displacement, plume spreading and uncertainty, *Water Resources Research*, 30(3), 791-815, 1994.

Dagan, G., *Flow and Transport in Porous Formations*, Springer-Verlag, 1989.

Davis, *Statistics and Data Analysis in Geology, 2nd Ed.*, John Wiley and Sons, 1973.

de Hoog, F.R., J.H. Knight and A.N. Stokes, An improved method for numerical inversion of Laplace transforms, *SIAM J. Sci. Stat. Comput.*, 3(3), 357-366, 1982.

Desai, C.S., and J.F. Abel, *An Introduction to the Finite Element Method*, Van Nostrand Reinhold, 1972.

Freyberg, D.L., A natural gradient experiment on solute transport in a sand aquifer 2. Spatial moments and the advection and dispersion of nonreactive tracers, *Water Resources Research*, 22(13), 2031-2046, 1986.

Frind, E.O., E.A. Sudicky and S.L. Schellenberg, Micro-scale modelling of plume evolution in heterogeneous media, *Stochastic Hydrol.*, 1, 241-262, 1987.

Garabedian, S.P., *Large-scale dispersive transport in aquifers: field experiments and reactive transport theory*, PhD Thesis, Massachusetts Institute of Technology, 1987.

Garabedian, S.P., D.R. LeBlanc, L.W. Gelhar and M.A. Celia, Large-scale natural gradient tracer test in sand and gravel, Cape Cod, Massachusetts 2. Analysis of spatial moments for a nonreactive tracer, *Water Resources Research*, 27(5), 911-924, 1991.

Gelhar, L.W. and C.L. Axness, Three-dimensional stochastic analysis of macrodispersion in aquifers, *Water Resources Research*, 19(1), 161-180, 1983.

Gelhar, L.W., and C. Welty, and K.R. Rehfeldt, A critical review of data on field-scale dispersion in aquifers, *Water Resources Research*, 28(7), 1955-1974, 1992.

Haley, D.F., E.A. Sudicky and R.L. Naff, Three-dimensional Monte Carlo analysis of spatial spreading during reactive solute transport by groundwater, in *Transport and Reactive Processes in Aquifers*, Dracos and Stauffer (eds), pp 437-443 A.A.Balkema/Brookfield, Rotterdam, 1994.

Halket, R.M., R.M. Allen-King, D.R. Gaylord and M.J.L. Robin, PCE sorption and hydraulic conductivity correlation with sedimentary facies in the Borden aquifer, *Water Resources Research* (submitted 1996).

Jenkins, G.M. and D.G. Watts, *Spectral Analysis and its Applications*, Holden-Day, California, 1968.

Massman, J. and R.E. Freeze, Groundwater contamination from waste management sites: The interaction between risk-based engineering and regulatory policy 1, Methodology, *Water Resources Research*, 23(2) 351-367, 1987

Massman, J. and R.E. Freeze, Groundwater contamination from waste management sites: The interaction between risk-based engineering and regulatory policy 2, Results, *Water Resources Research*, 23(2) 368-380, 1987

Naff, R.L., D.F. Haley and E.A. Sudicky, High-resolution Monte-Carlo simulation of flow and conservative transport in heterogeneous porous media: 1, Methodology and flow results, *Water Resources Research* (submitted 1996).

Naff, R.L., D.F. Haley and E.A. Sudicky, High-resolution Monte-Carlo simulation of flow and conservative transport in heterogeneous porous media: 2, Transport results, *Water Resources Research* (submitted 1996).

Press, W.H., B.P. Flannery, S.A. Teukolski, W.T. Vetterling, *Numerical Recipes, The Art of Scientific Computing,* Cambridge University Press, 1986.

Priestly, M.B., *Spectral Analysis and Time Series*, Academic Press, London, 1981.

Robin, M.J.L., *Migration of Reactive Solutes in Three-Dimensional Heterogeneous Porous Media*, PhD Thesis, University of Waterloo, 1991.

Robin, M.J.L., A.L. Gutjahr, E.A. Sudicky and J.L. Wilson, Cross-Correlated Random Field Generation With the Direct Fourier Transform Method, *Water Resources Research*, 29(7), 2385-2397, 1993.

Robin, M.J.L., E.A. Sudicky, R.W. Gillham and R.G. Kachanoski, Spatial Variability of Strontium Distribution Coefficients and Their Correlation With Hydraulic Conductivity in the Canadian Forces Base Borden Aquifer, *Water Resources Research*, 27(10), 2619-2632, 1991.

Snedecor, G.W. and Cochran, W.G., *Statistical Methods, 7th Ed.*, Iowa State University Press, 1980.

Sudicky, E.A., A natural gradient experiment on solute transport in a sand aquifer: spatial variability of hydraulic conductivity and its role in the dispersion process, *Water Resources Research*, 22(13), 2069-2082, 1986.

Sudicky, E.A., The Laplace Transform Galerkin technique: a time-continuous finite element theory and application to mass transport in groundwater, *Water Resources Research*, 25(8), 1833-1846, 1989.

Sudicky, E.A., S.L. Schellenberg and K.T.B. MacQuarrie, *Assessment of the behaviour of conservative and biodegradable solutes in porous media*, J.H. Cushman (ed.), Academic Press, 429-461, 1990.

Thompson, A.F.B., Numerical simulation of chemical migration in physically and chemically heterogeneous porous media, *Water Resources Research*, 29(11), 3709-3726, 1993.

Thompson, A.F.B. and L.W. Gelhar, Numerical simulation of solute transport in three-dimensional randomly heterogeneous porous media, *Water Resources Research*, 26(10), 2541-2562, 1990.

Vomvoris, E.G. and L.W. Gelhar, Stochastic analysis of the concentration variability in three-dimensional heterogeneous aquifer, *Water Resources Research*, 26(10), 2591-2602, 1987.

Wagner, B.J. and S.M. Gorelick, Optimal groundwater quality management under parameter uncertainty, *Water Resources Research*, 23(7), 1162-1174, 1987.

Wagner, B.J. and S.M. Gorelick, Reliable aquifer remediation in the presence of spatially varying hydraulic conductivity: From data to design, *Water Resources Research*, 24(4), 566-578, 1989.

Zhang, Y.K. and J. A. Chi, An evaluation of nonlinearity in spatial second moments of ensemble mean concentration in heterogeneous porous media, *Water Resources Research*, 31(12), 2991-3005, 1995.

Zar, J.H., *Biostatistical Analysis, 2nd Ed.*, Prentice-Hall, New Jersey, 1984.

APPENDIX A
Repeated measures ANOVA results for effect of type of correlation between velocity and retardation on the zeroth moment (mass)

The repeated measures model used was:

$$Mass = time + time*cross + time*auto + time*cross*auto + \epsilon$$

applied to the zeroth moments for every realization. The variable *time* refers to the time step, *auto* refers to the type of autocorrelation and the variable *cross* refers to the type of cross-correlation. The raw data is located at the end of this appendix.

The ANOVA was performed using SYSTAT (version 5.02), and the output from the test follows. The output of primary interest is the p-value for each variable, or combination of variables.
The p-value indicates the probability of committing an error in declaring an effect significant; 1-p is the confidence level.

SYSTAT output:

LEVELS ENCOUNTERED DURING PROCESSING ARE:
XCORS
1 2 3
AUTOS
1 2 3

NUMBER OF CASES PROCESSED: 21

DEPENDENT VARIABLE MEANS:

T1	T2	T3	T4	T5	T6
0.135	0.131	0.124	0.120	0.119	0.119

UNIVARIATE AND MULTIVARIATE REPEATED MEASURES ANALYSIS

BETWEEN SUBJECTS

SOURCE	*SS*	*DF*	*MS*	*F*	*P*
XCORS	0.269	2	0.134	4.480	0.035
AUTOS	0.030	2	0.015	0.507	0.614
XCORS*AUTOS	0.114	4	0.029	0.952	0.468
ERROR	0.360	12	0.030		

WITHIN SUBJECTS

SOURCE	*SS*	*DF*	*MS*	*F*	*P*	*G-G*	*H-F*
time	0.003	5	0.001	2.326	0.054	0.134	0.093
time*XCORS	0.004	10	0.000	1.815	0.077	0.178	0.126
time*AUTOS	0.001	10	0.000	0.368	0.956	0.783	0.891
time*XCORS*AUTOS	0.001	20	0.000	0.290	0.998	0.938	0.986
ERROR	0.014	60	0.000				

GREENHOUSE-GEISSER EPSILON: 0.3106
HUYNH-FELDT EPSILON : 0.5860

The results of the ANOVA indicate that the effect of the time step on mass is not

significant (p=0.054) and that this effect depends on neither the type of correlation nor the interaction. The lack of significance indicates that variations in mass over time are random, which is what we would expect if a plume encounters zones of high and low K_d at random.

The following table shows the mass of contaminant in solution for each scenario, and each time step. The headings Auto and Cross refer to the types of auto and cross-correlation between the K and K_d fields. The headings T1,...,T6 refer to the time steps (T1=200, T2=300, T3=400, T4=450, T5=500, T6=550 days).

Cross-correlation types are as follows:
1. Small negative cross-correlation between K and K_d
2. Variable correlation (negative at small scales, positive at scales larger than 1 m)
3. Perfect positive correlation

Autocorrelation types are as follows:
1. $\lambda_3 = 20$ cm
2. $\lambda_3 = 20$ cm, small-scale periodicity added
3. $\lambda_3 = 7$ cm

Zeroth moments for all realizations, according to time step.

Cross	Auto	T1	T2	T3	T4	T5	T6
1	1	0.082	0.084	0.083	0.083	0.086	0.088
1	1	0.116	0.099	0.089	0.086	0.084	0.082
1	2	0.062	0.063	0.069	0.072	0.074	0.075
1	2	0.063	0.063	0.067	0.069	0.071	0.071
1	3	0.092	0.084	0.087	0.09	0.092	0.094
1	3	0.059	0.055	0.054	0.053	0.054	0.054
2	1	0.079	0.075	0.073	0.072	0.073	0.073
2	1	0.067	0.061	0.063	0.065	0.068	0.071
2	2	0.061	0.061	0.063	0.065	0.066	0.066
2	2	0.076	0.07	0.065	0.062	0.06	0.059
2	3	0.081	0.076	0.074	0.075	0.077	0.078
2	3	0.059	0.054	0.052	0.053	0.054	0.056
3	1	0.157	0.16	0.149	0.138	0.131	0.128
3	1	0.152	0.111	0.091	0.082	0.077	0.076
3	2	0.33	0.314	0.294	0.274	0.256	0.236
3	2	0.448	0.43	0.392	0.372	0.375	0.395
3	2	0.209	0.254	0.248	0.242	0.234	0.228
3	2	0.087	0.082	0.091	0.097	0.103	0.105
3	2	0.254	0.255	0.218	0.202	0.188	0.179
3	3	0.077	0.072	0.072	0.076	0.082	0.089
3	3	0.222	0.223	0.208	0.198	0.192	0.191

APPENDIX B
ANOVA results for effect of type of correlation between velocity and retardation on the first moment (centre of mass)

The ANOVA model

$$M_{100} = auto + \epsilon$$

was applied to the centres of mass for a non-reactive solute for the third time step. The variable *auto* refers to the type of autocorrelation, the type of cross-correlation has no impact on the results of the non-reactive simulations, and thus is not considered for this ANOVA. The raw data is located at the end of this appendix.

The ANOVA was performed using SYSTAT (version 5.02), and the output from the test follows. The output of primary interest is the p-value for each variable, or combination of variables. The p-value indicates the probability of committing an error in declaring an effect significant; 1-p is the confidence level.

The first ANOVA result is for the centre of mass calculations based on a retardation factor calculated from the arithmetic mean of the truncated K_d field (M^*_{100A}).

SYSTAT output:

```
>MODEL M100NA = CONSTANT + AUTOS

WED 1/15/97 10:40:47 AM  H:\MONTE\SYSTAT\M1\COFM_T3.SYS
LEVELS ENCOUNTERED DURING PROCESSING ARE:
AUTOS
 1       2       3

DEP VAR: M100NA    N:    18 MULTIPLE R: 0.500 SQUARED MULTIPLE R: 0.250

            ANALYSIS OF VARIANCE

SOURCE     SUM-OF-SQUARES     DF     MEAN-SQUARE   F-RATIO     P
AUTOS          33.702          2        16.851        2.501    0.115
ERROR         101.050         15         6.737
```

For a non-reactive solute there was no significant effect of the type of autocorrelation (p=0.115) on the position of the plume centres of mass.

The ANOVA model

$$M_{100} = cross + auto + cross*auto + \epsilon$$

was applied to the first moments for a reactive solute (M_{100}), also at the third time step.

SYSTAT output:

MODEL M100 = CONSTANT + XCOR$+AUTO$+XCOR$*AUTO$

LEVELS ENCOUNTERED DURING PROCESSING ARE:
XCOR$
1 2 3
AUTO$
1 2 3

DEP VAR: M100 N: 18 MULTIPLE R: 0.903 SQUARED MULTIPLE R: 0.815

ANALYSIS OF VARIANCE

SOURCE	*SUM-OF-SQUARES*	*DF*	*MEAN-SQUARE*	*F-RATIO*	*P*
XCOR$	18.795	2	9.397	11.715	0.003
AUTO$	5.166	2	2.583	3.220	0.088
XCOR$*AUTO$	7.880	4	1.970	2.456	0.121
ERROR	7.220	9	0.802		

POST HOC TESTS

COL/ ROW	XCOR$	AUTO$
1 1	1	
2 1	2	
3 1	3	
4 2	1	
5 2	2	
6 2	3	
7 3	1	
8 3	2	
9 3	3	

USING MODEL MSE OF .802 WITH 9. DF.

MATRIX OF PAIRWISE MEAN DIFFERENCES:

	1	2	3	4	5	
1	0.000					
2	-0.200	0.000				
3	-2.950	-2.750	0.000			
4	-3.450	-3.250	-0.500	0.000		
5	-3.270	-3.070	-0.320	0.180	0.000	
6	-3.135	-2.935	-0.185	0.315	0.135	
7	-0.360	-0.160	2.590	3.090	2.910	
8	-1.625	-1.425	1.325	1.825	1.645	
9	-1.590	-1.390	1.360	1.860	1.680	

	6	7	8	9
6	0.000			
7	2.775	0.000		
8	1.510	-1.265	0.000	
9	1.545	-1.230	0.035	0.000

BONFERRONI ADJUSTMENT.
MATRIX OF PAIRWISE COMPARISON PROBABILITIES (p-values):

	1	2	3	4	5	
1	1.000					
2	1.000	1.000				
3	0.336	0.480	1.000			
4	0.140	0.198	1.000	1.000		
5	0.191	0.271	1.000	1.000	1.000	
6	0.242	0.345	1.000	1.000	1.000	

7	1.000	1.000	0.642	0.262	0.360
8	1.000	1.000	1.000	1.000	1.000
9	1.000	1.000	1.000	1.000	1.000

	6	7	8	9
6	1.000			
7	0.459	1.000		
8	1.000	1.000	1.000	
9	1.000	1.000	1.000	1.000

COL/
ROW XCOR$
1 1
2 2
3 3

USING MODEL MSE OF .802 WITH 9. DF.
MATRIX OF PAIRWISE MEAN DIFFERENCES:

	1	2	3
1	0.000		
2	-2.235	0.000	
3	-0.142	2.093	0.000

BONFERRONI ADJUSTMENT.
MATRIX OF PAIRWISE COMPARISON PROBABILITIES (P-values):

	1	2	3
1	1.000		
2	0.006	1.000	
3	1.000	0.009	1.000

COL/
ROW AUTO$
1 1
2 2
3 3

USING LEAST SQUARES MEANS.

USING MODEL MSE OF .802 WITH 9. DF.
MATRIX OF PAIRWISE MEAN DIFFERENCES:

	1	2	3
1	0.000		
2	-0.428	0.000	
3	-1.288	-0.860	0.000

BONFERRONI ADJUSTMENT.
MATRIX OF PAIRWISE COMPARISON PROBABILITIES (P-values):

	1	2	3
1	1.000		
2	1.000	1.000	
3	0.103	0.392	1.000

For a reactive solute, the location of the centre of mass (M_{100}) depends on the type of cross-correlation (p=0.003) but not on the type of autocorrelation (p=0.088) nor on the interaction between auto and cross-correlation (p=0.121). Post-hoc tests indicated that

there was no single scenario that differed significantly from any other, however, when grouping the scenarios according to cross-correlation type, results indicated that the centre of mass of a reactive solute travelled significantly less far for a variable correlation between the ln(K) and ln(K_d) fields, than for a small negative correlation (p=0.006) or a perfect positive correlation (p=0.009).

The following table contains the centre of mass values for a reactive solute a non-reactive solute at the third time step, for each Monte Carlo scenario.

Cross-correlation types are as follows:
1. Small negative cross-correlation between K and K_d
2. Variable correlation (negative at small scales, positive at scales larger than 1 m)
3. Perfect positive correlation

Autocorrelation types are as follows:
1. $\lambda_3 = 20$ cm
2. $\lambda_3 = 20$ cm, small-scale periodicity added
3. $\lambda_3 = 7$ cm

Cross	Auto	M_{100} (Reactive solute)	M_{100} (Non-reactive solute)
1	1	13.2	20.3
1	1	15.3	17.5
1	2	13.1	21.5
1	2	15	22.2
1	3	12.2	17.4
1	3	10.4	15.4
2	1	10.7	16.8
2	1	10.9	19.4
2	2	11.49	19.0
2	2	10.47	15.5
2	3	11.4	10.08
2	3	10.83	16.67
3	1	13.69	15.38
3	1	14.09	15.58
3	2	13.2	18.75
3	2	12.05	19.98
3	3	12.39	19.12
3	3	12.93	18.28

APPENDIX C
Calculation of adjusted first moments and adjusted time steps.

Table CI shows the original centres of mass of the non-reactive solute for three scenarios (Cases 11, 12 and 13).

Table CI: Raw first moments with original time steps (non-reactive solute, x-direction)

Real. #	time (d)	Case 11	Case 12	Case 13
1	69	11	11.4	10.6
1	103	15.6	16.5	13.8
1	138	20.3	21.5	17.4
1	155	22.5	23	19.3
1	172	24.2	23.7	21.1
1	190	25.5	24.3	23
2	69	11.2	12.9	9.31
2	103	14.4	17.6	12.2
2	138	17.5	22.2	15.4
2	155	19	23.9	17
2	172	20.4	25	18.7
2	190	21.8	25.6	20.5

Because output retardation factors varied between realizations, first moment values for a non-reactive solute could not be compared directly to those for a reactive solute: the non-reactive solute first moments needed an adjustment to reflect the varying retardation coefficients. This adjustment took the following form: because the first moment versus time (velocity) curves were linear, a linear interpolation was performed to determine the adjusted first moment values. The formula used was:

$$M^{*}_{100} = \frac{dM_{100}}{dt} t^{*} + 3.45$$

where M^{*}_{100} is the adjusted centre of mass location, dM_{100}/dt is the average plume velocity, t^{*} is the adjusted time value, and the final term (3.45) is the x-coordinate of the centre of mass of the source, in metres. The adjusted time value was calculated from:

$$t^* = \frac{t}{R}$$

where t is the corresponding time step for the reactive case, and R is either the output arithmetic retardation (R_A) factor or the geometric retardation factor (R_G) (based on the arithmetic or geometric mean of the ln(K_d) fields, respectively). M^*_{100A} represents the adjusted first moment calculated using R_A, and M^*_{100G} represents the one calculated using R_G.

Table CII shows the adjusted centres of mass, with the corresponding adjusted times

Table CII: Adjusted first moments, with corresponding time steps (non-reactive solute, x-direction).

R_A	Case 11		Case 12		Case 13	
Real. #	t^* (d)	M^*_{100A}	t^* (d)	M^*_{100A}	t^* (d)	M^*_{100A}
1	46	9.58	41	9.41	45	8.07
1	69	12.64	61	12.40	68	10.38
1	92	15.71	81	15.38	90	12.68
1	103	17.24	92	16.87	101	13.84
1	114	18.77	102	18.36	113	14.99
1	126	20.30	112	19.85	124	16.15
2	44	7.32	42	9.11	44	7.36
2	67	9.26	62	11.94	66	9.32
2	89	11.19	83	14.78	88	11.27
2	100	12.16	94	16.19	98	12.25
2	111	13.13	104	17.61	109	13.23
2	122	14.10	114	19.02	120	14.21

(using R_A) for the same three scenarios as shown in Table CI (Cases 11, 12 and 13).

For example, for Case 11 and the first time step of realization 1 (originally 200 days), t^* = 200/4.374 = 46 days and M^*_{100} = (0.133)(46) + 3.45 = 9.58 m.

Table CIII shows the adjusted centres of mass, with the corresponding adjusted times, using R_G (the retardation coefficient calculated from the geometric mean of the field K_d), for the same three scenarios as shown in Table CI (Cases 11 ,12 and 13).

Table CIII: Adjusted first moments, with corresponding time steps (non-reactive solute, x-direction).

	Case 11		Case 12		Case 13	
Real. #	t^* (d)	M^*_{100G}	t^* (d)	M^*_{100G}	t^* (d)	M^*_{100G}
1	49	10.08	48	10.42	49	8.48
1	74	13.39	71	13.91	74	10.99
1	99	16.70	95	17.40	98	13.50
1	111	18.36	107	19.14	110	14.76
1	124	20.02	119	20.88	123	16.01
1	136	21.67	131	22.63	135	17.27
2	50	7.80	49	10.10	49	7.82
2	75	9.97	73	13.43	73	10.01
2	96	12.14	98	16.75	98	12.20
2	112	13.23	110	18.41	110	13.29
2	124	14.32	122	20.08	122	14.38
2	137	15.40	134	21.74	135	15.48

Table CIV shows the centres of mass for the corresponding reactive simulations. Only three cases are shown in the tables, however the adjustment was made for all cases.

The point of interest here is in a comparison of the M^*_{100} columns of Tables CII and CIII with the corresponding M_{100} columns of Table CIV. See Appendix D for the ANOVA results of this comparison.

Table CIV: First moments for a reactive solute.

Real. #	Time (days)	M_{100}		
		Case 11	Case 12	Case 13
1	200	7.65	7.49	8.6
1	300	10.1	9.85	10.4
1	400	13.2	13.1	12.2
1	450	14.9	14.7	13.1
1	500	16.5	16.2	14.1
1	550	18	17.4	15.1
2	200	9.94	9.67	7.34
2	300	12.8	12.3	8.97
2	400	15.3	15	10.4
2	450	16.3	16.3	11.1
2	500	17.2	17.4	11.8
2	550	17.9	18.4	12.6

APPENDIX D

Repeated measures ANOVA results to test for differences between locations of centres of mass for a non-reactive solute at time t/R and a reactive solute at time t (400 days)

The ANOVA model

$$M_{100} = solute + solute*cross + solute*auto + solute*cross*auto + \epsilon$$

was applied first to compare the arithmetically adjusted centre of mass for a non-reactive solute plume (M^*_{100A}) with the centre of mass for the reactive solute plume (M_{100}). The variable *solute* refers to the type of solute (reactive or non-reactive), *auto* and *cross* refer to the types of auto and cross-correlation, respectively. The variable *solute* is treated as a repeated measure because of the correlation caused by using the same flow field. The raw data is located at the end of this appendix.

The ANOVA was performed using SYSTAT (version 5.02), and the output from the test follows. The output of primary interest is the p-value for each variable, or combination of variables. The p-value indicates the probability of committing an error in declaring an effect significant; 1-p is the confidence level.

The first ANOVA results are for a comparison between M^*_{100A} and M_{100}.

SYSTAT output:

```
>CATEGORY XCORS AUTOS
>MODEL R NR = CONSTANT + XCORS+AUTOS+XCORS*AUTOS /REPEAT=2 NAMES='solute'

LEVELS ENCOUNTERED DURING PROCESSING ARE:
XCORS
 1       2       3
AUTOS
 1       2       3

NUMBER OF CASES PROCESSED:    18

DEPENDENT VARIABLE MEANS
              R         NR
            12.408    12.989


UNIVARIATE REPEATED MEASURES ANALYSIS

BETWEEN SUBJECTS
```

SOURCE	*SS*	*DF*	*MS*	*F*	*P*
XCORS	13.380	2	6.690	8.968	0.007
AUTOS	4.280	2	2.140	2.869	0.109
XCORS*AUTOS	15.575	4	3.894	5.219	0.019
ERROR	6.714	9	0.746		

WITHIN SUBJECTS

SOURCE	SS	DF	MS	F	P	G-G	H-F
solute	3.045	1	3.045	1.839	0.208	.	.
solute*XCOR$	7.834	2	3.917	2.366	0.149	.	.
solute*AUTO$	2.422	2	1.211	0.732	0.508	.	.
solute*XCOR$*AUTO$	2.457	4	0.614	0.371	0.824	.	.
ERROR	14.900	9	1.656				

GREENHOUSE-GEISSER EPSILON: .
HUYNH-FELDT EPSILON : .

There was no significant difference between the two sets of first moment data (p=0.208) due to the type of solute. This means that there is no significant difference between the location of the centre of mass for a non-reactive solute at time t/R_A and the location of the centre of mass for a reactive solute at time t, where R_A is the retardation coefficient calculated from the arithmetic average of K_d.

These second ANOVA results are for a comparison of M^*_{100G} with M_{100}.

SYSTAT results:

SUN 1/05/97 11:58:35 AM H:\MONTE\SYSTAT\M1\COFM_T3G.SYS
LEVELS ENCOUNTERED DURING PROCESSING ARE:
XCOR$
1 2 3
AUTO$
1 2 3

NUMBER OF CASES PROCESSED: 18

DEPENDENT VARIABLE MEANS

R	NR
12.408	14.207

UNIVARIATE REPEATED MEASURES ANALYSIS

BETWEEN SUBJECTS

SOURCE	SS	DF	MS	F	P
XCOR$	14.497	2	7.248	9.152	0.007
AUTO$	7.179	2	3.589	4.532	0.043
XCOR$*AUTO$	18.665	4	4.666	5.892	0.013
ERROR	7.128	9	0.792		

WITHIN SUBJECTS

SOURCE	SS	DF	MS	F	P	G-G	H-F
solute	29.126	1	29.126	16.722	0.003	.	.
solute*XCOR$	7.296	2	3.648	2.094	0.179	.	.
solute*AUTO$	4.035	2	2.017	1.158	0.357	.	.
solute*XCOR$ *AUTO$	3.272	4	0.818	0.470	0.757	.	.
ERROR	15.676	9	1.742				

GREENHOUSE-GEISSER EPSILON: .
HUYNH-FELDT EPSILON : .

The above results indicate that the location of the centre of mass of a reactive solute

plume at time t is significantly greater (farther along) than that of a non-reactive plume at time t/R_G (p=0.003), where R_G is the retardation factor based on the geometric mean of the K_d field. This effect did not depend on the type of cross-correlation (p=0.179, the type of autocorrelation (p=0.357, or the specific scenario (p=0.757).

The following table contains the centre of mass values for the reactive case (M_{100}) and the adjusted calculations for the non-reactive case (M^*_{100A} and M^*_{100G}) for each Monte Carlo scenario.
Cross-correlation types are as follows:
1. Small negative cross-correlation between K and K_d
2. Variable correlation (negative at small scales, positive at scales larger than 1 m)
3. Perfect positive correlation

Autocorrelation types are as follows:
1. $\lambda_3 = 20$ cm
2. $\lambda_3 = 20$ cm, small-scale periodicity added
3. $\lambda_3 = 7$ cm

First moments for reactive solute plume at time T3 (M_{100}) and non-reactive solute plumes at times $T3/R_A$ (M^*_{100A}) and $T3/R_G$ (M^*_{100A}).

Cross	Auto	M_{100} Reactive	M^*_{100A} Non-reactive	M^*_{100G} Non-reactive
1	1	13.2	15.71	16.704
1	1	15.3	11.19	12.143
1	2	13.1	15.38	17.396
1	2	15	14.78	16.75
1	3	12.2	12.68	13.501
1	3	10.4	11.27	12.198
2	1	10.7	12.05	12.797
2	1	10.9	13.58	14.888
2	2	11.49	12.61	14.066
2	2	10.47	11.76	13.132
2	3	11.4	13.86	14.806
2	3	10.83	12.96	14.065
3	1	13.69	12.67	13.837
3	1	14.09	11.82	12.823
3	2	13.2	12.34	13.811
3	2	12.05	13.52	14.982
3	3	12.39	12.89	14.03
3	3	12.93	12.74	13.792

APPENDIX E
ANOVA results for effect of type of correlation between velocity and retardation on the retardation coefficient

The ANOVA model

$$R = cross + auto + cross*auto + \epsilon$$

was applied to R_A, R_G, and R_V successively, where R_A is the arithmetic retardation coefficient, R_G is the geometric retardation coefficient, and R_V is the retardation coefficient based on the ratio of the velocity of the non-reactive solute plume and the reactive solute plume. The variables *auto* and *cross* refer to the types of auto and cross-correlation, respectively. The raw data is located at the end of this appendix.

The ANOVA was performed using SYSTAT (version 5.02), and the output from the test follows. The output of primary interest is the p-value for each variable, or combination of variables.
The p-value indicates the probability of committing an error in declaring an effect significant; 1-p is the confidence level.

SYSTAT output for R_A:

```
>ESAV 'H:\MONTE\SYSTAT\M1\RARGRV.SYS'

>MODEL RA = CONSTANT + XCOR$+AUTO$+XCOR$*AUTO$

LEVELS ENCOUNTERED DURING PROCESSING ARE:
XCOR$
 1        2        3
AUTO$
 1        2        3

DEP VAR:    RA    N:    18  MULTIPLE R: 0.859  SQUARED MULTIPLE R: 0.738

             ANALYSIS OF VARIANCE

SOURCE          SUM-OF-SQUARES   DF   MEAN-SQUARE   F-RATIO      P
XCOR$                    0.029    2         0.014     0.678    0.532
AUTO$                    0.485    2         0.242    11.350    0.003
XCOR$*AUTO$              0.029    4         0.007     0.336    0.847
ERROR                    0.192    9         0.021

COL/
ROW  XCOR$    AUTO$
 1 1      1
 2 1      2
 3 1      3
 4 2      1
 5 2      2
 6 2      3
 7 3      1
 8 3      2
 9 3      3

USING MODEL MSE OF      .021 WITH     9. DF.
```

MATRIX OF PAIRWISE MEAN DIFFERENCES:

	1	2	3	4	5
1	0.000				
2	0.420	0.000			
3	0.065	-0.355	0.000		
4	0.110	-0.310	0.045	0.000	
5	0.400	-0.020	0.335	0.290	0.000
6	0.075	-0.345	0.010	-0.035	-0.325
7	0.055	-0.365	-0.010	-0.055	-0.345
8	0.480	0.060	0.415	0.370	0.080
9	0.240	-0.180	0.175	0.130	-0.160

	6	7	8	9
6	0.000			
7	-0.020	0.000		
8	0.405	0.425	0.000	
9	0.165	0.185	-0.240	0.000

BONFERRONI ADJUSTMENT.

MATRIX OF PAIRWISE COMPARISON PROBABILITIES (P-values)

	1	2	3	4	5
1	1.000				
2	0.660	1.000			
3	1.000	1.000	1.000		
4	1.000	1.000	1.000	1.000	
5	0.826	1.000	1.000	1.000	1.000
6	1.000	1.000	1.000	1.000	1.000
7	1.000	1.000	1.000	1.000	1.000
8	0.340	1.000	0.698	1.000	1.000
9	1.000	1.000	1.000	1.000	1.000

	6	7	8	9
6	1.000			
7	1.000	1.000		
8	0.781	0.625	1.000	
9	1.000	1.000	1.000	1.000

COL/
ROW XCORS
1 1
2 2
3 3

USING MODEL MSE OF .021 WITH 9. DF.
MATRIX OF PAIRWISE MEAN DIFFERENCES:

	1	2	3
1	0.000		
2	0.033	0.000	
3	0.097	0.063	0.000

BONFERRONI ADJUSTMENT.

MATRIX OF PAIRWISE COMPARISON PROBABILITIES (P-values):

	1	2	3
1	1.000		

```
      2     1.000     1.000
      3     0.844     1.000     1.000

COL/
ROW  AUTOS
 1 1
 2 2
 3 3

USING MODEL MSE OF      .021 WITH    9. DF.
MATRIX OF PAIRWISE MEAN DIFFERENCES:

             1         2         3

      1     0.000
      2     0.378     0.000
      3     0.072    -0.307     0.000
BONFERRONI ADJUSTMENT.

MATRIX OF PAIRWISE COMPARISON PROBABILITIES (P-values):

             1         2         3

      1     1.000
      2     0.005     1.000
      3     1.000     0.016     1.000
```

The addition of small scale periodicity to the autocorrelation structure of the fields significantly increased R_A (p=0.003), however, neither the type of cross-correlation (p=0.532) nor the interaction (p=0.847) significantly affected R_A.

SYSTAT output for R_G:

```
>MODEL RG = CONSTANT + XCORS+AUTOS+XCORS*AUTOS

LEVELS ENCOUNTERED DURING PROCESSING ARE:
XCORS
 1         2         3
AUTOS
 1         2         3

DEP VAR:    RG    N:    18  MULTIPLE R: 0.690  SQUARED MULTIPLE R: 0.475

              ANALYSIS OF VARIANCE

SOURCE          SUM-OF-SQUARES     DF     MEAN-SQUARE     F-RATIO     P
XCORS                    0.012      2           0.006       0.475     0.636
AUTOS                    0.063      2           0.031       2.478     0.139
XCORS*AUTOS              0.029      4           0.007       0.563     0.696
ERROR                    0.114      9           0.013
```

The geometric mean retardation coefficient, R_G, did not depend on the autocorrelation (p=0.139), the cross-correlation (p=0.636), nor on the interaction (p=0.696).

SYSTAT output for R_V:

```
>MODEL RV = CONSTANT + XCORS+AUTOS+XCORS*AUTOS

LEVELS ENCOUNTERED DURING PROCESSING ARE:
XCORS
```

1 2 3
AUTO$
1 2 3

DEP VAR: RV N: 18 MULTIPLE R: 0.930 SQUARED MULTIPLE R: 0.864

ANALYSIS OF VARIANCE

SOURCE	*SUM-OF-SQUARES*	*DF*	*MEAN-SQUARE*	*F-RATIO*	*P*
XCOR$	3.878	2	1.939	12.691	0.002
AUTO$	2.438	2	1.219	7.979	0.010
XCOR$*AUTO$	2.436	4	0.609	3.987	0.039
ERROR	1.375	9	0.153		

COL/
ROW XCOR$ AUTO$
1 1 1
2 1 2
3 1 3
4 2 1
5 2 2
6 2 3
7 3 1
8 3 2
9 3 3

POST HOC TEST OF RV

USING MODEL MSE OF .153 WITH 9. DF.
MATRIX OF PAIRWISE MEAN DIFFERENCES:

	1	2	3	4	5
1	0.000				
2	0.960	0.000			
3	1.555	0.595	0.000		
4	1.610	0.650	0.055	0.000	
5	1.230	0.270	-0.325	-0.380	0.000
6	1.695	0.735	0.140	0.085	0.465
7	-0.410	-1.370	-1.965	-2.020	-1.640
8	1.045	0.085	-0.510	-0.565	-0.185
9	0.510	-0.450	-1.045	-1.100	-0.720

	6	7	8	9
6	0.000			
7	-2.105	0.000		
8	-0.650	1.455	0.000	
9	-1.185	0.920	-0.535	0.000

BONFERRONI ADJUSTMENT.

MATRIX OF PAIRWISE COMPARISON PROBABILITIES (P-values):

	1	**2**	**3**	**4**	**5**
1	**1.000**				
2	**1.000**	**1.000**			
3	**0.116**	**1.000**	**1.000**		
4	**0.094**	**1.000**	**1.000**	**1.000**	
5	**0.425**	**1.000**	**1.000**	**1.000**	**1.000**
6	**0.068**	**1.000**	**1.000**	**1.000**	**1.000**
7	**1.000**	**0.240**	**0.026**	**0.021**	**0.084**
8	**0.917**	**1.000**	**1.000**	**1.000**	**1.000**
9	**1.000**	**1.000**	**0.917**	**0.728**	**1.000**

	6	7	8	9
6	1.000			
7	0.016	1.000		
8	1.000	0.171	1.000	
9	0.511	1.000	1.000	1.000

COL/
ROW XCOR$
1 1
2 2
3 3

USING MODEL MSE OF .153 WITH 9. DF.
MATRIX OF PAIRWISE MEAN DIFFERENCES:

	1	2	3
1	0.000		
2	0.673	0.000	
3	-0.457	-1.130	0.000

BONFERRONI ADJUSTMENT.
MATRIX OF PAIRWISE COMPARISON PROBABILITIES (P-values):

	1	2	3
1	1.000		
2	0.046	1.000	
3	0.221	0.002	1.000

COL/
ROW AUTO$
1 1
2 2
3 3

USING MODEL MSE OF .153 WITH 9. DF.
MATRIX OF PAIRWISE MEAN DIFFERENCES:

	1	2	3
1	0.000		
2	0.678	0.000	
3	0.853	0.175	0.000

BONFERRONI ADJUSTMENT.

MATRIX OF PAIRWISE COMPARISON PROBABILITIES (P-values):

	1	2	3
1	1.000		
2	0.044	1.000	
3	0.013	1.000	1.000

R_V depends on the type of cross-correlation between velocity and retardation (p=0.002), on the type of autocorrelation within the fields (p=0.010) and to a lesser degree on the interaction between the auto and cross-correlation scenarios (p=0.039).

Post-hoc analysis revealed that retardation coefficients were significantly elevated when there was a variable cross-correlation between K and Kd compared to a small negative

cross-correlation (p=0.046) or a perfect positive cross-correlation (p=0.002). R_V was also elevated when the correlation lengths were 20 cm compared to the same correlation lengths with the addition of periodicity (p=0.044), or to correlation lengths of 7 cm and no periodicity (p=0.013).

A repeated measures ANOVA was performed to look for significant differences between R_G and R_V. The ANOVA model was

$$R = retard + retard*cross + retard*auto + retard*cross*auto + \epsilon$$

where *retard* refers to either R_V or R_G.

SYSTAT output:

```
>MODEL RG RV = CONSTANT + XCOR$+AUTO$+XCOR$*AUTO$ /REPEAT=2 NAMES='retard'

LEVELS ENCOUNTERED DURING PROCESSING ARE:
XCOR$
 1        2        3
AUTO$
 1        2        3

NUMBER OF CASES PROCESSED:    18

DEPENDENT VARIABLE MEANS
              RG       RV
           4.119    5.146

UNIVARIATE REPEATED MEASURES ANALYSIS

BETWEEN SUBJECTS
----------
SOURCE              SS     DF     MS        F        P
XCOR$             1.864    2    0.932    11.793   0.003
AUTO$             1.548    2    0.774     9.794   0.006
XCOR$*AUTO$       1.388    4    0.347     4.392   0.030
ERROR             0.711    9    0.079

WITHIN SUBJECTS
----------
SOURCE                   SS     DF     MS        F        P      G-G    H-F
retard                 9.486    1    9.486   109.790   .2E-05     .      .
retard*XCOR$           2.026    2    1.013    11.722   0.003      .      .
retard*AUTO$           0.953    2    0.476     5.512   0.027      .      .
retard*XCOR$*AUTO$     1.076    4    0.269     3.114   0.072      .      .
ERROR                  0.778    9    0.086

GREENHOUSE-GEISSER EPSILON:    .
HUYNH-FELDT EPSILON    :    .
```

There was a very significant difference between the types of retardation (R_V and R_G) (p=0.2E-05), which depended on the type of cross-correlation (p=0.003) and on the type of auto-correlation (p=0.027) but not on the interaction (p=0.072).

To give a different perspective, the ratio of R_V to R_G was tested for a dependence on the

correlation scenario.

SYSTAT output:

>MODEL RVOVERRG = CONSTANT + XCOR$+AUTO$+XCOR$*AUTO$

LEVELS ENCOUNTERED DURING PROCESSING ARE:
XCOR$
1 2 3
AUTO$
1 2 3

DEP VAR:RVOVERRG N: 18 MULTIPLE R: 0.913 SQUARED MULTIPLE R: 0.833

ANALYSIS OF VARIANCE

SOURCE	*SUM-OF-SQUARES*	*DF*	*MEAN-SQUARE*	*F-RATIO*	*P*
XCOR$	0.247	2	0.124	11.318	**0.003**
AUTO$	0.112	2	0.056	5.147	**0.032**
XCOR$*AUTO$	0.129	4	0.032	2.963	**0.081**
ERROR	0.098	9	0.011		

COL/ ROW	XCOR$	AUTO$
1 1	1	
2 1	2	
3 1	3	
4 2	1	
5 2	2	
6 2	3	
7 3	1	
8 3	2	
9 3	3	

USING MODEL MSE OF .011 WITH 9. DF.
MATRIX OF PAIRWISE MEAN DIFFERENCES:

	1	2	3	4	5
1	0.000				
2	0.202	0.000			
3	0.367	0.165	0.000		
4	0.374	0.172	0.008	0.000	
5	0.262	0.060	-0.105	-0.113	0.000
6	0.401	0.199	0.034	0.027	0.139
7	-0.097	-0.299	-0.464	-0.471	-0.359
8	0.192	-0.010	-0.174	-0.182	-0.069
9	0.080	-0.122	-0.286	-0.294	-0.181

	6	7	8	9
6	0.000			
7	-0.498	0.000		
8	-0.208	0.290	0.000	
9	-0.320	0.178	-0.112	0.000

BONFERRONI ADJUSTMENT.

MATRIX OF PAIRWISE COMPARISON PROBABILITIES (P-values):

	1	**2**	**3**	**4**	**5**
1	**1.000**				
2	**1.000**	**1.000**			
3	**0.239**	**1.000**	**1.000**		
4	**0.214**	**1.000**	**1.000**	**1.000**	

5	1.000	1.000	1.000	1.000	1.000
6	0.144	1.000	1.000	1.000	1.000
7	1.000	0.674	0.059	0.053	0.270
8	1.000	1.000	1.000	1.000	1.000
9	1.000	1.000	0.826	0.735	1.000

	6	7	8	9
6	1.000			
7	0.037	1.000		
8	1.000	0.782	1.000	
9	0.487	1.000	1.000	1.000

COL/
ROW XCOR$
1 1
2 2
3 3

USING MODEL MSE OF .011 WITH 9. DF.
MATRIX OF PAIRWISE MEAN DIFFERENCES:

	1	2	3
1	0.000		
2	0.156	0.000	
3	-0.131	-0.287	0.000

BONFERRONI ADJUSTMENT.

MATRIX OF PAIRWISE COMPARISON PROBABILITIES (P-values):

	1	2	3
1	1.000		
2	0.089	1.000	
3	0.175	0.003	1.000

COL/
ROW AUTO$
1 1
2 2
3 3

USING MODEL MSE OF .011 WITH 9. DF.
MATRIX OF PAIRWISE MEAN DIFFERENCES:

	1	2	3
1	0.000		
2	0.126	0.000	
3	0.190	0.064	0.000

BONFERRONI ADJUSTMENT.

MATRIX OF PAIRWISE COMPARISON PROBABILITIES (P-values):

	1	2	3
1	1.000		
2	0.197	1.000	
3	0.035	0.953	1.000

The type of cross-correlation had a significant effect (p=0.003) on the ratio of R_V to R_G, and the autocorrelation had a less significant effect (p=0.032), while the interaction was not significant. Post hoc tests revealed that within the individual scenarios, only Case 23

(variable cross-correlation, $\lambda_3 = 7$ cm) was significantly higher than Case 31 (perfect positive correlation, $\lambda_3 = 20$ cm) (p=0.037).

The following table contains retardation coefficients for every realization. RA refers to the arithmetic retardation coefficient, R_A, RG refers to the geometric retardation coefficient R_G, and RV refers to the retardation coefficient calculated from a ratio of the non-reactive solute plume to the reactive solute plume.

Retardation coefficients for all realizations

Cross	Auto	RA	RG	RV	RV/RG
1	1	4.37	4.041	4.21	1.042
1	1	4.51	4.017	4.26	1.06
1	2	4.91	4.199	5.01	1.193
1	2	4.81	4.096	5.38	1.313
1	3	4.44	4.079	5.54	1.358
1	3	4.57	4.088	6.04	1.477
2	1	4.53	4.168	5.44	1.305
2	1	4.57	4.046	6.25	1.545
2	2	4.91	4.239	5.36	1.264
2	2	4.77	4.094	5.57	1.361
2	3	4.49	4.107	5.66	1.378
2	3	4.54	4.066	6.2	1.525
3	1	4.69	4.163	4.16	0.999
3	1	4.3	3.841	3.49	0.909
3	2	5.1	4.378	4.91	1.122
3	2	4.74	4.138	5.65	1.365
3	3	4.77	4.257	5.05	1.186
3	3	4.59	4.123	4.44	1.077

APPENDIX F
ANOVA results for effect of type of correlation between velocity and retardation on the macrodispersivity

The ANOVA model

$$A_{ii} = auto + \epsilon$$

was applied to the non-reactive solute macrodispersivities in each direction (longitudinal, transverse horizontal, transverse vertical). The variable *auto* refers to the type of autocorrelation. The raw data is located at the end of this appendix.

The ANOVA was performed using SYSTAT (version 5.02), and the output from the test follows. The output of primary interest is the p-value for each variable, or combination of variables.
The p-value indicates the probability of committing an error in declaring an effect significant; 1-p is the confidence level.

SYSTAT output for non-reactive solute plume (longitudinal direction):

LEVELS ENCOUNTERED DURING PROCESSING ARE:
AUTOS
a b c

DEP VAR: DISP N: 18 MULTIPLE R: 0.411 SQUARED MULTIPLE R: 0.169

ANALYSIS OF VARIANCE

SOURCE	*SUM-OF-SQUARES*	*DF*	*MEAN-SQUARE*	*F-RATIO*	*P*
AUTOS	0.137	2	0.068	1.524	0.250
ERROR	0.673	15	0.045		

SYSTAT output for non-reactive solute plume (transverse vertical direction):

LEVELS ENCOUNTERED DURING PROCESSING ARE:
AUTOS
a b c

DEP VAR: DISP N: 18 MULTIPLE R: 0.524 SQUARED MULTIPLE R: 0.275

ANALYSIS OF VARIANCE

SOURCE	*SUM-OF-SQUARES*	*DF*	*MEAN-SQUARE*	*F-RATIO*	*P*
AUTOS	.831000E-05	2	.415500E-05	2.844	0.090
ERROR	.219150E-04	15	.146100E-05		

SYSTAT output for non-reactive solute plume (transverse horizontal direction):

LEVELS ENCOUNTERED DURING PROCESSING ARE:
AUTOS
a b c

DEP VAR: DISP N: 18 MULTIPLE R: 0.222 SQUARED MULTIPLE R: 0.049

ANALYSIS OF VARIANCE

SOURCE	*SUM-OF-SQUARES*	*DF*	*MEAN-SQUARE*	*F-RATIO*	*P*
AUTO$	.127633E-04	2	.638167E-05	0.388	0.685
ERROR	.246417E-03	15	.164278E-04		

The above results indicate that there was no significant difference between types of auto-correlation in any direction for the non-reactive case (p=0.250, p=0.090, p=0.685 for the x, y and z directions respectively).

The ANOVA

$$A_{ii} = cross + auto + cross*auto + \epsilon$$

was used to determine whether the macrodispersivities of a reactive solute plume depended on the correlation scenario. The variable *cross* refers to the type of cross-correlation.

SYSTAT output for reactive solute, longitudinal (x) direction:

model A_ii = XCOR + AUTO + XCOR*AUTO + ERROR
LEVELS ENCOUNTERED DURING PROCESSING ARE:
XCOR$
1 2 3
AUTO$
a b c

DEP VAR: DISP N: 21 MULTIPLE R: 0.915 SQUARED MULTIPLE R: 0.838

ANALYSIS OF VARIANCE

SOURCE	*SUM-OF-SQUARES*	*DF*	*MEAN-SQUARE*	*F-RATIO*	*P*
XCOR$	4.1242	2	2.0621	18.8370	0.0002
AUTO$	1.6518	2	0.8259	7.5445	0.0076
AUTO$*XCOR$	1.0470	4	0.2618	2.3911	0.1087
E RROR	1.3137	12	0.1095		

COL/
ROW XCOR$
1 1
2 2
3 3

USING MODEL MSE OF .109 WITH 12 DF.
MATRIX OF PAIRWISE MEAN DIFFERENCES:

	1	2	3
1	0.0000		
2	-0.4165	0.0000	
3	-1.0919	-0.6754	0.0000

BONFERRONI ADJUSTMENT.
MATRIX OF PAIRWISE COMPARISON PROBABILITIES (P-values):

	1	2	3
1	1.0000		
2	0.1496	1.0000	
3	0.0002	0.0087	1.0000

Comparison of auto-correlation types:

COL/
ROW AUTOS
1 a
2 b
3 c

USING LEAST SQUARES MEANS.

USING MODEL MSE OF .109 WITH 12 DF.
MATRIX OF PAIRWISE MEAN DIFFERENCES:

	1	2	3
1	0.0000		
2	0.4454	0.0000	
3	-0.2408	-0.6863	0.0000

BONFERRONI ADJUSTMENT.
MATRIX OF PAIRWISE COMPARISON PROBABILITIES (P-values):

	1	2	3
1	1.0000		
2	0.0904	1.0000	
3	0.6941	0.0078	1.0000

Comparison of both auto- and cross-correlation:

COL/
ROW AUTOS XCORS
1 a 1
2 a 2
3 a 3
4 b 1
5 b 2
6 b 3
7 c 1
8 c 2
9 c 3

USING MODEL MSE OF .109 WITH 12 DF.
MATRIX OF PAIRWISE MEAN DIFFERENCES:

	1	2	3	4	5	
1	0.0000					
2	-0.5565	0.0000				
3	-1.0925	-0.5360	0.0000			
4	0.6320	1.1885	1.7245	0.0000		
5	0.1200	0.6765	1.2125	-0.5120	0.0000	
6	-1.0647	-0.5082	0.0278	-1.6967	-1.1847	
7	-0.5680	-0.0115	0.5245	-1.2000	-0.6880	
8	-0.7490	-0.1925	0.3435	-1.3810	-0.8690	
9	-1.0545	-0.4980	0.0380	-1.6865	-1.1745	

	6	7	8	9
6	0.0000			
7	0.4967	0.0000		
8	0.3157	-0.1810	0.0000	
9	0.0102	-0.4865	-0.3055	0.0000

BONFERRONI ADJUSTMENT.
MATRIX OF PAIRWISE COMPARISON PROBABILITIES (P-values):

	1	2	3	4	5
1	1.0000				
2	1.0000	1.0000			
3	0.2274	1.0000	1.0000		
4	1.0000	0.1332	0.0078	1.0000	
5	1.0000	1.0000	0.1166	1.0000	1.0000
6	0.0838	1.0000	1.0000	0.0018	0.0385
7	1.0000	1.0000	1.0000	0.1249	1.0000
8	1.0000	1.0000	1.0000	0.0465	0.7963
9	0.2814	1.0000	1.0000	0.0095	0.1439

	6	7	8	9
6	1.0000			
7	1.0000	1.0000		
8	1.0000	1.0000	1.0000	
9	1.0000	1.0000	1.0000	1.0000

In the longitudinal direction (reactive case), both the effects of the type of cross-correlation and auto-correlation were found to be significant (p=0.0002 and p=0.0076, respectively). The effect of the interaction was not significant (p=0.1087) indicating that the effect of the type of autocorrelation did not depend on the type of cross-correlation.

SYSTAT output for reactive solute plume (transverse horizontal direction):

LEVELS ENCOUNTERED DURING PROCESSING ARE:
XCOR$
1 2 3
AUTO$
B a c

DEP VAR: DISP N: 21 MULTIPLE R: 0.565 SQUARED MULTIPLE R: 0.319

ANALYSIS OF VARIANCE

SOURCE	*SUM-OF-SQUARES*	*DF*	*MEAN-SQUARE*	*F-RATIO*	*P*
XCOR$	.203205E-04	2	.101603E-04	2.2996	0.1427
AUTO$	.128205E-06	2	.641026E-07	0.0145	0.9856
AUTO$*XCOR$	.316667E-05	4	.791667E-06	0.1792	0.9448
ERROR	.530200E-04	12	.441833E-05		

SYSTAT output for reactive solute plume (transverse vertical direction):

LEVELS ENCOUNTERED DURING PROCESSING ARE:
XCOR$
1 2 3
AUTO$
B C a

DEP VAR: DISP N: 21 MULTIPLE R: 0.601 SQUARED MULTIPLE R: 0.361

ANALYSIS OF VARIANCE

SOURCE	*SUM-OF-SQUARES*	*DF*	*MEAN-SQUARE*	*F-RATIO*	*P*
XCOR$	.250274E-04	2	.125137E-04	0.8060	0.4694
AUTO$	.122658E-04	2	.613292E-05	0.3950	0.6821
AUTO$*XCOR$	.684920E-04	4	.171230E-04	1.1029	0.3993
ERROR	0.0002	12	.155257E-04		

In the transverse horizontal and transverse vertical directions, for the reactive scenarios, the type of auto and cross-correlation had no significant effect on macrodispersivity ($p>0.1427$), and there was no interaction between the auto and cross-correlation ($p>0.3993$).

The following table gives macrodispersivity values for all cases, where X, Y, and Z refer to the longitudinal, transverse horizontal and transverse vertical directions, respectively, and the subscripts R and NR refer to reactive and non-reactive solute plumes, respectively.

Macrodispersivities for all realizations, all directions.

Cross	Auto	XR	YR	ZR	XNR	YNR	ZNR
1	1	0.636	0.013	0.016	0.22	0.013	0.019
1	1	1.591	0.013	0.012	0.495	0.013	0.007
1	2	1.908	0.012	0.006	0.698	0.009	0.005
1	2	1.583	0.014	0.012	0.463	0.011	0.008
1	3	0.467	0.011	0.012	0.141	0.012	0.011
1	3	0.624	0.014	0.012	0.246	0.011	0.007
2	1	0.453	0.009	0.003	0.711	0.011	0.007
2	1	0.661	0.011	0.009	0.148	0.01	0.013
2	2	1.834	0.01	0.019	0.751	0.009	0.016
2	2	0.633	0.012	0.005	0.354	0.01	0.011
2	3	0.209	0.011	0.011	0.153	0.009	0.009
2	3	0.52	0.009	0.014	0.416	0.013	0.006
3	1	0.021	0.012	0.008	0.304	0.011	0.011
3	1	0.021	0.01	0.008	0.616	0.011	0.007
3	2	0.034	0.007	0.009	0.546	0.01	0.007
3	2	0.051	0.009	0.013	0.134	0.011	0.013
3	2	0.039	0.012	0.009			
3	2	0.079	0.015	0.011			
3	2	0.041	0.011	0.005			
3	3	0.064	0.011	0.011	0.572	0.012	0.006
3	3	0.054	0.012	0.008	0.153	0.011	0.013

APPENDIX G
ANOVA results for effect a comparison of macrodispersivities between the reactive and non-reactive solute plumes

The ANOVA model which was used to perform the repeated measures analysis was

$$A_{ii} = solute + solute*xcor + solute*auto + solute*xcor*auto + \epsilon$$

where the type of solute was the repeated measure (either reactive or non-reactive) because of the inherent correlation due to the same flow field. The variable *solute* refers to the type of solute and variables *auto* and *cross* refer to the types of auto and cross-correlation, respectively. The raw data is located at the end of this appendix.

The ANOVA was performed using SYSTAT (version 5.02), and the output from the test follows. The output of primary interest is the p-value for each variable, or combination of variables.
The p-value indicates the probability of committing an error in declaring an effect significant; 1-p is the confidence level.

SYSTAT output:

LEVELS ENCOUNTERED DURING PROCESSING ARE:
AUTO$
1 2 3
XCOR$
1 2 3

NUMBER OF CASES PROCESSED: 18

DEPENDENT VARIABLE MEANS

RDISP	NRDISP
0.631	0.396

UNIVARIATE REPEATED MEASURES ANALYSIS

BETWEEN SUBJECTS

SOURCE	*SS*	*DF*	*MS*	*F*	*P*
XCOR$	1.819	2	0.910	6.129	**0.021**
AUTO$	1.211	2	0.606	4.081	**0.055**
XCOR$*AUTO$	0.737	4	0.184	1.241	**0.360**
ERROR	1.336	9	0.148		

WITHIN SUBJECTS

SOURCE	*SS*	*DF*	*MS*	*F*	*P*	*G-G*	*H-F*
solute	0.500	1	0.500	8.321	**0.018**	.	.
solute*XCOR$	1.846	2	0.923	15.347	**0.001**	.	.
solute*AUTO$	0.371	2	0.185	3.084	**0.095**	.	.
solute*XCOR$*AUTO$	0.196	4	0.049	0.815	**0.547**	.	.
ERROR	0.541	9	0.060				

GREENHOUSE-GEISSER EPSILON: .
HUYNH-FELDT EPSILON : .

When all values were taken together (ignoring differences between reactive and non-reactive simulations), there was a marginally significant effect of cross-correlation ($p=0.021$) and of auto-correlation ($p=0.055$) on macrodispersivity. However, when reactive and non-reactive macrodispersivities were taken as repeated measures, the effect of the type of solute was significant and depended on the type of cross-correlation ($p=0.001$) but not on the type of auto-correlation ($p=0.095$).

The following table contains longitudinal macrodispersivities for every realization. Aii(R) and Aii(NR) refer to macrodispersivities for the reactive and non-reactive solute plumes, respectively.

Longitudinal macrodispersivities for all realizations.

Cross	Auto	Aii(R)	Aii(NR)
1	1	0.636	0.22
1	1	1.591	0.495
1	2	1.908	0.698
1	2	1.583	0.463
1	3	0.467	0.141
1	3	0.624	0.246
2	1	0.453	0.711
2	1	0.661	0.148
2	2	1.834	0.751
2	2	0.633	0.354
2	3	0.209	0.153
2	3	0.52	0.416
3	1	0.021	0.304
3	1	0.021	0.616
3	2	0.034	0.546
3	2	0.051	0.134
3	3	0.064	0.572
3	3	0.054	0.153

APPENDIX H
ANOVA results for effect of type of correlation between velocity and retardation on A^*

The ANOVA model

$$A^* = cross + auto + cross*auto + \epsilon$$

was applied to the ratio

$$A^* = \frac{A_R - A_{NR}}{A_{NR}}$$

where the subscripts *R* and *NR* refer to the reactive and non-reactive solute plume macrodispersivities, respectively. The variables *auto* and *cross* refer to the type of auto and cross-correlation. The raw data is located at the end of this appendix.

The ANOVA was performed using SYSTAT (version 5.02), and the output from the test follows. The output of primary interest is the p-value for each variable, or combination of variables. The p-value indicates the probability of committing an error in declaring an effect significant; (1-p) is the confidence level.

SYSTAT output:

```
>MODEL ASTAR = CONSTANT + XCORS+AUTOS+XCORS*AUTOS

LEVELS ENCOUNTERED DURING PROCESSING ARE:
XCORS
 1       2       3
AUTOS
 1       2       3

DEP VAR:  ASTAR     N:    18 MULTIPLE R: 0.874  SQUARED MULTIPLE R: 0.764

             ANALYSIS OF VARIANCE

SOURCE          SUM-OF-SQUARES     DF    MEAN-SQUARE      F-RATIO      P
XCORS              24.989           2        12.495          13.681     0.002
AUTOS               0.528           2         0.264           0.289     0.756
XCORS*AUTOS         1.132           4         0.283           0.310     0.864
ERROR               8.220           9         0.913
```

Post-hoc tests

```
>HYPOTHESIS
>POST xcors, autos/ BONF

COL/
ROW  XCORS     AUTOS
 1 1       1
 2 1       2
 3 1       3
 4 2       1
```

```
 5 2       2
 6 2       3
 7 3       1
 8 3       2
 9 3       3

USING LEAST SQUARES MEANS.

USING MODEL MSE OF      .913 WITH    9. DF.
MATRIX OF PAIRWISE MEAN DIFFERENCES:
             1       2       3       4       5

       1   0.000
       2   0.024   0.000
       3  -0.128  -0.152   0.000
       4  -0.501  -0.525  -0.373   0.000
       5  -0.937  -0.961  -0.809  -0.437   0.000
       6  -1.745  -1.768  -1.616  -1.244  -0.807
       7  -3.001  -3.025  -2.873  -2.500  -2.064
       8  -2.831  -2.855  -2.703  -2.330  -1.894
       9  -2.820  -2.844  -2.692  -2.319  -1.883

             6       7       8       9

       6   0.000
       7  -1.256   0.000
       8  -1.087   0.170   0.000
       9  -1.076   0.181   0.011   0.000


BONFERRONI ADJUSTMENT.
MATRIX OF PAIRWISE COMPARISON PROBABILITIES (p-values):
             1       2       3       4       5

       1   1.000
       2   1.000   1.000
       3   1.000   1.000   1.000
       4   1.000   1.000   1.000   1.000
       5   1.000   1.000   1.000   1.000   1.000
       6   1.000   1.000   1.000   1.000   1.000
       7   0.429   0.412   0.533   1.000   1.000
       8   0.572   0.550   0.712   1.000   1.000
       9   0.583   0.560   0.725   1.000   1.000

             6       7       8       9

       6   1.000
       7   1.000   1.000
       8   1.000   1.000   1.000
       9   1.000   1.000   1.000   1.000


>HYPOTHESIS
>POST xcor$/ BONF

COL/
ROW   XCOR$
 1 1
 2 2
 3 3

USING LEAST SQUARES MEANS.

USING MODEL MSE OF      .913 WITH    9. DF.
MATRIX OF PAIRWISE MEAN DIFFERENCES:
```

```
            1       2       3

1       0.000
2      -1.026   0.000
3      -2.849  -1.823   0.000

BONFERRONI ADJUSTMENT.
MATRIX OF PAIRWISE COMPARISON PROBABILITIES (p-values):
            1       2       3

1       1.000
2       0.288   1.000
3       0.002   0.028   1.000


COL/
ROW   AUTOS
 1 1
 2 2
 3 3

USING LEAST SQUARES MEANS.

USING MODEL MSE OF      .913 WITH    9. DF.
MATRIX OF PAIRWISE MEAN DIFFERENCES:
            1       2       3

1       0.000
2      -0.081   0.000
3      -0.397  -0.316   0.000

BONFERRONI ADJUSTMENT.
MATRIX OF PAIRWISE COMPARISON PROBABILITIES (p-values):
            1       2       3

1       1.000
2       1.000   1.000
3       1.000   1.000   1.000
```

The above results indicate that there is reduced spreading for the case of a perfect positive correlation (p=0.002), however neither the type of autocorrelation or the specific scenario (interaction) significantly affects A^* (p=0.755 and p=0.864, respectively). Post-hoc pairwise comparisons indicate that there are no specific pairs of cases which significantly differ from one another. In fact, this ANOVA model procures no new information, simply confirming the results obtained from previous ANOVA's.

The table below displays reactive (Rdisp) and non-reactive (NRdisp) solute plume longitudinal macrodispersivities. All values are in metres.

Cross	Auto	Rdisp	NRdisp	A*
1	1	0.636	0.22	1.891
1	1	1.591	0.495	2.214
1	2	1.908	0.698	1.734
1	2	1.583	0.463	2.419

1	3	0.467	0.141	2.312
1	3	0.624	0.246	1.537
2	1	0.453	0.711	-0.363
2	1	0.661	0.148	3.466
2	2	1.834	0.751	1.442
2	2	0.633	0.354	0.788
2	3	0.209	0.153	0.366
2	3	0.52	0.416	0.25
3	1	0.021	0.304	-0.931
3	1	0.021	0.616	-0.966
3	2	0.034	0.546	-0.938
3	2	0.051	0.134	-0.619
3	3	0.064	0.572	-0.888
3	3	0.054	0.153	-0.647

APPENDIX I
Spectral analysis

Spectral analysis is a tool that allows a researcher to apply standard statistical methods to evaluate the spatial behaviour of variability in a data set or sets. The main advantage of spectral analysis is that it gives an indication of the variability associated with a specific wavelength, or wavelengths (similar to the autocovariance and the cross-covariance, which give an indication of the variability in the data set associated with different separations, or lags), however, the corresponding spectral functions are uncorrelated. Before proceeding on the subject of spectral analysis, a short discussion of auto and cross-covariance follows.

The autocovariance function (ACF) gives a measure of how a variable is correlated with itself in space or time. More specifically, the ACF gives the co-variance between pairs of measurements separated by a given distance, the lag. In typical geological applications measurements that are close together (small lags) show a large positive covariance (they are highly correlated); the covariance then decreases to zero as the distance separating the measurements increases and the measurements become uncorrelated. Because the covariance for each lag is calculated from the same data set, the autocovariance estimates at different lags are correlated to one another.

The Cross-Covariance Function (CCF) measures how two variables co-vary with each other in space or time. Specifically, it is a measure of the covariance between variable A at a point x and variable B at a point $x + lag$. Similar to the autocovariance, the cross-covariance estimates are also correlated to one another. Because of this correlation, we cannot compare the covariance values at different lags using standard statistical tools. However, if the autocovariance (and cross-covariance) functions were to be orthogonalized in lag space, each measurement would be independent of the other and standard statistical methods would be applicable. This is achieved is through the use of the Fourier transform.

The principle behind the Fourier transform is that all single-valued, continuous functions can be expressed as the sum of orthogonal sinusoidal functions. In effect, the Fourier transform partitions the variability in a data set into the portions contributed by the distance (length or time) over which the variability is measured. This is done by representing the series as a sum of sinusoidal curves, each of which is orthogonal to one another (*Davis, 1973*). The sum of these sinusoidal curves produces the original series, and therefore the sum of the variations in the individual curves (the amplitudes) produces the series variance. The Power spectrum is a plot of the amplitudes of the sinusoidal curves as a function of their frequency. Frequency has units of cycles/m (in one dimension) and its reciprocal, the wave length, can be interpreted as the scale over which the measurements take place.

Thus the power spectrum can be interpreted as variability as a function of the scale over which the measurements are made. Similarly, the cross-spectrum gives the degree of co-variability between two spatially distributed variables (also as a function of the scale over which the measurements are made). The power spectrum and cross-spectrum are closely related to the autocovariance and cross-covariance functions, respectively. In fact the power spectrum and the autocovariance function are a Fourier transform pair; and likewise for the cross-spectrum and the cross-covariance function.

The spectra and covariance functions therefore contain essentially the same information but, as mentioned above, their statistical properties are very different. Contrary to the spectral estimates, the covariances estimated at different lags by the ACF or the CCF are not independent of each other, which precludes many statistical tests (as mentioned earlier). As a result the interpretations from ACF's and CCF's are often more descriptive in nature and more qualitative. On the other hand, spectral estimates are independent of each other and can therefore undergo more rigorous statistical testing. The cost of this increased rigour is that spectral estimates are more complicated to calculate and, arguably, to interpret.

To be more rigorous now, the Power Spectral Density Function actually gives the density of variance as a function of frequency. Thus the integral of the power spectrum over a frequency range gives the variance contributed by that frequency range (or range of scales). Since the spectral estimates are independent of each other, it is possible to use the standard Fisher-Snedecor Test to compare variance contributions at various scales.

Given a stationary (space invariant) process $\psi(\vec{x})$, it's perturbation, $\psi'(\vec{x}) = \psi(\vec{x}) - \mu_\psi$ can be represented in the Fourier domain by a complex variable $dZ_\psi(\vec{\omega}) = dZ(\omega_1)\, dZ(\omega_2)\, dZ(\omega_3)$, where:

$$\psi'(\vec{x}) = \int_{-\infty}^{\infty}\int\int \exp\,(i\vec{\omega}\cdot\vec{x})\; dZ_\psi(\vec{\omega})$$

$$= \int_{-\infty}^{\infty}\int\int \frac{dZ_\psi(\vec{\omega})}{d\vec{\omega}} \exp\,(i\vec{\omega}\cdot\vec{x}) d\vec{\omega}$$

$$= \int_{-\infty}^{\infty}\int\int \frac{dZ_\psi(\vec{\omega})}{d\vec{\omega}} [\cos(\vec{\omega}\cdot\vec{x}) + i\sin(\vec{\omega}\cdot\vec{x})] d\vec{\omega}$$

and $i = \sqrt{-1}$ and $\vec{\omega} = 2\pi f$ is the angular frequency. We define the Power spectrum as the magnitude of the Fourier representation of the perturbation:

$$S_{\psi\psi}(\vec{\omega}) = |dZ_\psi(\vec{\omega})|$$

$$= dZ_\psi(\vec{\omega})\; dZ_\psi^*(\vec{\omega})$$

where the asterisk denotes complex conjugation. The Power spectrum is a real function, and is the inverse Fourier transform of the autocovariance function:

$$S_{\psi\psi}(\vec{f}) = \frac{1}{(2\pi)^3} \int_{-\infty}^{\infty}\int\int \rho_{\psi\psi}(\vec{s}) \exp\left(-i\vec{f}\cdot\vec{x}\right) d\vec{s}$$
$$= (2\pi)^3 \mathcal{F}^{-1}\left(\rho_{\psi\psi}(\vec{s})\right)$$

The corresponding function, the Fourier-domain representation of the cross-covariance, is called the Cross-spectrum:

$$S_{\psi_1\psi_2} = (2\pi)^3 \mathcal{F}^{-1}\left(\rho_{\psi_1\psi_2}(\vec{s})\right)$$
$$= dZ_{\psi_1}(\vec{\omega})\, dZ^{*}_{\psi_2}(\vec{\omega})$$
$$= Co(\vec{\omega}) + i\, Quad(\vec{\omega})$$

which is a complex variable, with a real part called the co-spectrum and an imaginary part called the quadrature spectrum. The co- and quadrature spectra measure the in- and out-of-phase covariance of the two variables. The in-phase covariance, or co-spectrum, measures the degree of covariance between the two series when they are not offset relative to one another. The out-of-phase covariance, or quadrature spectrum, measures the degree of covariance between the two series when they are offset relative to one another. The size of the offset is the delay associated with the quadrature spectrum.

The ratio of the magnitude of the cross-spectrum to the product of the two spectra is called the Coherency spectrum. It is the spectral equivalent of the correlation coefficient; it gives the degree of correlation between the two variables as a function of frequency (or scale).

The previous paragraphs explain the theory behind and general background of spectral analysis. The following section summarizes methods for calculating the power spectrum.

There are two categories of methods which are used to calculate power spectra, direct methods, and indirect methods. In the case of the indirect methods, the power spectrum is simply calculated from the Fourier transform of the autocovariance function. In the case of the direct methods, the autocovariance is not calculated, the power spectrum is estimated directly from the data. The direct method usually incorporates the use of the Fast Fourier Transform algorithm (in fact, this is the algorithm applied by the Random Field Generator used for this research) since it is capable of quickly dealing with a large data set, however, another approach is to use the Discrete Fourier Transform method using sines and cosines. This method is illustrated for the one-dimensional case below (*Kachanoski and de Jong, 1988*):

$$S_{\psi\psi}(f_k) = \frac{2\,\Delta x}{(2m+1)N^2} \sum_{l=-m}^{m} \left(A_{\psi}^2(f_{k+l}) + i\, B_{\psi}^2(f_{k+l}) \right)$$

$$A_{\psi}(f_k) = \sum_{j=1}^{N} \psi_j \cos(2\pi j \Delta x f_k)$$

$$B_{\psi}(f_k) = \sum_{j=1}^{N} \psi_j \sin(2\pi j \Delta x f_k)$$

where Δx is the sampling interval and f_k is the frequency coordinate:

$$f_k = \begin{cases} k/(N\Delta x),\ k=1,2,\ldots,N/2; & N \text{ even} \\ k/((N-1)\Delta x),\ k=1,2,\ldots,(N-1)/2; & N \text{ odd} \end{cases}$$

The cross-spectrum can also be estimated using the Discrete Fourier Transform method, as shown below (modified from *Brillinger, 1981*):

$$S_{\psi_1\psi_2}(f_k) = \frac{1}{(2m+1)N^2} \sum_{l=-m}^{m} \left(C_{i\psi_1\psi_2}(f_{k+l}) + Q_{i\psi_1\psi_2}(f_{k+l}) \right)$$

$$C_{i\psi_1\psi_2} = A_{i\psi_1} A_{i\psi_2} + B_{i\psi_1} B_{i\psi_2}$$

$$Q_{i\psi_1\psi_2} = A_{i\psi_2} B_{i\psi_1} - A_{i\psi_1} B_{i\psi_2}$$

where $A_{i\psi}$ and $B_{i\psi}$ are as above and $C_{i\psi\psi}$ and $Q_{i\psi\psi}$ represent the co- and quadrature spectra, respectively.

The cross-spectrum can be normalized to obtain the squared coherency spectrum, $R^2_{\psi\psi}(f_k)$:

$$R^2_{\psi_1\psi_2}(f_k) = \frac{|S_{\psi_1\psi_2}(f_k)|^2}{S^2_{\psi_1\psi_1}(f_k)\; S^2_{\psi_2\psi_2}(f_k)}$$

As mentioned earlier, the coherency spectrum is a measure of the correlation between the two variables as a function of frequency (or scale).

The random field generator used in this work exploits the functional relations above to produce random fields of prescribed power-spectral and cross-spectral properties. Essentially the method consists of obtaining deterministic values of $A_{i\psi}$ and $B_{i\psi}$, based on the input power-spectra and the input cross-spectrum; randomizing these values according to a Chi-Squared distribution; and performing an inverse Fourier transform on

the randomized $A_{i\psi}$ and $B_{i\psi}$ values to obtain random fields.

REFERENCES

Brigham, E.O., *The Fast Fourier Transform and its Applications*, Prentice Hall, New Jersey, 1988

Brillinger, D.R., *Time Series: Data Analysis and Theory, Second Edition*, San Francisco: Holden Day, 1981

Davis, *Statistics and Data Analysis in Geology, 2nd Ed.*, John Wiley and Sons, 1973

Robin, M.J.L., E.A. Sudicky, R.W. Gillham and R.G. Kachanoski, Spatial Variability of Strontium Distribution Coefficients and Their Correlation With Hydraulic Conductivity in the Canadian Forces Base Borden Aquifer, *Water Resources Research*, 27(10), 2619-2632, 1991.

Kachanoski and deJong, 1988.

Jenkins, G.M., and D.G. Watts, Spectral Analysis and its Applications, Holden-Day, Oakland, California, 1968.

Priestly, M.B., Spectral Analysis and Time Series, Academic Press, London, 1981.

APPENDIX J
Analysis of Variance

An Analysis of Variance (ANOVA) is performed when testing a multi sample hypothesis; that is, when comparing multiple means. For instance, if one wanted to test whether three samples came from the same population one might test the null hypothesis that the means are equal; H_0: $\mu_1 = \mu_2 = \mu_3$ by testing each pair-wise equality individually: H_0: $\mu_1 = \mu_2$, H_0: $\mu_1 = \mu_3$ and H_0: $\mu_2 = \mu_3$. This procedure, however, is invalid since the probability of falsely rejecting the three pair-wise null hypotheses would be much higher than that of rejecting the single multiple-comparison.

The ANOVA is actually based on comparisons of variabilities (expressed as variances); hence the name. If the variability between means is larger than the variability of the elements within each mean, then we reject the null hypothesis that all means are from the same population, and we declare that there is a significant difference between the means (with probability of error p). Since the underlying hypothesis is that all means are from the same population, the variances within each mean must all be estimates of the same sample variance. This variance, called the error, is obtained by replicating each element in the means. That the error is uniform from one mean to another is one of the main assumptions upon which the ANOVA technique is based; it is referred to as the assumption of homogeneity of variance. In other words, the variability associated with the replication of the experiment should be consistent between samples, or treatments.

The type of ANOVA used in this study was the two-factor Analysis of Variance, since the effect of two principal factors were examined: both the type of autocorrelation and the type of cross-correlation, each with three levels. Each of the nine possible combinations of the three levels of each factor is called a "treatment". The possibility that the effect of one factor on the dependent variable could be affected by the level of the other factor was also examined. This effect is called the "interaction". The ANOVA procedure effectively partitions the overall variability into the variability contributed by the two factors, the interaction and the error. The real advantage to using a Factorial design is that, by replicating each treatment and by combining the error estimates from each treatment, a very good estimate of the error can be obtained with relatively few replications. This is a substantial advantage when the cost of laboratory analyses is large or, as in this study, when the time required for each realization is very large.

The results of the ANOVA are based on the comparison of the variability between means of each factor level and the error. This variability is estimated by the Mean Squared Deviation from the Mean - "Mean Squared" or MS for short. If the ratio of the MS due to one factor to the MS of the error is significantly larger than 1, we declare that the factor in question has a significant effect on the dependent variable (with probability of error p). The ratio of mean squares is called the F-statistic and it is distributed according to the Fisher-Snedecor Distribution. The p-value is the probability that the real F-statistic is as

large or larger than the measured F-statistic; it is therefore the probability of committing an error in rejecting the null hypothesis. Most software packages will give both the F-statistic and the p-value; (1-p) is the confidence level.

REFERENCES

Snedecor, G.W. and Cochran, W.G., *Statistical Methods, 7th Ed.*, Iowa State University Press, 1980

Zar, J.H., *Biostatistical Analysis, 2nd Ed.*, Prentice-Hall, New Jersey, 1984